



**MECHANICAL BEHAVIOR OF CRACKED PANELS
REPAIRED WITH BONDED COMPOSITE PATCH**

THESIS

Michael A. Hansen, Captain, USAF

AFIT/GA/ENY/05-J01

**DEPARTMENT OF THE AIR FORCE
AIR UNIVERSITY**

AIR FORCE INSTITUTE OF TECHNOLOGY

Wright-Patterson Air Force Base, Ohio

APPROVED FOR PUBLIC RELEASE; DISTRIBUTION UNLIMITED

The views expressed in this thesis are those of the author and do not reflect the official policy or position of the United States Air Force, Department of Defense, or the United States Government

AFIT/GA/ENY/05-J01

MECHANICAL BEHAVIOR OF CRACKED PANELS
REPAIRED WITH BONDED COMPOSITE PATCH

THESIS

Presented to the Faculty

Department of Aeronautics and Astronautics

Graduate School of Engineering and Management

Air Force Institute of Technology

Air University

Air Education and Training Command

In Partial Fulfillment of the Requirements for the
Degree of Master of Science in Astronautical Engineering

Michael A. Hansen, BS

Captain, USAF

June, 2005

APPROVED FOR PUBLIC RELEASE; DISTRIBUTION UNLIMITED.

AFIT/GA/ENY/05-J01

MECHANICAL BEHAVIOR OF CRACKED PANELS
REPAIRED WITH BONDED COMPOSITE PATCH

Michael A. Hansen, BS

Captain, USAF

Approved:

Dr. Shankar Mall (Chairman)

date

Dr. Marina B. Ruggles-Wrenn

date

Dr. Robert A. Canfield

date

Abstract

This research focuses on investigating the mechanical behavior of cracked aluminum panels repaired with bonded boron/epoxy composite patches. The effects of crack initiation and growth on the residual strength of the repaired panels are characterized. This research establishes a correlation between damage modes, residual strength and evolution of strain within as well as outside the patch. Monotonic tensile tests on specimens with a perfectly bonded patch were used to determine the base line strength. Likewise, fatigue tests on specimens with a perfectly bonded patch served to establish baseline fatigue life. In addition, several specimens with a perfectly bonded patch were subjected to different fractions of the expected fatigue life, introducing damage, which were quantified by NDE techniques. These specimens were then subjected to a monotonic tensile test to failure in order to characterize the residual strength and the evolution of strain within and outside the patch, and the correlation between the disbonds and strain measurements at various locations on the specimen. This research looks to help in extending the service life of military and commercial aging aircraft, by using bonded composite patches on developing cracks in the structure. Bonded composite patches may be able to replace the crack patching technique of using bolted joints, which have the disadvantage of requiring holes to be machined in the metallic structure, which decreases its load-carrying capacity, creating stress concentrations and sites for crack initiation.

In this study it was learned how the strain values increase as the crack grows. And despite differing crack growth rates, the strain values followed the growth of the crack closely throughout all the tests. The effects of overload situations were seen, and how this produces a retardation effect in the rate of growth of the crack.

Table of Contents

	Page
Abstract.....	iv
Table of Contents	vi
List of figures	viii
List of Tables	xii
I. Introduction	1
1.1 Aging Aircraft	1
1.2 Repair Options	3
1.3 Research	5
II. Background	8
2.1 Elementary Fracture Mechanics.....	8
2.2 Composite Repair Design	14
2.2.1 Patch Design	14
2.2.2 Patch Material Selection	16
2.2.3 Adhesive Selection	18
2.2.4 Surface Preparation.....	20
2.3 History of Composite Repair and Past Research.....	21
2.3.1 Origin of Composite Repair	21
2.3.2 Examples of Composite Repair	24
2.3.2.1 F-111 Lower Wing Skin Repair Substantiation	24
2.3.2.2 F-16 Fuel Vent-Hole Repairs	26
2.3.3 Research Studies	27
III. Experimental Setup and Procedure	30
3.1 Materials and Specimen Description.....	30
3.2 Test Equipment	33
3.3 Test Procedure	38
3.4 Scanning Acoustic Microscopy	40
IV. Test Results and Discussion	42
4.1 Pre-Test Curvature	43
4.2 Fatigue Testing	48
4.2.1 Crack Growth Analysis	49
4.2.2 Overloading and Retardation Effects	54

	Page
4.2.3 Strain Measurements	57
4.3 Tensile Loading and Fracture	78
4.4 Debonds	79
4.4.1 Photographic and Acoustic Imaging	79
4.4.2 IR Imaging	87
4.5 Data Comparisons	89
V. Summary, Conclusions, and Recommendations.....	93
Bibliography.....	96

List of figures

Figure	Page
1. Specimen diagram.....	6
2. Crack in an infinite plate.....	8
3a. The engineering problem, Crack Growth Curve.....	9
3b. The Engineering Problem, Residual Strength Curve.....	9
4. The three modes of loading.....	10
5. Elastic stress σ_y at the crack tip.....	11
6. Load Flow into a Repair.....	13
7. Bending Caused by Neutral Axis Shift in Single Sided Repair.....	15
8. Loading on Adhesive Bonds.....	15
9. Strain Gage Diagram, Patched Side.....	34
10. Strain Gage Diagram, Unpatched Side.....	35
11. Gaertner Traveling Microscope.....	36
12. Gaertner Microscope Digital Readout.....	36
13. FLIR IR Camera.....	37
14. Master-Mite Heat Gun.....	38
15. Specimen Grips.....	39
16. Scanning Acoustic Microscopy System.....	41
17. Oscilloscope Screen.....	41
18. Specimen Curvature Data Points and Polynomial Fit Line.....	43
19. Average Initial Strain Values for Strain Gages 1-6, 13, 14.....	46

Figure	Page
20. Average Initial Strain Values for Strain Gages 7-12.....	46
21. Crack Growth Rate.....	49
22. Fitted Crack Growth Curve Lines.....	50
23. Test 1 Initial Max-Min Fatigue loading showing small overloads.....	51
24. Representative Initial Max-Min Fatigue Loads Showing Larger Overloads.	51
25. Test 6 Tapered Initial Max-Min Fatigue Loading.....	52
26. Crack Growth Rate vs. Number of Cycles.....	53
27. Crack Growth Rate vs. Crack Length.....	54
28. Retardation as a Result of Overloads (2024-T3 Al-alloy).....	55
29. Residual Compressive Stresses at Crack Tip as a Result of Overload.....	56
30a. Max - Min Strain Versus Crack Length (mm):Strain Gage 1.....	58
30b. Max Strain Versus Crack Length (mm):Strain Gage 1.....	58
30c. Min Strain Versus Crack Length (mm):Strain Gage 1.....	59
31a. Max - Min Strain Versus Crack Length (mm):Strain Gage 2.....	59
31b. Max Strain Versus Crack Length (mm):Strain Gage 2.....	60
31c. Min Strain Versus Crack Length (mm):Strain Gage 2.....	60
32. Max - Min Strain Versus Crack Length (mm):Strain Gage 3.....	61
33. Max - Min Strain Versus Crack Length (mm):Strain Gage 4.....	61
34. Max - Min Strain Versus Crack Length (mm):Strain Gage 5.....	62
35. Max - Min Strain Versus Crack Length (mm):Strain Gage 6.....	62
36. Max - Min Strain Versus Crack Length (mm):Strain Gage 7.....	63
37. Max - Min Strain Versus Crack Length (mm):Strain Gage 8.....	63

Figure	Page
38. Max - Min Strain Versus Crack Length (mm):Strain Gage 9.....	64
39. Max - Min Strain Versus Crack Length (mm):Strain Gage 10.....	64
40. Max - Min Strain Versus Crack Length (mm):Strain Gage 11.....	65
41. Max - Min Strain Versus Crack Length (mm):Strain Gage 12.....	65
42. Max - Min Strain Versus Crack Length (mm):Strain Gage 13.....	66
43. Max - Min Strain Versus Crack Length (mm):Strain Gage 14.....	66
44. Change in Strain Versus Crack Length (mm):Strain Gage 1.....	71
45. Change in Strain Versus Crack Length (mm):Strain Gage 2.....	71
46. Change in Strain Versus Crack Length (mm):Strain Gage 3.....	72
47. Change in Strain Versus Crack Length (mm):Strain Gage 4.....	72
48. Change in Strain Versus Crack Length (mm):Strain Gage 5.....	73
49. Change in Strain Versus Crack Length (mm):Strain Gage 6.....	73
50. Change in Strain Versus Crack Length (mm):Strain Gage 7.....	74
51. Change in Strain Versus Crack Length (mm):Strain Gage 8.....	74
52. Change in Strain Versus Crack Length (mm):Strain Gage 9.....	75
53. Change in Strain Versus Crack Length (mm):Strain Gage 10.....	75
54. Change in Strain Versus Crack Length (mm):Strain Gage 11.....	76
55. Change in Strain Versus Crack Length (mm):Strain Gage 12.....	76
56. Change in Strain Versus Crack Length (mm):Strain Gage 13.....	77
57. Change in Strain Versus Crack Length (mm):Strain Gage 14.....	77
58. Test 2 acoustic Microscopy Image.....	80
59. Test 3 Acoustic Microscopy Image.....	81

Figure	Page
60. Acoustic Microscopy Image of Test 4 Specimen.....	82
61. Photographic Image of Test 5 Specimen.....	83
62. Close Up Photo of Test 5 Specimen.....	83
63. Photo of the Back Side of the Patch of Test 5 Specimen.....	84
64. Acoustic Microscopy Image of Specimen from Test 1.....	85
65. Acoustic Microscopy Image of Specimen from Test 6.....	86
66. Photo Image of Specimen 6 Patch Debond Area.....	86
67. Thermal IR Scan of Test 6 Sample at 63 mm Crack Length.....	88
68. Thermal IR Scan of Test 4 Sample After Failure.....	88
69. Thermal IR Scan of Test 5 Sample at 63 mm Crack Length.....	89

List of Tables

Table	Page
1. US Air Force Aircraft Age Comparison.....	2
2. Patch Materials.....	17
3. Structural Adhesives.....	21
4. Recent Bonded Repair Applications.....	24
5. Aluminum 7075-T6 Mechanical Properties.....	30
6. Boron Epoxy Mechanical Properties.....	31
7. Strain gages used on each test.....	33
8. Testing Summary.....	42
9. Initial Strains in Microstrain ($10^{-6} mm/mm$) at No Loading.....	44
10. Initial Strains in Microstrain ($10^{-6} mm/mm$) at 6.89 MPa Stress.....	44
11. Initial Strains in Microstrain ($10^{-6} mm/mm$) at 103.42 MPa Load Stress.....	45
12. Initial Strains in Microstrain ($10^{-6} mm/mm$) at 206.84 MPa Stress.....	45
13. Fracture Strength with Associated Crack Length.....	78
14. Crack Length Comparison: Real Loads to Theoretical Loads with No Patch.	90

I. Introduction

1.1 Aging Aircraft

Today the average lifespan of aircraft in service is increasing significantly. With the cost of new aircraft always increasing, and the US military being forced to survive with decreasing resources, many aircraft are now staying in service years past their original expected lifespan. These older aircraft are being continually subjected to load stresses in flight as well as the harsh elements, leading to cracking due to corrosion and fatiguing.

In 1967 the average age of the USAF fleet was only 8.45 years. By 2004 the average age had increased to 23.3 years. Some airframes have even longer average lifespans. (Table 1)[1,2,3] When it is seen that the B-52H has an average age of 42.8 years, the KC-135 of 43.1 years, C-130E of 39.5 years, and T-37B of 40.8 years, just to name a few, it is obvious that the USAF is dealing with many aging aircraft. In addition many fighter engines have on-going service life extensions. Approximately two-thirds of the GE F-110 engines in the fleet are past their original design service life, and half of the P&W F-100 engines are past their original design service life[1].

Commercial airlines are also struggling with aging aircraft. They are always fighting to stay financially competitive, while the cost of new jet aircraft are increasing with the cost of the latest technological advancements. The aging affects of commercial airlines was never more apparent than on Aloha Airline flight 243 where part of the fuselage ripped off causing the death of a flight attendant. The cause was linked to stress corrosion cracking due to its high flight hours and environmental effects. [4,5] As a

direct result of this tragedy, the US government established the National Aging Aircraft Research Program under the direction of the Federal Aviation Administration (FAA) and the Airframe Structural Integrity Program under the direction of the National Aeronautics and Space Administration(NASA) [5]

Table 1. US Air Force Aircraft Age Comparison

Aircraft	Year Fielded	Planned Retire Date	Avg. Age (yrs)	Retire Age (yrs)	Original Service Life hrs.	Extended Life hrs.	Desired Life hrs.
A-10	1977	2028	23.3	51.0	6,000	8,000	16,000
B-1B	1986	2016	17.1	30.0	9,681		14,850
B-52H	1962	2040	42.8	78.0	5,000	12,000	32,000
C-5 A	1969	2040	33.0	71.0	30,000		45,000
C-5 B	1986	2040	16.8	54.0	30,000		45,000
C-130	1961	2030	39.5	69.0	30,000		40,000
C-141	1965	2006	37.5	41.0	30,000		
E-3A	1977	2025	24.5	48.0	30,000		45,000
E-8	1997	2014	4.8	17.0	60,000	+20,000	80,000
F-15 A/B	1975	99-05	26.3	30.0	8,000	12,000	
F-15 C/D	1979	2007-2012	21.4	33.0	8,000	12,000	
F-15 E	1989	Unknown	12.5		8,000	12,000	
F-16	1980	2008	19.5	28.0	8,000		
KC-135	1957	2040	43.1	83.0	undefined		
T-1A	1993	2017	9.9	24.0	18,000		
T-37B	1957	2011	40.8	54.0	8,000	25,000	
T-38	1961	2020	36.9	59.0	7,000		
U-2	1956	Unknown	21.2		undefined	20,000	75,000
C-9	1968	2013	31.8	45.0	30,000		65,000
C-12	1974	Unknown	24.4				
C-20	1983	Unknown	15.8		20,000		
C-21A	1984	Unknown	19.7		Unlimited		
C-22B	1984	1999		15.0	60,000		
C-26	1989	Unknown	10.4		35,000		
E-4B	1980	2020	30.3	40.0	60,000		24,000
KC-10A	1982	Unknown	19.7		30,000		
T-3A	1994	2020	9.6	26.0	18,000		
T/CT-43A	1974	2025	30.5	51.0	51,000		35,000

1.2 Repair Options

When aging aircraft begin to show signs of wear and damage, there are several options available. The entire aircraft can be replaced, the damaged part can be replaced, or the damaged part can be repaired. In most cases, replacing the entire aircraft is not an option. With the high prices of aircraft this is generally not an option. If just one part is damaged, part replacement is preferred. With part replacement there is a good new part that will run well into the future. However, sometimes procuring these parts can be difficult. With some of the older aircraft approaching 40 years old and older, some parts are no longer in production. This means that if a new part is needed for an aircraft, it will have to be custom made. This also can be expensive. Replacing an entire aircraft part, depending on the part, is often not a trivial job, and can take a long time to finish the replacement. If fleet-wide, depot-level maintenance needs to be done to replace a given part, it could take a very long time. The only option left is part repair. Repairing a damaged part will be the cheapest and quickest method of returning an aircraft to flight status. Only cosmetic or sealing repairs may be needed to repair minor damage, but often times structural repair is required due to the strength having been reduced below the design limits, or has the potential of being reduced in subsequent services.[6]

There have been two options for part repair: mechanically bolted or riveted repairs, or adhesively bonded composite patches. Mechanically fastened repairs, while being the most well known and established repair method, have several disadvantages. These repairs introduce further local stress concentrations at the additional fastener holes which in turn can result in increased fatigue cracking. Cracks may end up forming from fastener holes due to poor quality hole drilling or riveting, which can be a common

problem under field conditions. Additionally cracks may initiate from hidden corrosion developing under a poorly sealed mechanical repair. Adhesively bonded repairs however provide a method of repair that eliminates stress concentrations [6,7]

Composite patches, while less well known, provide many advantages. The high directional stiffness they have allows for the use of thin patches, allowing reinforcement to be applied only in the desired directions. Their high failure strain and durability under cyclic loading minimizes the danger of patch failure at high elastic strain levels in the parent metal structure. The low density of the composite patch is an important advantage where the balance or mass of the control surface must be maintained. The composite materials' excellent formability allows for low-cost manufacture of patches with complex contours. Composite patches tend to reduce repair time. For example the normal metallic structural repair for a C-141 center wing panel may take up to six weeks. With the boron composite patch, the repair downtime may be only around two weeks. The actual repair itself consists of only a few hours to prepare the surface with eight hours cure time. After the repair is done the inspection intervals can be increased (from 800 to 4000 hours on the C-141 vertical stabilizer), which translates to higher aircraft availability rates. This increased interval is allowed because of reduced potential fatigue sites and reduced stress levels. [8]

There are some drawbacks however in using adhesively bonded composite patches. Drawbacks include the need for a "clean" surface through extensive surface preparation. Heat and pressure over time are required to produce a quality cure. While room temperature adhesives can be used, elevated temperatures of 120°C yield a stronger bond. Composite patch repair is often designed for depot level repair. This is

necessary to provide proper environmental control in the work area due to the toxic nature of composite materials. Because of this technicians must be specifically certified for the process. [8]

1.3 Research

To date a fair amount of research has been done in the area of bonded composite repairs. Testing has been done to see the effects of repairs on thin structures and thick structures, to include studies by Conley, Schubbe, Denny, Mills, and Ryan. [11,13,22] Other studies have looked at the effects on stiffened panels such as that done by Avraam.[5] Other studies have looked at different patch repair materials, and the effects of debonds on the repair to include Fredell and Avraam. [5, 21] The background section will go into further detail on the objectives of the individual studies. To date little has been done in the way of looking at the mechanical properties, gathering strain data, and looking at the residual strength of the repair. This study will look at the relationship between the stress and strain readings and the crack growth throughout the life of the specimen.

A series of fatigue and tensile tests will be performed with six specimens in this study. The specimens used are 914.4 mm long by 152.4 mm wide, by 0.4763 mm thick of unclad 7075-T6 aluminum, cut into a dogbone shape with a 127 mm gage section. Cracks were machined at the center of each specimen. A 6.35 mm diameter hole was cut on the center of each specimen with 1.27 mm EDM notches cut into each side of the hole. Starter Cracks of about 1.27 mm were then grown from the notches. (See figure 1) Each specimen had a 16 ply, 76.2 mm wide long boron/epoxy 5521 patch centered on the hole. The patches were tapered at the ends with a 20:1 ratio of overlap length to patch

thickness. The length of the longest patch ply is 215.9 mm. With a nominal 0.14224 mm ply thickness, the length of the tapered region at each end of the patch is 39.624 mm and the constant thickness patch length is 139.7 mm. The patches are all unidirectional plies, with the fibers oriented along the length of the specimen. The patches were bonded to the aluminum with a nominal 0.0381 mm layer of FM-73 knit carrier adhesive with a nominal weight of 0.085 Newtons per square meter. [9]

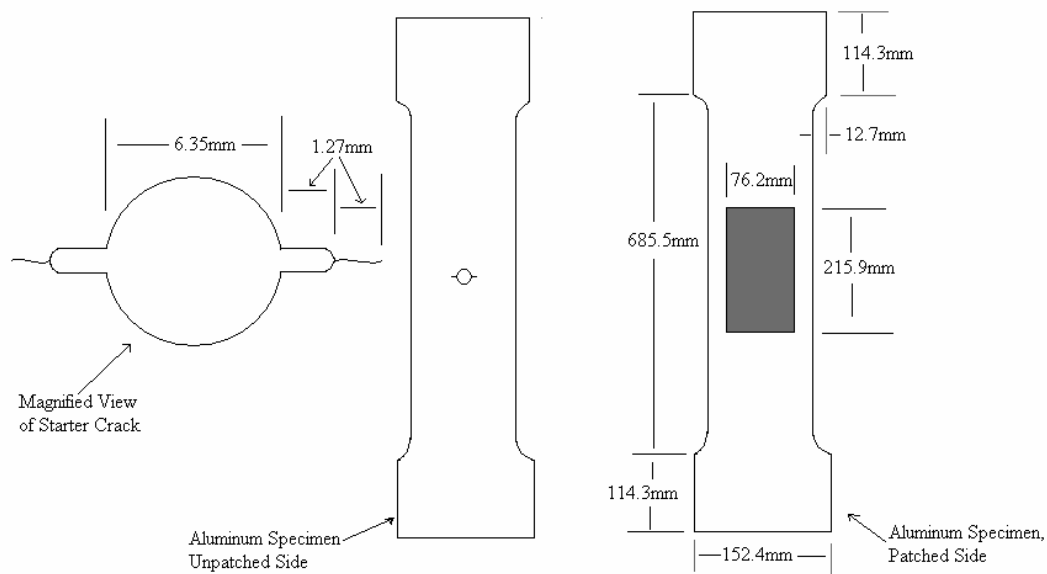


Figure 1. Specimen diagram

This thesis has been separated into five distinct chapters, each summarizing a different area of the study. The first chapter covers the motivation behind this research. The second chapter discusses the background theory and previous efforts in bonded repair technology. Chapter three will cover the experimental setup and testing procedures. The fourth chapter will detail the results of this study. Chapter five will provide a brief summary of the report and where to go in the future.

II. Background

2.1 Elementary Fracture Mechanics

To better understand how aircraft repair works, and the differences between mechanically fastened and adhesively bonded repairs, it helps to have a basic understanding of the theory behind cracks in a metallic structure. This section will cover the basic theory behind Linear Elastic Fracture Mechanics (LEFM).

Consider first a crack in an infinite plate (Figure 2). From the inherent flaws in the material this crack may have grown due to structural loading, environmental conditions or both. Over time the crack will continue to grow due to combinations of further environmental effects, and additional loading.

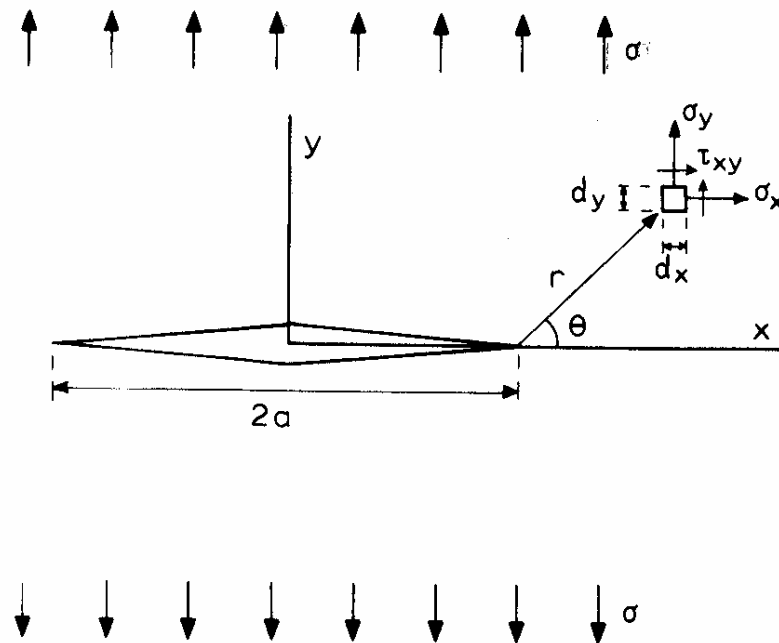


Figure 2. Crack in an infinite plate.[10]

As the crack gets larger over time (Figure 3), the structures residual strength will decrease, decreasing its load capability, and ultimately decrease the time to failure for the given structure.

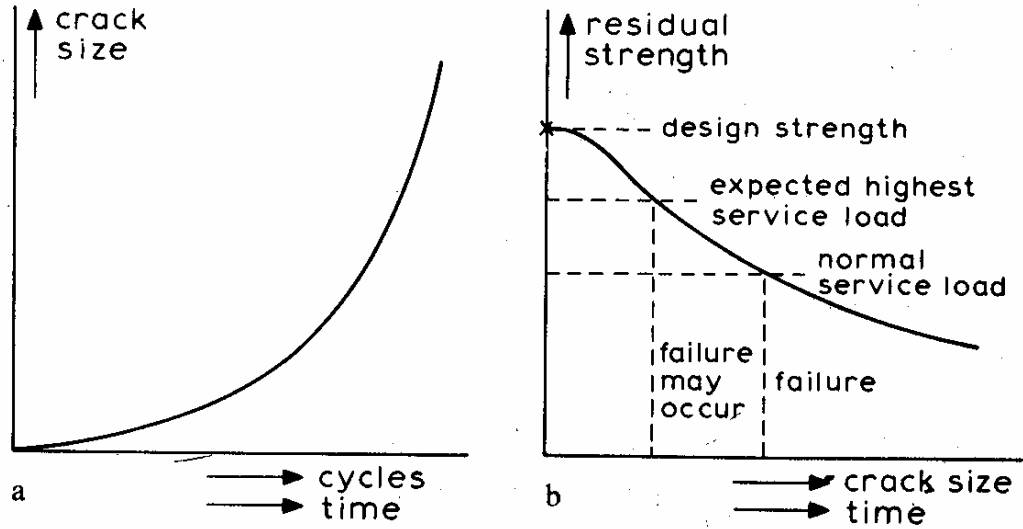


Figure 3 The Engineering Problem
 a. Crack Growth Curve; b. Residual Strength Curve.[10]

Stresses on a crack can occur in any of three different loading modes as shown in Figure 4. Mode I loading is often referred to as the opening mode. In mode I the loading is in-plane and perpendicular to the crack, where the loading is causing the crack to be pulled open. Mode II loading is called the sliding mode. In mode II the loading is in plane and parallel to the crack causing a sliding motion. Mode III is referred to as the tearing mode. Mode III occurs as the result of out-of-plane loading parallel to the crack which causes an associated tearing motion. In a cracked aircraft structure mode I is the primary loading situation. This loading will be focused upon for this discussion. The reader is referred to any fracture mechanics text for further information on mode II and mode III loading.

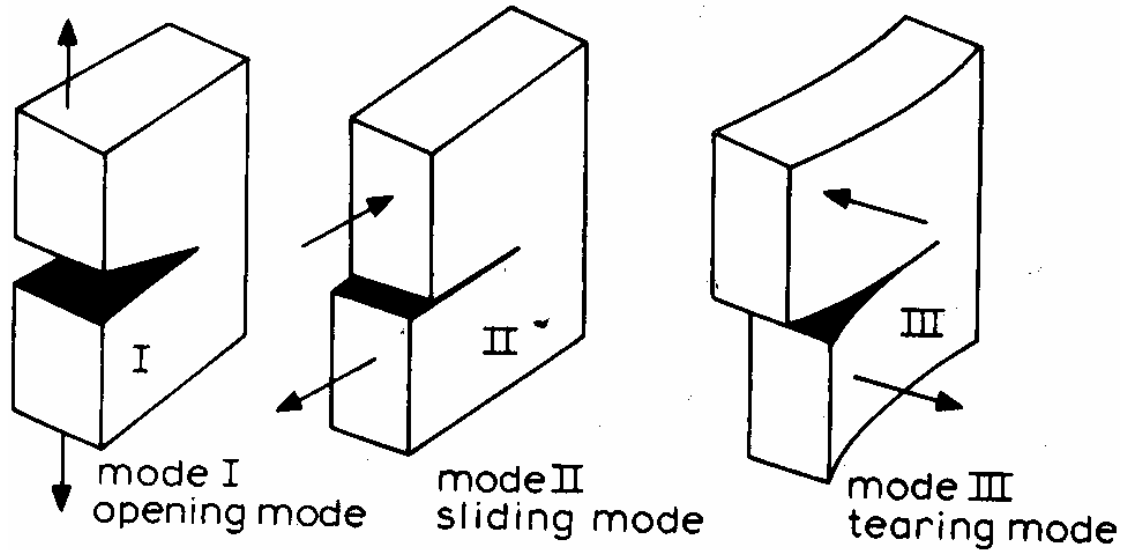


Figure 4 The three modes of loading.[10]

Again the cracked infinite plate in Figure 2 is considered. To understand the stresses at the crack, the stress intensity factor K must first be defined. For the given crack and loading in a mode I situation, the stress intensity factor is given by

$$K_I = \sigma\sqrt{\pi a} \quad (1)$$

Where σ = the applied stress, and a = half the crack length.

In this situation, with the crack in an infinite plate, there are no geometry effects, such as thickness, proximity to an edge, or another crack, that have to be considered.

Near the crack tip the stress field is given by

$$\sigma_x = \frac{K_I}{\sqrt{2\pi r}} \sqrt{\frac{a}{2r}} \cos\left(\frac{\theta}{2}\right) \left[1 - \sin\left(\frac{\theta}{2}\right) \sin\left(\frac{3\theta}{2}\right) \right] \quad (2)$$

$$\sigma_y = \frac{K_I}{\sqrt{2\pi r}} \sqrt{\frac{a}{2r}} \cos\left(\frac{\theta}{2}\right) \left[1 + \sin\left(\frac{\theta}{2}\right) \sin\left(\frac{3\theta}{2}\right) \right] \quad (3)$$

$$\tau_{xy} = \frac{K_I}{\sqrt{2\pi r}} \sqrt{\frac{a}{2r}} \sin\left(\frac{\theta}{2}\right) \cos\left(\frac{\theta}{2}\right) \sin\left(\frac{3\theta}{2}\right) \quad (4)$$

$$\sigma_z = 0 \quad (\text{plane stress}) \quad (5)$$

$$\sigma_z = \nu(\sigma_x + \sigma_y) \quad (\text{plane strain}) \quad (6)$$

The stress intensity factor K_I at first can be difficult to comprehend in seeing that it has units of stress * $\sqrt{\text{length}}$. The stress intensity factor is the value that helps us quantify the stress field at and in front of the crack tip. The crack in the plate leads to larger stress values around the crack (see fig 5).

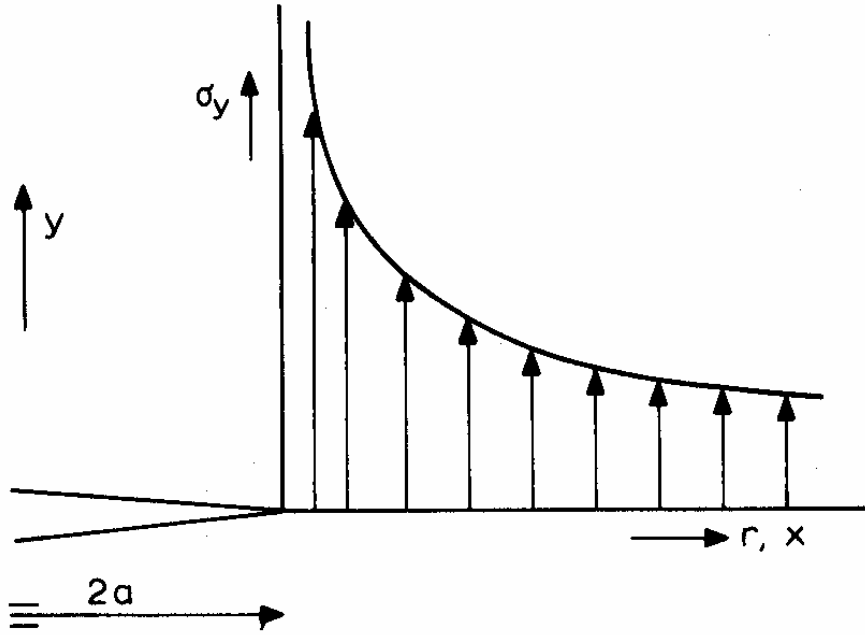


Figure 5. Elastic stress σ_y at the crack tip [10]

However, in reality there is no such thing as an infinitely wide plate, while some plates can be accurately modeled as such, a correction factor α is often needed to adjust for plate width.

$$K_I = \alpha\sigma\sqrt{\pi a} \quad (7)$$

This correction factor will be different for different geometries. These correction factors will be found in any fracture mechanics text. For the center cracked specimen, the stress intensity factor for a finite width plate is given as

$$K_I = \sigma\sqrt{\pi a} \left(\sec \frac{\pi a}{W} \right)^{1/2} \quad (8)$$

Where W = width of the cracked plate.

Now that the stress intensity factor and stress fields are defined, they need to be related to crack growth. One of the simplest and very useful relationships is the Paris Law.

$$\frac{da}{dN} = c\Delta K^m \quad (9)$$

Where da = change in crack length

dN = change in the number of loading cycles

$$\Delta K = K_{\max} - K_{\min}$$

c, m = material constants

This relationship shows us that the larger the stress intensity factor, the larger the crack growth rate. In fracture mechanics and crack patching the primary goal is to reduce the stress system's stress intensity factor so that the crack growth rate will also be reduced. The stresses around the crack are reduced, which reduces the stresses at the

crack tip itself, where these stresses are the primary source of crack growth. This is the goal in crack patching. When a patch is put on the specimen, the stress field in the plate is partially rerouted through the patch, instead of into the crack tip (Figure 6). The stresses that would have gone into opening the crack are now rerouted through the patch. Fewer stresses at the crack tip in turn reduce the crack growth rate, if not stop the crack growth completely.

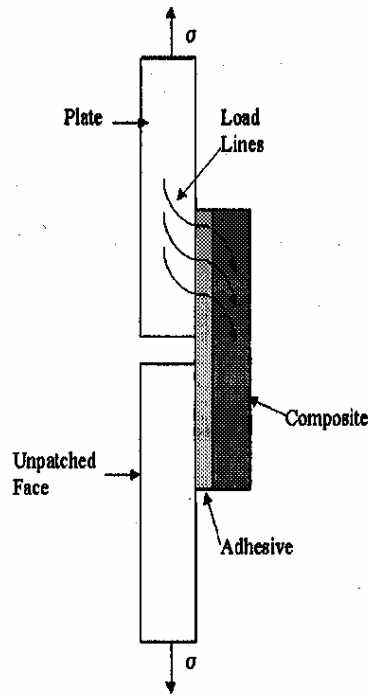


Figure 6. Load Flow into a Repair.[11]

2.2 Composite Repair Design

2.2.1 Patch Design

“The goal of a properly designed bonded repair is to restore the damaged structure’s ultimate load carrying capability. Damage growth should either be arrested or significantly retarded. The repair must be carried out without causing further damage or creating a weak link in the structure. In short, the repair allows the structure to fulfill its original intended function. [11]”

A lot of planning goes into designing an efficient composite repair for a specific structure. However the first place to start is in understanding what loads there are in the region of the planned repair. This study examines a single sided repair in mode I loading, so that is what will be looked at here. The repaired system will be seeing stresses in both the repaired structure and in the repair itself. Loading will be transferred from the structure to the repair through shear stresses in the adhesive.

While the plate is loaded in tension, the patch, in picking up a portion of the loading, creates a neutral axis shift. This, in addition to any bending caused through a difference of coefficients of thermal expansion between the structure and the patch during the repair process, creates normal stresses in the form of out-of-plane bending that acts on the tips of the patch as shown in Figure 7.

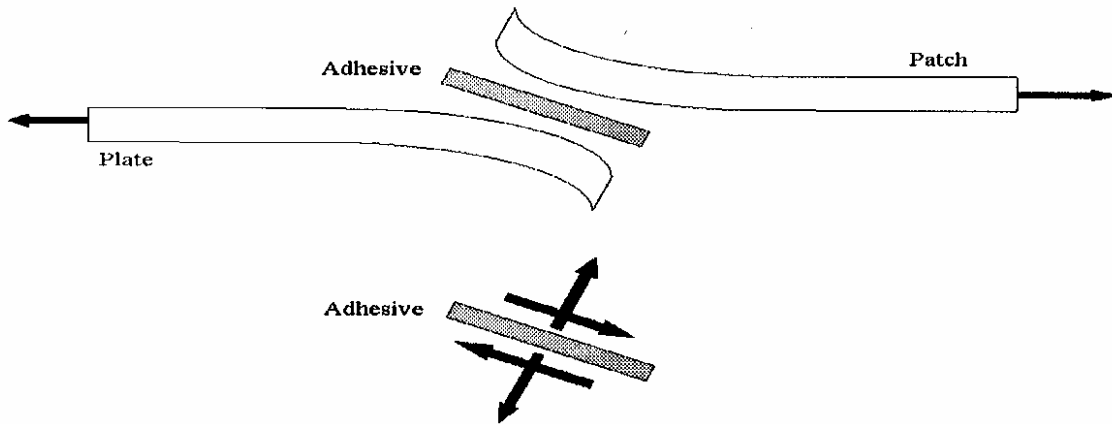


Figure 7. Bending Caused by Neutral Axis Shift in Single Sided Repair [11].

The combination of shear and normal stresses may potentially lead to two common bond line failures known as peel and cleavage as shown in Figure 8.

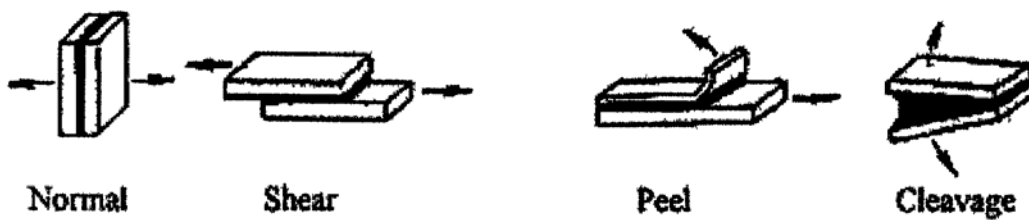


Figure 8 Loading on Adhesive Bonds[5].

Designing an adhesively bonded composite repair is quite technical, there are a few guidelines, or “rules of thumb” that have been established to aid in the successful design of composite repairs. They include [11, 12,13]:

- Choose repair materials that have static load-carrying capabilities greater than or equal to that of the parent material.
- Use a double lap arrangement whenever practical to eliminate the bending problems associated with a neutral axis shift.
- Use overlap distances of roughly 30 times the thickness of the parent structure for double lap repairs and 80 times for single lap repairs.
- Taper the thickness of the repair patch tips to relieve adhesive peel stresses. The taper slope should be approximately 1:10.
- Ensure a smooth fillet is produced in the bonding process to reduce stress concentrations that occur at the edge of the overlap.
- Maintain a stiffness ratio (S) of $1 \leq E_r t_r / E_p t_p \leq 1.5$, where E_r and E_p are the Young's modulus of the repair and panel respectively and t_r and t_p are the thicknesses of the repair and panel.

2.2.2 Patch Material Selection.

Here the factors used in deciding which composite to use in the repair will be examined. The primary requirements here are the strength and stiffness requirements, in addition to the operating environment of the structure being repaired. There are many different patch materials that can be used in the repair process. Just a few of them are laid out in Table 2 [5,14]. Boron/Epoxy was the patch material chosen for this study. Here E designates the Young's Modulus, with the subscripts L and T referring to the

longitudinal and transverse directions. Poissons ration is represented by ν , and α is the Coefficient of thermal expansion.

Table 2. Patch Materials

Material	$E_L (GPa)$	$E_T (GPa)$	Strength (Mpa)	ν	CTE, $\alpha, (10^{-6} / ^\circ C)$
AS4/3501-6 Carbon Epoxy	148	10.5	2137	0.3	-0.8
T300/5208 Carbon Epoxy	132	10.8	1513	0.24	-0.77
Boron/Epoxy	195	25	1520	0.21	4.5
Kevlar/Epoxy	76.8	5.5	1380	0.34	-4
Boron/Al	227	139	1290	0.24	5.94
SCS-6/Ti-15-3	221	145	1517	0.27	6.15
S-2 glass/epoxy	43.5	11.2	1724	0.27	6.84
Glare 2	65.6	50.7	1590	0.17	4.5

The two most important physical properties of the patch that will be looked at are the strength and stiffness (Young's Modulus, E). It is these properties of composite materials that allow the manufacture of thinner and lighter patches than are found in metallic repairs. The thinner and lighter the patch is, the less it will affect the aerodynamic properties of the repaired structure, which is highly desirable. A strong thin patch is desirable in that it will reduce out of plane bending due to the neutral axis shift that occurs, and thus reduces the patch tip peel stresses, giving a higher quality repair. However the patch should be produced to match the strength of the repaired structure reasonably well. A patch that is too stiff will have loads more quickly transfer to it from the cracked panel, possibly damaging the surrounding structure. Naturally the patch needs to maintain a certain level of strength in order to carry the load. To best design a

patch criteria have been put down for the stiffness ratio, S , between the repaired structure and the attached patch, as seen below [5].

$$S = \frac{E_p t_p}{E_s t_s} \quad (10)$$

Where

E_p = Young's modulus of the patch

t_p = Thickness of the patch

E_s = Young's modulus of the structure

t_s = Thickness of the structure

2.2.3 Adhesive Selection.

There are many different types of adhesives that can be chosen to bind a repair to the damaged structure. When selecting the adhesive there are certain properties that must be considered. The adhesive must have a good strength and toughness throughout its expected operating temperature range, it must be resistant to environment effects; it must be able to bond well with the chosen surface preparation agents, and the curing temperature must be considered and the resources available to meet these requirements.

An adhesive with a high shear modulus will transfer its stresses from the cracked component to the patch most efficiently, better reducing the associated stresses at the crack tip, reducing crack growth and leading to a successful repair, increasing the aircraft life. The adhesive should have a good peel strength in order to offset loads caused by out of plane bending. In regards to cure temperature, while a lower temperature cures are easier to perform, those adhesives don't perform as well at the higher temperatures that are often experienced by aircraft. At the same time a higher cure temperature adhesive creates unwanted concerns over residual thermal stresses and mismatches in the coefficient of thermal expansion. These higher temperature cure adhesives are often

more desired when possible, especially for high performance aircraft. In general low cure temperature repairs are only best when doing temporary battle damage repairs, but when permanent repairs are being done, a higher cure temperature adhesive should be used.

There are three main types of adhesives that are used: foam, pasted, and film. Foam adhesives will expand during the cure process and will fill large cracks or holes, and can be used to repair rough or damaged bondlines. Paste adhesives can come in one or two part mixtures. For the case of two part mixtures, each part must be carefully measured out and mixed. The paste is then manually spread using a flat instrument such as a spatula. Paste adhesives are nice in that they can often be stored at room temperature with long shelf lives, and are fairly easy to use. However there is a lot of room for human error in the mixing of pastes, and in producing a smooth bond without air bubbles. Pastes are often most useful for making temporary repairs. For long term repairs a film adhesive is the best to use. Film adhesives provide the best strength and durability properties. As they are supplied in tape form, they are easy to apply and provide a uniform bondline thickness. They do however have higher costs, require refrigerator storage, and need high temperature and pressure during the curing process. This makes film adhesives very difficult to use in making field repairs. Table 3 below provides several examples of each type of adhesive and some of their properties. [7]. Note that the adhesive used in this study is FM-73.

Table 3 Structural Adhesives.

Adhesive	Adhesive Type	Cure Time/Temp	Storage	Supplier
FM-39	Foam	1hr / 121°C	6 mo. @ -18°C	American Cyanamid
AF-3002	Foam	1hr / 177°C	6 mo. @ -18°C or 7 days @ 24°C	3M
EA-9309	Paste	3 days / Room Temp. or 1 hour / 66°C	12 mo. @ Room Temp.	Dexter Corp/ Hysol
EA-1386	Paste	60 min / 177°C	4.5°C or Below	3M
FM-73	Film	1hr / 121°C	6 mo. @ -18°C	American Cyanamid
AF-163-2	Film	1hr / 121°C	6 mo. @ -18°C	3M
Metlbond 328	Film	90 min / 177°C or 15 min / 365°C	6 mo. @ -18°C	Narmco

2.2.4 Surface Preparation.

“Surface Preparation of the metal adherend is the keystone upon which the structural adhesive bond is formed.” [15] If the surface where the patch is to be adhered is not prepared appropriately before hand there is a high risk for repair degradation and failure. Almost all bonded repairs end up failing as a result of environmental attacks on the adhesive structure interface. A proper surface preparation will prevent many bonding failures, and ensure the success of the repair. There a few different surface preparation techniques that can be used.

The method of phosphoric acid anodizing (PAA) was developed by Boeing and is known to provide a good, durable, long-lasting bond, that will well withstand environmental attacks. This process requires degreasing the surface of the damaged area and submerging it in a series of acid etch baths. Since this requires the damaged part to be removed from the parent structure, this is not always feasible. A variation of this

method was developed by the USAF known as phosphoric acid containment system (PACS). This allows the repair to be performed on the aircraft itself but also produces additional hazards. If extreme caution is not used, the chemical acids involved will get into other parts of the aircraft that may not be easily reached and end up causing damage.

Another surface preparation method is known as grit blast/silane (GBS). This is the method that was used on the specimens in this study. GBS involves degreasing, deoxidizing, grit blasting, and finally applying a silane solution (SiH_4) to promote adhesion. This process will provide both a physical and chemical bond between the adhesive and metal. This process is widely used because it is able to be performed on the aircraft itself, providing a similar bond to PAA. GBS has the advantage of not using any acids on the aircraft, and as such is the most environmentally friendly. However there are disadvantages involved in containing the grit on the aircraft. This process runs the risk of aluminum oxide grit getting into and damaging aircraft components. To combat this problem the USAF has designed a grit containment box, preventing the grit from getting into other parts of the aircraft.

2.3 History of composite repair, and past research.

2.3.1 Origin of Composite Repair

Adhesively bonded repair technology was first researched by the USAF in the early 1970's on the F-111. A boron doubler modification was installed onto the F-111 left wing and placed into a test jig at Convair Aerospace Division Structures Test Facility, San Diego California. The boron doubler survived for 100 test blocks which correlates to 40,000 test hours, and an additional 10,000 cycles at 75% of its design limit. [5,16]

US bonded repair technology however did not take off. In the early 1970's and 1980's the US department of defense had large budgets with a fairly young fleet. These two factors produced little concern for aging aircraft issues in the United States. The US thus did not pursue much further research into bonded repair, resulting in a lack of faith in the ability of the technology to perform over a long period of time in harsh environments. Australia however was in a very different situation at this time. They had a much smaller defense budget, and were working with more aged aircraft. They heavily pursued bonded repair studies in order to keep their aircraft flying longer, and the technology first began to take off, under the Australians. Australia's first efforts in bonded repairs were on their F-111's purchased from the US. These F-111's were fitted with bonded boron doublers prior to delivery, which helped Australia's Aeronautical Research Laboratory (ARL) (now the Aeronautical and Maritime Research Laboratory (AMRL)) get their adhesively bonded repair technology off the ground.[5]

The ARL became very proficient in bonded repair technology. They made most of the initial advancements in bonded repair technology, to include inventing the first successful grit blast/silane surface preparation technique used to create higher quality bonds between the patch and the material surface. Early on Australia was by far the most aggressive in doing actual adhesively bonded repairs on aircraft, and with much success. [5]

One of the US's first efforts into adhesive bonding technology was the Primary Adhesively Bonded Structure Technology (PABST) program of 1978. The purpose of this study was to investigate the effects of different surface treatments for adhesives on the durability of bonded joints. This program proved that adhesive bonded structures are

far more tolerant of quite large flaws than had been previously believed. The PABST fuselage was produced on development tooling and not production tooling which could have been refined after the manufacturing had begun. Every panel was accepted for the structure with most of the flaws left unrepaired in order to be monitored during the testing. Because the PABST was not a flawless structure, the success of the program was of an even greater significance than had a perfect laboratory test coupon been used. Because the bond flaws did not grow, there was great confidence in the reliability of adhesively bonded structures. The program also monitored three disbonds located in the fuselage splice joints to determine their impact on the structure. These disbonds showed no decrease in joint strength and no increase in adhesive shear stress or strain. It was thus concluded that most disbonds can go unrepaired except for those at the edges of the bonded joint, and in this case, a sealant not an adhesive, should be used to protect the bondline from the environment. In fact, in many cases, the repair of the patch served only to reduce the service life by providing additional paths for moisture to ingress. Had such flaws been unrepaired, the structures would have been just as strong and lasted much longer. [11, 17]

In the 1990's the United States found themselves in a very different position than in previous decades. With defense spending decreasing, and attention gained from recent aircraft failures like Aloha Airlines' Flight 243, concern for their aging aircraft began to rise. Here the US began to follow the lead of the Australians, and began to more aggressively pursue bonded repair research and technology.

2.3.2 Examples of Recent Composite Repair.

Slowly composite patch repair is becoming increasingly used as more people become aware of its advantages. Table 4 shows just a few examples of where composite patch repair has been used in real world situations. Here a few of those applications will be looked at a little more closely. These and other examples are expanded upon more fully in “Advances in the Bonded Composite Repair of Metallic Aircraft Structure Volume 2” by Baker, Rose, and Jones. [18]

Table 4. Recent Bonded Repair Applications.

Aircraft	User	Application
F-111	RAAF	Lower Wing Skin Repair Substantiation
L-1011	FAA	Composite Doubler Installation
F-111	RAAF	Wing Pivot Fitting Reinforcement
F/A-18	RAAF	Y470.5 Centre Fuselage Bulkhead
C-5A	USAF	Fuselage Crown Cracking
F-16	USAF	Fuel Vent-hole Repairs
F/A-18	Multiple	Inboard Aileron Hinge
Concord	UK	Wing leading edge panels, elevons, body fairing panels
747	UK	engine cowling, pylon fairing panels
CF-116	Canada	Upper Wing Skin Fatigue Enhancement Boron Doubler
CH-47	USAF	Cargo Hook Beam
T-38	USAF	Lower Wing Skin
C-141	USAF	Inner Wing Lower Service Weep Holes

2.3.2.1 F-111 Lower Wing Skin Repair Substantiation [19]

During a routine visual inspection of a Royal Australian Air Force (RAAF) F-111 aircraft, a crack was discovered on the lower wing skin in the area of previously noticed fuel seepage that led to the initial inspection. A more detailed inspection revealed a

through thickness crack 48 mm long, tip to tip. Using a handbook value for fracture toughness of $46 \text{ MPa}\sqrt{m}$, the residual strength for this portion of the aircraft was determined to be 168MPa, which is considerably lower than the Design Ultimate Stress of 358 MPa specified for this portion of the wing. A mechanically fastened metallic repair was initially considered but discarded due to undesirable aerodynamic implications, and the uninspectability of the underlying structure that would result. The final decision, and only viable alternative next to scrapping the wing, was to use a bonded repair.

Before the aircraft could fly again, approval and final certification of the repair was required, using a comprehensive validation program. This was necessary for safety concerns, due to the inherent weakness of the aircraft wing prior to the repair. The crack had reduced the residual strength well below the specified design limit stress of 238 MPa. The validation for this procedure would provide confidence in its use for other, less critical applications.

Ultimately the aircraft was certified and flew for two more years, accumulation 665.9 flight hours. The repair was regularly monitored, inspections occurring at least every 100 hours, for any evidence of disbonds and crack growth. Some debonds were detected at the corners of the repair, but were believed to be present since the repair was originally applied, as they had not developed any further. These disbonds are believed to be due to poor application methods at the time.

The cracked wing has now been retired, and has since been used for full scale fatigue testing. The wing has been subjected to 8074.4 hours of testing under a number

of different tests by the RAAF, with no evidence of crack growth or degradation of the repair. The area around where the initial disbonds were discovered appears to be still intact in these small regions. While still under investigation, it appears to be due to the adhesive consolidation. As a result of the success of this first repair, three additional wings have been repaired using this process and have been returned to fully operational status.

2.3.2.2 F-16 Fuel Vent-Hole Repairs [20]

Several F-16 aircraft developed cracks between 2500 and 3500 flight hours, near the fuel vent hole in the lower left wing skin. These cracks were noticed in the first 144 aircraft prior to a design modification.

A traditional metal repair was initially considered. This method had several disadvantages to include the possibility of foreign object damage, the possibility of damage to nearby vent tubing, the potential for fuel leaks to appear, likely depot level maintenance being required, excessive costs and aircraft down time.

A bonded boron/epoxy repair was evaluated and found to have several advantages. It is lighter with lower external moldline profile, more efficient load transfer capability, no additional fasteners required to prevent new cracks and fuel leaks. The patch is easier to apply in less time, and crack detection is more easily done using eddy-current or ultrasonic NDI. The patch could be applied in the field with a minimal impact on aircraft readiness at a much lower cost than its mechanically fastened alternative.

The F-16 fuel vent hole bonded repairs have been considered highly successful. No crack growth or disbonds have been detected since the patches were originally applied in 1993.

2.3.3 Research Studies.

A variety of research studies have been done in the area of adhesive bonded repair. Fredell conducted tests using Boron/Epoxy and Glare (aluminum/fiberglass laminate) to investigate the effects of the coefficient of thermal expansion (CTE) mismatch on the life of bonded repairs. His studies showed several advantages of Glare for fuselage skin repairs due to an improved thermal expansion compatibility between the aluminum and Glare. He showed that a closer match in the CTE would prolong the life of the repair, and that large mismatches of the CTE could cause the crack to open, reducing the life of the repair. [11,21]

Denny did a series of experiments to investigate the effects of disbonds on the fatigue response of cracked thin aluminum panels ($t = 1$ mm) repaired with bonded composite patches. The effects of disbond location and size were compared to a completely bonded patch and a cracked panel without a patch. It was found that a disbond around the crack resulted in greater crack growth rate and shorter life as compared to a disbond away from the crack and a completely bonded patch. It was also found that increasing the peak stress level resulted in an increased adhesive shear strain, causing greater levels of cyclic disbonding about the crack faces and reduced the specimen life. A higher stress ratio, R , reduced the repaired stress intensity factor range

and increased patch efficiency; however, cyclic debonding was similar for the same peak stress level, because the adhesive shear strain is a function of the peak stress level. [22]

Mills and Ryan carried on the work started by Denny by considering repairs to thicker structures of 1 mm to 3.15 mm. Their results also showed a decrease in life with an increased debond size, still finding significant increases in life over the unrepaired case, as well as finding little to no growth of the artificially induced disbond. [5,11]

Ratwani approached the problem from an entirely analytical method. He used an empirically weighted analytical method which used experimental results from both thick and thin plates to formulate his weighting factor. A semi-analytical method was used that involved through-the-thickness stress-distribution and strip mode of the plate to determine different back face stress intensity factors for plates of different thicknesses with single sided repairs. While his results were comparable with that for thin plates, they lost accuracy as the plate thickness increased. [5,11]

Schubbe investigated the effects of the repair geometry and stiffness ratios on single sided repairs of thick plates (3.15mm to 6.35mm). His research showed that for thicker plates, a stiffness ratio of 1, as opposed to the more commonly used 1.4 in thin cases, provided the largest improvement in life. This was due to reduced thermal stresses and bending, which proved to have a noticeable impact on the life of the repair. Schubbe also developed a finite element model known as the 3-layer technique and used it along with empirical data to formulate a weighting factor for predicting ΔK_r and as a result the life of the repair. [5,11,13]

Conley studied the effects of thickness on composite patch repairs. He made several observations in his research. He found that at a given stress level, increased panel

thickness causes increased crack growth rate and decreased life span. He also showed that longer patches on thin plates reduce initial thermal curvature which increases the fatigue life. On the other hand, longer patches on thick panels increase curvatures and thus increase bending stresses when the panel is loaded, increasing crack growth rates, and reducing fatigue life. He found that patch width had only a small effect on crack growth rate, and similar rates were found regardless of width. Thus the patch width should be governed primarily by the maximum allowable crack size. He also found that disbond growth is dependent on crack size rather than on patch configuration, but that asymmetric repairs will cause significant plate bending resulting in non-uniform crack front progression in thick specimens. [11]

Avraam studied the fatigue response of thin stiffened aluminum cracked panels repaired with bonded composite patches. In studying disbond effects he found that disbonds were most detrimental to the fatigue life of a repaired panel when they were closer to the crack. Also that crack propagation rate was not significantly affected by the disbond until it was in the crack wake, supporting Bakers previous observations that disbonds in front of the crack tip have little effect on fatigue crack propagation rates. He found that, while debonds greatly reduced the repair life, the life was still significantly greater than had there been no repair. [5]

III. Experimental Setup and Procedure

This Chapter will detail the test equipment that was used in the experiments, along with the procedures used.

3.1 Materials and Specimen Description

For this study, six cracked aluminum panels with a centered composite patch, underwent a series of tests. The specimens used are 914.4 mm long by 152.4 mm wide by 0.4763 mm thick of unclad 7075-T6 aluminum sheet (see Table 5 for properties), cut into a dogbone shape with a 127 mm gauge section. The L grain direction is parallel to the long dimension of the specimen. [9,23]

Table 5. Aluminum 7075-T6 Mechanical Properties

Mechanical Properties	Metric	English	Comments
Tensile Strength, Ultimate	570 MPa	82700 psi	
Tensile Strength, Yield	505 MPa	73200 psi	
Elongation at Break	11 %	11 %	In 5 cm; Sample 1.6 mm
Modulus of Elasticity	72 GPa	10400 ksi	
Poisson's Ratio	0.33	0.33	
Fatigue Strength	160 MPa	23200 psi	500,000,000 Cycles
Fracture Toughness	20 MPa-m ^{1/2}	18.2 ksi-in ^{1/2}	K(IC) in S-L direction.
Fracture Toughness	25 MPa-m ^{1/2}	22.8 ksi-in ^{1/2}	K(IC) for T-L orientation
Fracture Toughness	29 MPa-m ^{1/2}	26.4 ksi-in ^{1/2}	K(IC) in L-T direction
Machinability	70 %	70 %	0-100 Scale of
Shear Modulus	26.9 GPa	3900 ksi	
Shear Strength	330 MPa	47900 psi	

Cracks were machined into the center of each specimen. A 6.35 mm diameter hole was cut into the center of each specimen with 1.27 mm EDM notches cut into each side of the hole. Starter cracks of about 1.27 mm were then grown. Refer back to Figure 1 for the specimen diagram. [9]

Each specimen had a 16 ply, 76.2 mm wide long boron/epoxy 5521 (see table 6) patch centered on the hole. The patches were tapered at the ends with a 20:1 ratio of overlap length to patch thickness. The length of the longest patch ply is 215.9 mm. With a nominal 0.14224 mm ply thickness, the length of the tapered region at each end of the patch is 39.624 mm and the constant thickness patch length is 139.7mm. The patches are all unidirectional plies, with the fibers oriented along the length of the specimen. The patches were bonded to the aluminum with a nominal 0.0381 mm layer of FM-73 knit carrier adhesive with a nominal weight of 0.085 Newtons per square meter. [9]

Table 6. 5521 Boron Epoxy Mechanical Properties

Mechanical Properties	Metric	English
Tensile Strength, Ultimate	1520 MPa	220000 psi
Elongation at Yield	0.8 %	0.8 %
Modulus of Elasticity	195 GPa	28300 ksi
Flexural Modulus	190 GPa	27600 ksi
Flexural Yield Strength	1790 MPa	260000 psi
Compressive Yield Strength	2930 MPa	425000 psi
Compressive Modulus	210 GPa	30500 ksi
Poisson's Ratio	0.21	0.21
Shear Modulus	6.3 GPa	914 ksi
Shear Strength	97 MPa	14100 psi

All specimens were fabricated at Boeing with the following fabrication procedure.

1. The boron plies are laid up in inverse pyramid – smallest ply first. The layup is debulked after every 5 plies.
2. Typical patches for an actual repair have a layer of FM73 over the top boron ply and then a layer of standard 191 fiberglass prepreg (121.1 °C cure). This provides a sacrificial covering and seal against the environment.
3. The patches are precured. The patches are vacuum bagged and autoclave cured at 345-414 KPa for 90 minutes at 121.1 °C degrees. Cure is single ramp with a heat up rate of 3 to 5 degrees per minute, cool down is 10 degrees per minute (still with full pressure) to 37.8 °C and then the pressure is dumped and the heat turned off for free fall.
4. The metal surfaces were Grit Blast/Silane treated for bonding, including a spray with CIAP primer (BR-127)
5. The patches are also wrapped (both sides, like a band-aid) in a nontreated resin rich peel ply which peeled off of the bond surface immediately prior to bonding.
6. The patches were secondarily bonded to the metal with the film adhesive (1 ply).

Some bowing of the specimens during and after the bonding cure occurs due to the thermal expansion coefficient mismatch between the patch and the aluminum plate, and the presence of the patch on only one side of the plate. [9]

3.2 Test Equipment

The following is a list of the test equipment used in this study:

- Mechanical Load system
- Strain Gages with strain measurements system
- Crack Measurement System
- Thermal Imaging System

The mechanical loading system consisted of the following:

- 100 kip MTS 810 Servohydraulic Testing Machine
- MTS Testar IIs Controller
- Compaq Personal Computer with Testar IIs software

Each test specimen was laid out with twelve 350 ohm strain gages. The strain gages were either 3.175 mm gages, or 1.5875 mm gages depending on their location. Fourteen strain gage positions were used throughout testing. The locations of certain strain gages changed to try to acquire better data in later tests. Refer to table 7 for which strain gage positions were used on which tests, and Figures 9 and 10 for the positions of each of the gage positions on the front and back side of the specimen.

Table 7 Strain gages used on each test

Test No.	gages 1-	gage 11	gage 12	gage 13	gage 14
1	Yes	Yes	Yes		
2	Yes		Yes	Yes	
3	Yes		Yes	Yes	
4	Yes		Yes	Yes	
5	Yes			Yes	Yes
6	Yes			Yes	Yes

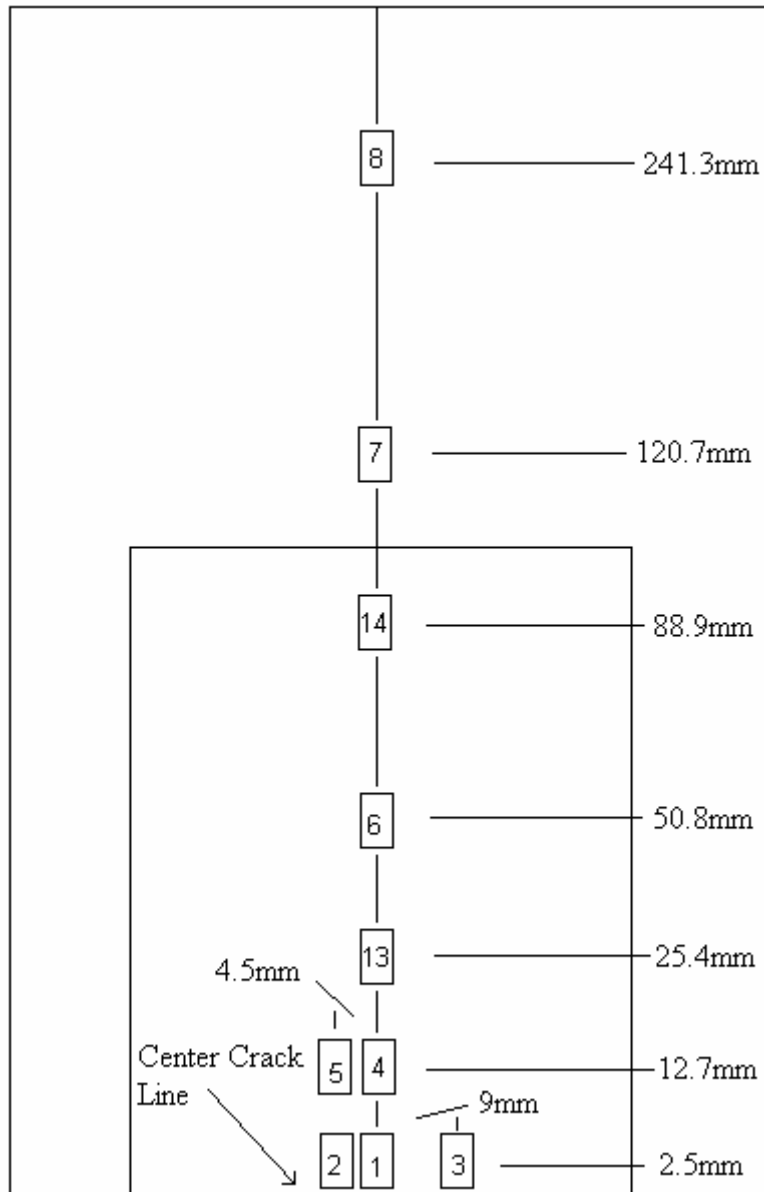


Figure 9. Strain Gage Diagram, Patched Side.

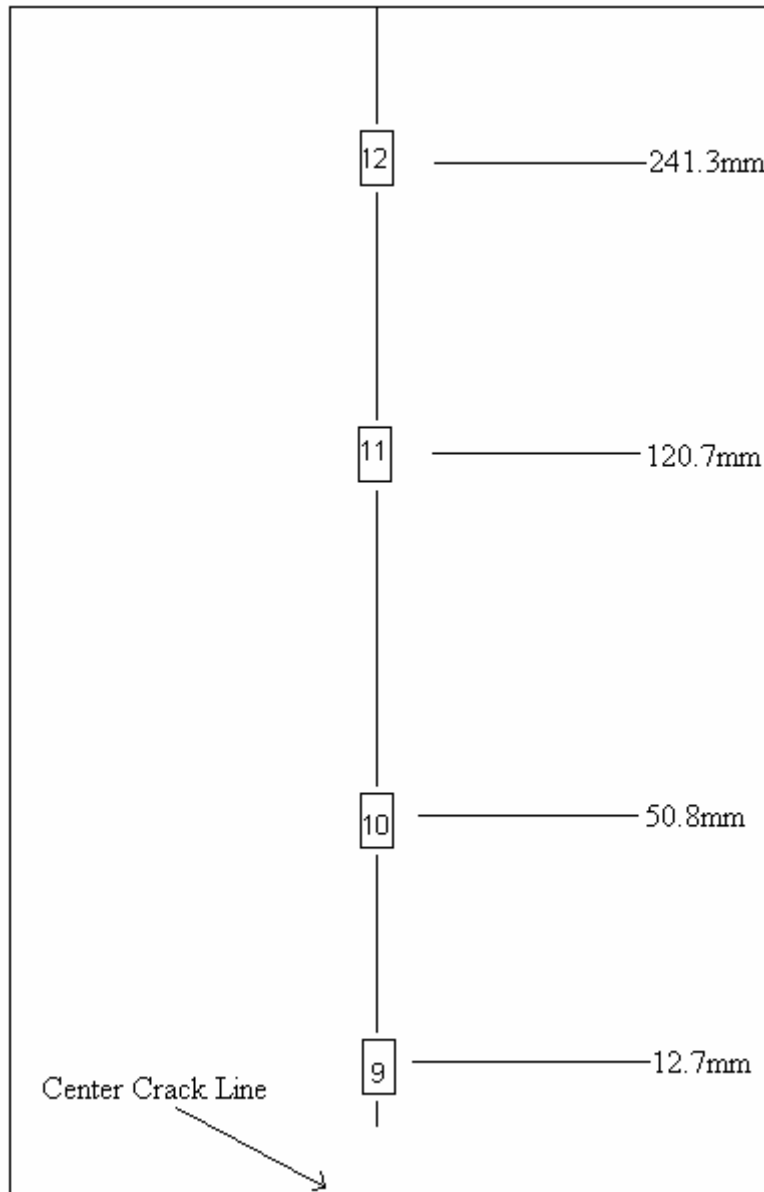


Figure 10. Strain Gage Diagram, Unpatched Side.

To measure the crack length a Gaertner travelling microscope with a digital readout system was used to optically measure the crack length periodically during the test (see Figures 11 and 12)

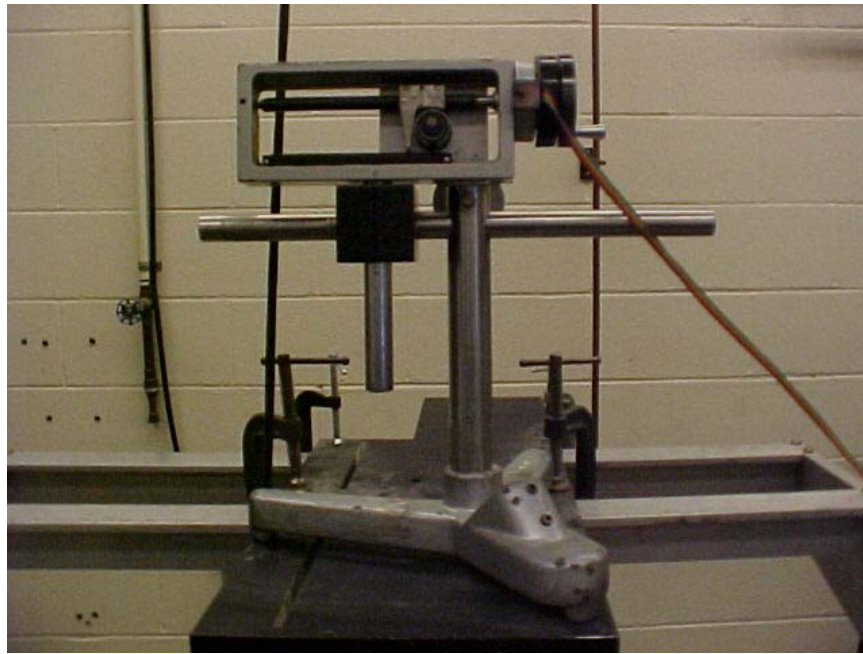


Figure 11. Gaertner Traveling Microscope



Figure 12. Gaertner Microscope Digital Readout

IR pictures were taken of the specimens using a FLIR IR camera, and analyzed with the associated software (see Figure13). A Master-Mite heat gun was used during the IR readings in order to quickly heat up the specimen, in order to best get the different IR readings as the areas of the disbond region would potentially heat up at a different rate than the rest of the sample (see Figure 14).



Figure 13. FLIR IR Camera



Figure 14. Master-Mite Heat Gun

Additional imaging was done on the finished specimens at the Air Force Research Labs, materials directorate using scanning acoustic microscopy. These scans give us a very detailed picture of the final size of the debond behind the patch.

3.3 Test Procedure

Each specimen was first laid out with 12 strain gages. The majority of the strain gages were put on the patched side of the specimen, and nearest to the center line crack (refer back to Figures 9 and 10 and table 7). Here is where the most interesting data will occur. To fit in the hydraulic machine specifically designed grips had to be attached (see Figure 15). Each specimen had to first have the five 12.7 mm diameter holes machined into the grip section, to accommodate the grips, so that it could be loaded into the machine.



Figure 15. Specimen Grips

Before the specimen was fully loaded into the machine all of the strain gages were zeroed out to get the zero stress strain conditions. After the specimen was gripped the strain readings were taken at stresses of 0 kip, 7.35 MPa, 110 MPa, and 221 MPa. Initial strains were recorded due to the initial curvature of the specimen.

After the specimen had been loaded into the hydraulic machine with all strain gages applied, and wired up to the conditioners, a series of tests was conducted. Fatigue and tensile tests were performed. Two of the tests were performed under pure fatigue conditions, one test was a pure tensile test, with the other three tests having a combination of fatigue and tensile conditions. These combination tests had the crack growing under fatigue conditions to a total crack length $2a$ equaling 25.4 mm, 55.88 mm, and 63.5 mm, before it was subjected to tensile loading.

During the fatigue portions of the testing, the specimen was subject to stresses from 7.35 MPa to 194 MPa at a frequency of 4 Hz. Periodically, after every few hundred cycles, the testing was paused to take optical measurements of the total crack length. A couple times, the tests would be paused for a longer time in order to take IR pictures of the sample.

During the tensile portions of the testing, the specimen would be put under load control and be slowly raised and lowered to successively higher loads in 34.47 MPa increments until the specimen failed. These tests had to be done after the testing was concluded to prevent damaging the specimen and tainting further results. This process is described below.

3.4 Scanning Acoustic Microscopy

When each test was finished, if some of the patch was still adhered, it was sent over to AFRL to be scanned to get the best pictures of the debond area behind the patch. Images of these specimens were taken using scanning acoustic microscopy. The specimen is submersed in a water tank, patch side down, so a submersed ultrasonic transducer can be scanned over the aluminum surface. The transducer height above the part is optimized to give the best signal from the back side (the aluminum surface of the side with the patch). This way the transducer is also optimized for the aluminum-patch interface. The system is used in a pulse-echo configuration in that a pulse is sent in to the part and the echo received back is from any surfaces and interfaces. Gates are set up in software on the received waveform (echo) to measure the amplitude and time of flight at different points of interest in the waveform. The points of interest are chosen to be the

places in the received waveform that appear to change the most when the transducer is moved across the area of the part that is to be imaged. After all the optimization steps, the ultrasonic transducer is then scanned over the area of the part to be scanned for a quick low resolution initial scan to make sure all the parameters are correct. Any adjustments are then made and a final higher resolution scan is performed. The spot size is approximately $500\mu\text{m}$ for the frequency used, 5 MHz. Refer to Figures 16 and 17 for rough diagrams of the procedure. [25]

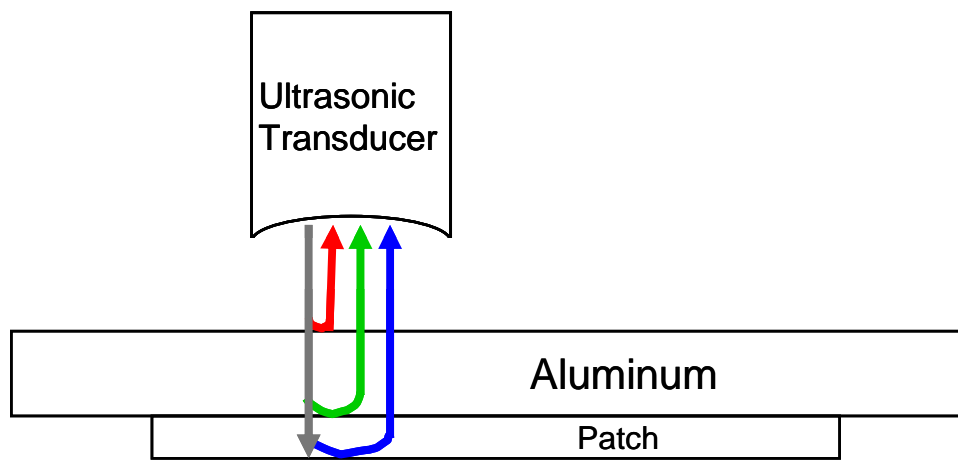


Figure: 16 Scanning Acoustic Microscopy System [25]

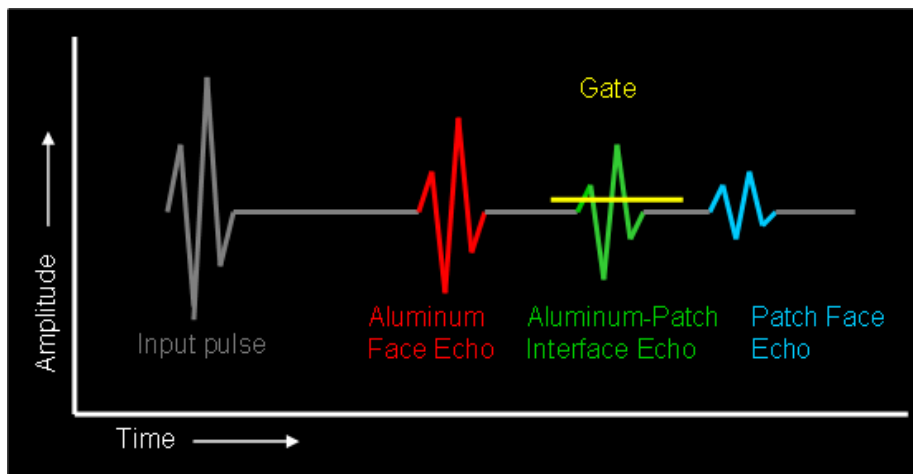


Figure: 17. Oscilloscope Screen [25]

IV. Test Results and Discussion

This Chapter will present the results of the experimental tests that were performed. A total of six tests were performed to include fatigue only tests, tensile only tests, and a combination of fatigue and tensile testing.

In test one the crack was grown to the width of the patch (76.2 mm), and stopped. Test two was a tensile only test, pulling the specimen in load control mode until the specimen broke. In test three the crack was fatigued to 25.4 mm and then subjected to tensile loading to break. In test four the crack was grown to 55.88 mm and pulled in tensile loading. In test five the crack was grown to 63.5 mm before it was subjected to tensile loading until it broke. In test six the specimen was fatigued until it failed at a crack length of 91.4 mm which is 15.2 mm longer than the 76.2 mm patch width. Table 8 briefly summarizes the tests, and their results.

Table 8 Testing Summary.

Test #	Test type	Details	Results
1	Fatigue	Fatigue 7.35 MPa to 194 MPa, to length of patch	Survived to 80 mm crack length
2	Tensile	Tensile to failure at 603 MPa	Failed at Grip
3	Fatigue / Tensile	Fatigue to 25.4 mm, Tensile to failure at 603 MPa	Failed at Grip
4	Fatigue / Tensile	Fatigue to 55.9 mm, Tensile to failure at 559 MPa	Clean break on center line
5	Fatigue / Tensile	Fatigue to 63.5 mm, Tensile to failure at 474 MPa	Break at center, patch shattered
6	Fatigue	Fatigue to Failure at 91.4 mm. 15.2 mm beyond patch width.	Patch delaminate from lower half

4.1 Pre-Test Curvature

Each specimen had an initial curvature to it after the patch was bonded. This is due to the differences in the coefficients of thermal expansion between the aluminum specimen and the composite patch during the patches application process. This initial curvature will lead to additional internal stresses within the specimen. The specimen's curvature has been plotted out in Figure 18. Here the patch is in place on the top of the curve in the out of plane direction. The x-axis zero line is in the center of the specimen, along the crack line. The y-axis dimensions are the out of plane displacement. A best-fit sixth degree polynomial was determined to be:

$$y(x) = -1 \cdot 10^{-7} x^6 + 2 \cdot 10^{-7} x^5 + 3 \cdot 10^{-5} x^4 - 4 \cdot 10^{-5} x^3 - 0.0041x^2 + 0.0017x + 0.442 \quad (11)$$

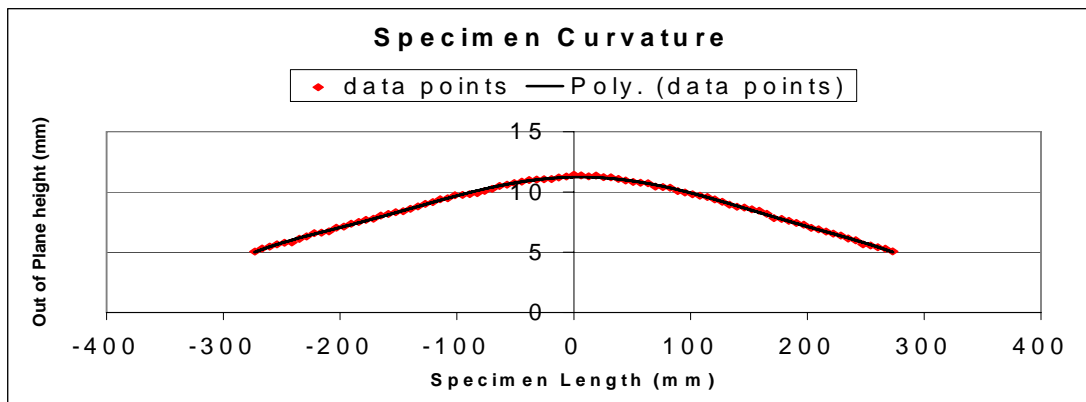


Figure 18 Specimen Curvature Data Points and Polynomial Fit Line

Before each specimen was loaded into the hydraulic machine the strain gages were zeroed out. After the specimen was loaded into the machine strain readings were taken at 0 MPa, 7.35 MPa, 110 MPa, and 221 MPa. Those initial strains can be seen in Table 9 through 12. Refer back to Figures 9 and 10 for where the locations of these strain gages on the specimen. Figures 19 and 20 show the average stress strain curves for each individual strain gage.

Table 9. Initial Strains in Microstrain ($10^{-6} mm/mm$) at No Loading

Gage #	Test 1	Test 2	Test 3	Test 4	Test 5	Test 6	Average
1	-110	-110	-117	-107	-92	-114	-108
2	-110	-86	-120	-104	-85	-107	-102
3	-110	-115	-109	-117	-115	-127	-116
4	-110	-92	-114	-102	-92	-105	-103
5	-100	-99	-119	-107	-94	-112	-105
6	-100	-87	-95	-94	-90	-105	-95
7	-410	-295	-429	-295	-360	-364	-359
8	-360	-260	-451	-209	-360	-324	-327
9	120	92	147	144	115	142	127
10	140	117	169	134	119	157	139
11	330						330
12	330	204	428	204			292
13		-94	-117	-114	-95	-110	-106
14					-127	-134	-131

Table 10. Initial Strains in Microstrain ($10^{-6} mm/mm$) at 7.35 MPa Stress

Gage #	Test 1	Test 2	Test 3	Test 4	Test 5	Test 6	Average
1	-208	-205	-206	-206	-216	-224	-211
2	-204	-186	-214	-199	-196	-205	-201
3	-213	-209	-204	-216	-241	-238	-220
4	-189	-177	-196	-191	-179	-198	-188
5	-194	-186	-206	-201	-171	-203	-194
6	-181	-171	-167	-172	-172	-186	-175
7	-402	-288	-371	-305	-360	-348	-346
8	-183	-74	-206	-33	-115	-109	-120
9	352	335	387	386	325	386	362
10	386	374	406	396	372	418	392
11	535						535
12	345	240	407	250			311
13		-184	-208	-203	-188	-203	-197
14					-188	-193	-191

Table 11. Initial Strains in Microstrain (10^{-6} mm/mm) at 110 MPa Stress

Gage #	Test 1	Test 2	Test 3	Test 4	Test 5	Test 6	Average
1	-172	-124	-70	-136	-204	-209	-153
2	-139	-85	-92	-100	-152	-152	-120
3	-154	-152	-104	-176	-218	-179	-164
4	-31	-11	-20	-16	-55	-40	-29
5	-47	-28	-38	-40	-52	-50	-43
6	-90	-85	-70	-84	-105	-89	-87
7	1732	1791	1787	1816	1678	1735	1756
8	1559	1551	1599	1661	1610	1618	1600
9	1796	1735	1801	1744	1843	1804	1787
10	2161	2148	2161	2153	2170	2173	2161
11	1710						1710
12	1727	1633	1703	1661			1681
13		-68	-75	-92	-112	-85	-86
14					176	142	159

Table 12. Initial Strains in Microstrain (10^{-6} mm/mm) at 220 MPa Stress

Gage #	Test 1	Test 2	Test 3	Test 4	Test 5	Test 6	Average
1	445	532	603	503	407	404	482
2	501	585	584	565	508	495	540
3	471	478	564	446	389	428	463
4	669	681	681	689	656	658	673
5	658	676	659	673	671	659	666
6	436	424	458	453	444	463	447
7	4125	4097	4125	4228	3976	4018	4095
8	3236	3152	3300	3316	3284	3283	3262
9	2640	2576	2653	2524	2665	2615	2612
10	3440	3444	3447	3410	3410	3419	3428
11	3038						3038
12	3394	3320	3338	3326			3345
13		579	567	540	523	552	552
14					935	835	885

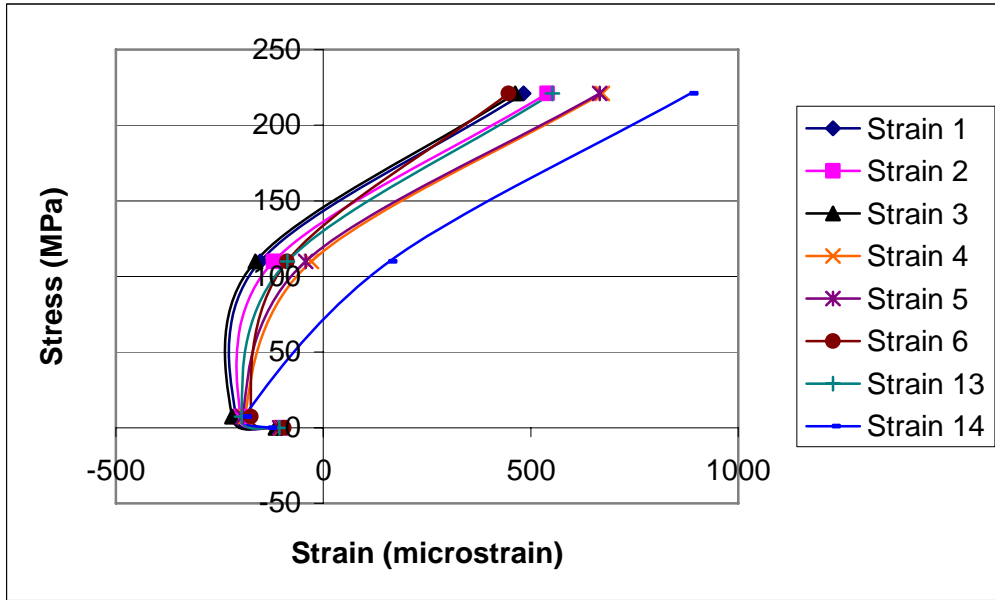


Figure 19. Average Initial Strain Values for Strain Gages 1-6, 13, 14

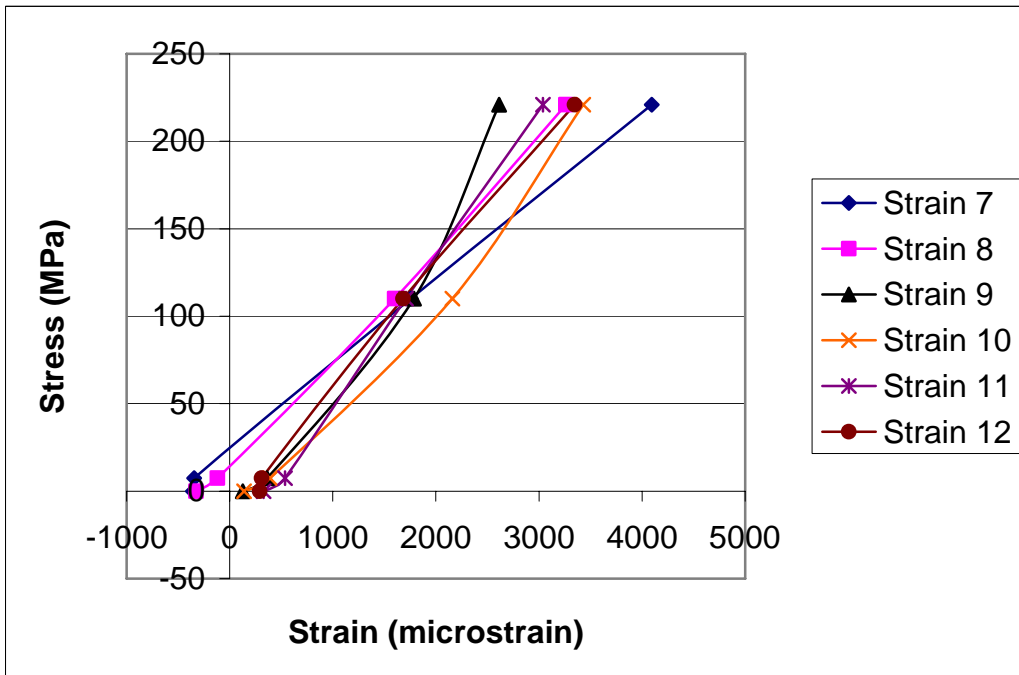


Figure 20. Average Initial Strain Values for Strain Gages 7-12

In Table 9 the initial strains are due to only the gripping action of the hydraulic machine. All of the strains on the patched side of the specimens begin with negative strains and those on the unpatched side with positive strains, as expected. The grips grabbing on to each end force a small amount of straightening on the specimen, even without any tensile load. With the initial curvature, this creates a bending moment on the specimen, resulting in compression on the patch side, and tension on the unpatched side, producing the appropriate strains seen.

From Table 10 it is seen that with 7.35 MPa of loading all of the strains on the patch itself get more negative, whereas all of the strains off of the patch are getting less negative. This is not completely unexpected. Under these low stress conditions the curvature effects of the specimen, and resultant strains due to the bending moment are still dominant. This initial load is providing much more strain due to the flattening effect on the specimen than due to tensile effects. This just leads to larger magnitudes of the strains that were seen under the no load condition.

As the stress increases to 110 MPa in Table 11 it is seen that the strains are larger than those under the 7.35 MPa condition, however strains 1 through 3, those right on the crack, are similar or more negative than the strains under the no load condition. Here it is seen more significantly, the strain effects of the tensile loading. Here the different moduli of elasticity for each material are seen to be 72 GPa for the aluminum and 195 GPa for the patch. According to the stress strain relationship for tensile loading [26]:

$$\sigma = Ee \quad (12)$$

where σ is the applied stress, E is the modulus of elasticity and e is strain.

From this equation it is seen that for the same applied stress, a material with a smaller modulus of elasticity will strain more, and a material with a larger modulus of elasticity will strain less under tensile loading. On strains gages 4-14, this is how the strains are now getting more positive then under the 7.35 MPa loading condition. The strains due to tensile loading are now having a greater impact then the stains due to the bending moment at these locations. However strains due to the bending of the specimen are still quite apparent here, especially in strains gages 1 through 3 which are still more negative then those under the no load condition. This area of the specimen has the highest curvature, and thus would experience the greatest strain due to the bending moment.

In Table 12 it is seen that under the 221 MPa load all of the strains have gone into positive value, those strains on the patch ranging from 400 to 1000 microstrain, and those off of the patch ranging from 2500 to 4500. Here the stress-strain relationship for tensile loading is the primary source for the strains in the specimen on all of the gages.

4.2 Fatigue Testing

In five of the six tests, the specimen was subjected to fatigue loading at 4 Hz at loads from 7.35 MPa to 194 MPa. Test number two was the only test not subject to fatigue loading, and only subject to tensile loading. This section examines how the strain values change under fatigue loading over the number of cycles as the crack grows, and at the crack growth rate under these conditions.

4.2.1 Crack Growth Analysis

In Figure 21 the total crack length versus the number of cycles is plotted, followed by Figure 22 which plots the associated trend lines. Each graph has a line at 76.2 mm showing the length of the patch. In these graphs it is seen that the crack growth did actually change somewhat significantly in the different tests. Specifically test number one was the most different from the other tests, however it is the closest to the results of previous tests on similar samples [9]. This appears to be due to poor compensators in hydraulic machine and changes in lab conditions between tests. The building has been under heavy construction, and the laboratory and hydraulic system went under a series of repairs between the individual tests. This likely led to the differences in the tests. The stress vs. time curves for the different crack growth patterns that were seen need to be examined. (Figures 23-25)

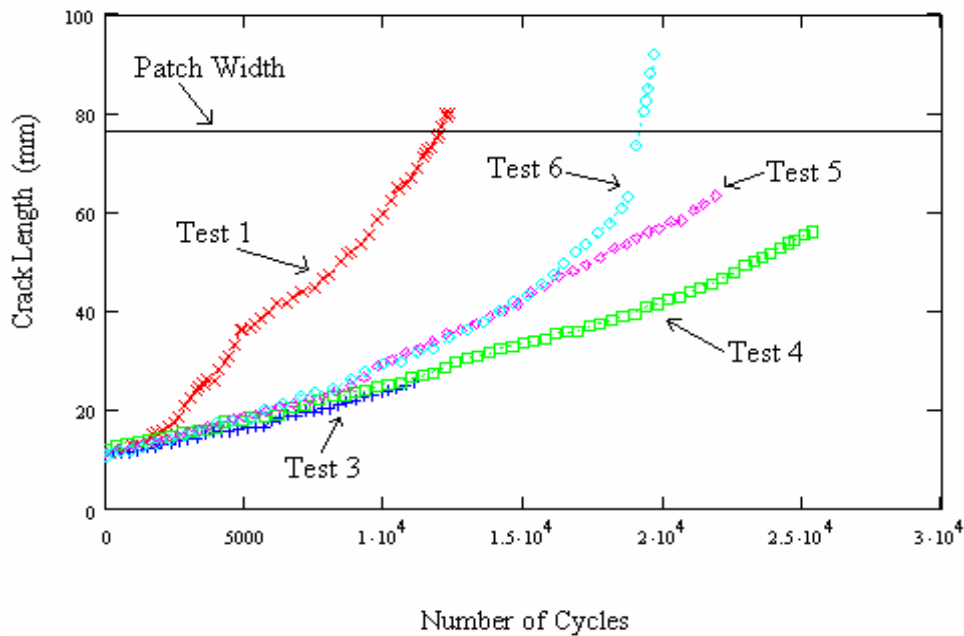


Figure 21. Crack Growth Rate.

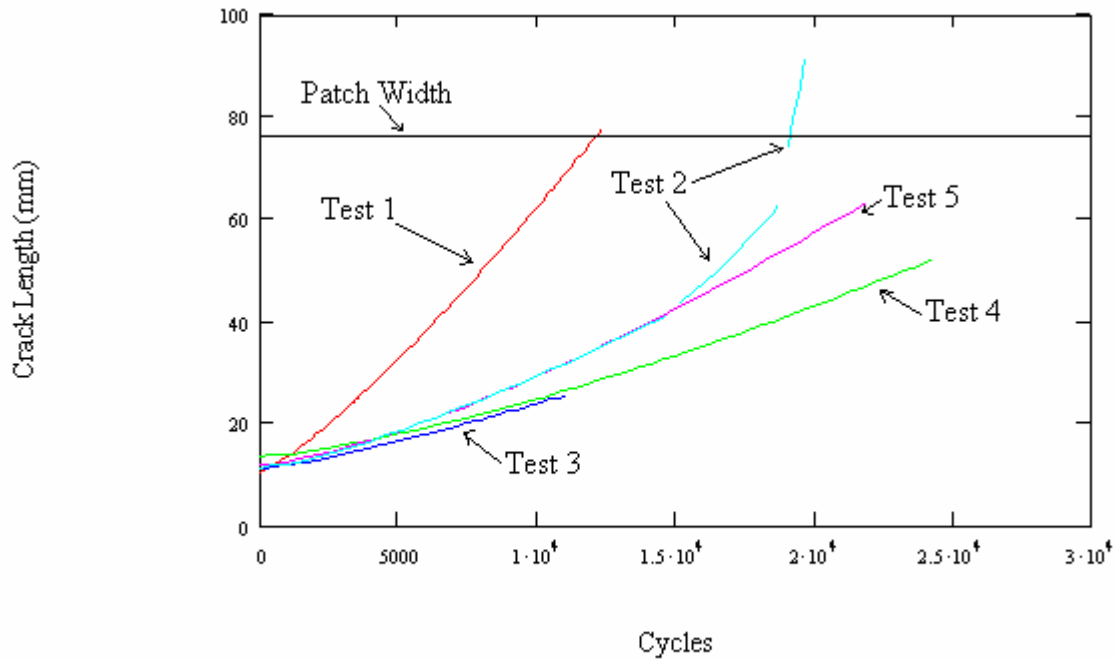


Figure 22. Fitted Crack Growth Curve Lines.

For the duration of the experiment the testing was stopped every few hundred cycles to take crack growth measurements. When the test was restarted, the machine took a second or two to have the compensators kick in fully. As a result, the loading would overshoot and undershoot the prescribed loading conditions for the first few cycles before it leveled off. This was seen throughout the length of each test. During the first test some overloading did occur (Figure 23), but not nearly to the degree that it did in the following tests, which all matched fairly closely (Figures 24).

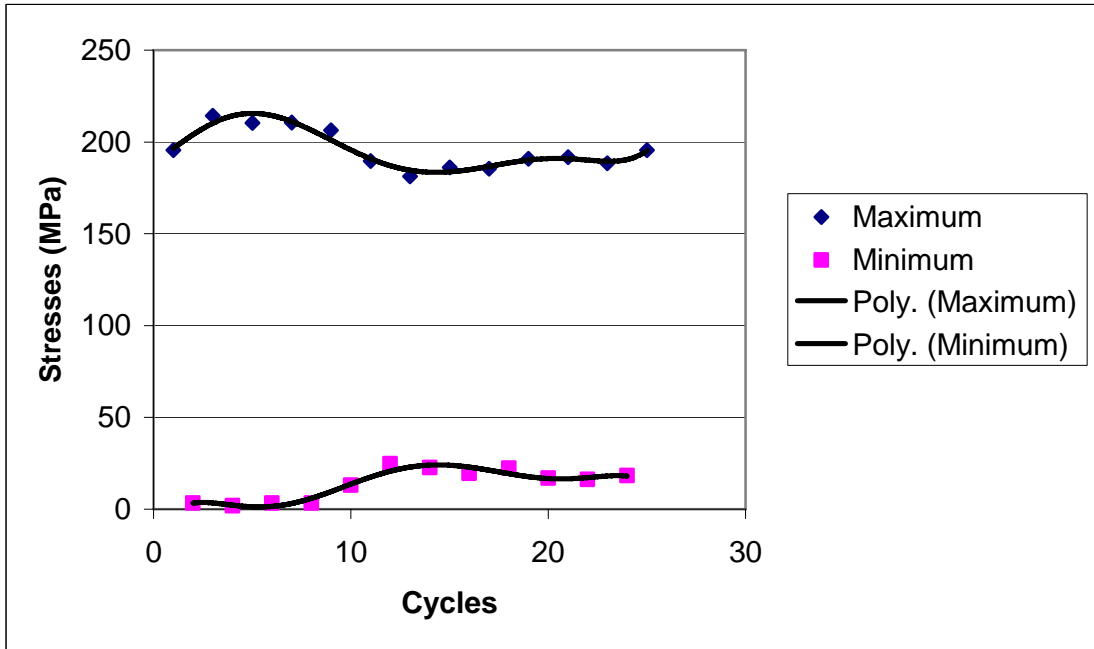


Figure 23. Test 1 Initial Max-Min Fatigue Loading Showing Small Overloads.

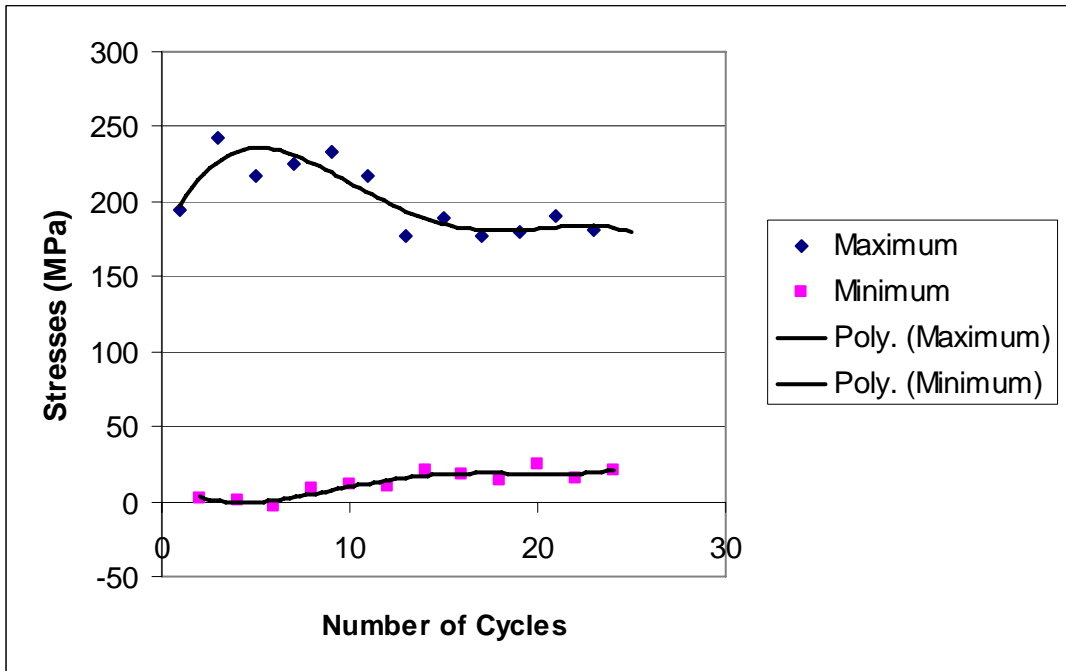


Figure 24. Tests 3-6 Representative Initial Max-Min Fatigue Loading Showing Larger Overloads.

The overloading problem was difficult to rectify, however part way through test 6 it was found that a tapered sine wave pattern could be used to avoid this initial over and undershooting (Figure 25). At around 15000 cycles in test six this was implemented. The machine would gradually increase the maximum and minimum loads over the first 10 cycles. This way it didn't get the sudden shock overshoot at the beginning. This let the system build up to the required loading conditions, instead of being forced into it suddenly and having to compensate. Here it is seen that at this point when test number six is no longer subjected to those initial overload conditions it begins to start growing quickly, and its rate of growth at this point is similar to that of the rate of growth of the first test when it started to grow and take off.

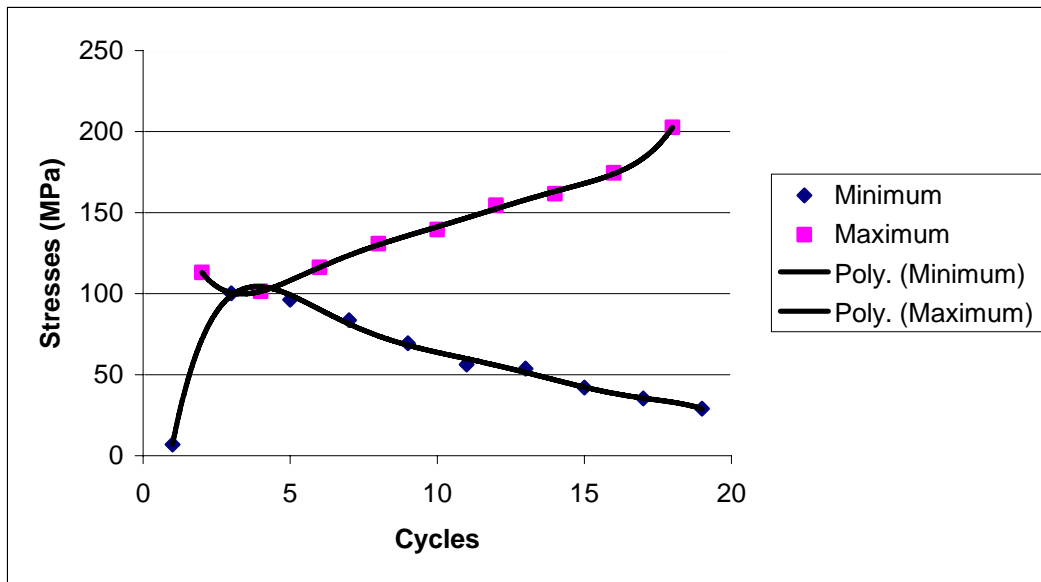


Figure 25. Test 6 Tapered Initial Max-Min Fatigue Loading.

The data points at the end of test six that grow rapidly are believed to be unreliable. Those data points were taken shortly after an IR reading. In this reading the specimen had a crack of 63.5 mm. It was heated up with the heat gun, and cooled down

with ice in order to attempt to capture the different temperatures in the debond area as it is expected to heat up and cool down at a different rate than the rest of the specimen. It is believed that this rapid heating and cooling in addition to the already high crack length additionally weakened the specimen causing the crack to grow much more rapidly than it would have otherwise.

In Figures 26-27 the crack growth rate in mm per cycle is examined. These growth rates are based on our trend lines from Figure 22. Here several different patterns are seen. Test one lies all by itself. Tests three and four have very similar growth rates. Tests five and six match up with similar growth rates most of the way through. It is also seen that test number six begins to rise to approach similar growth rates to that of test after it switched over to the tapered growth pattern for the initial fatiguing.

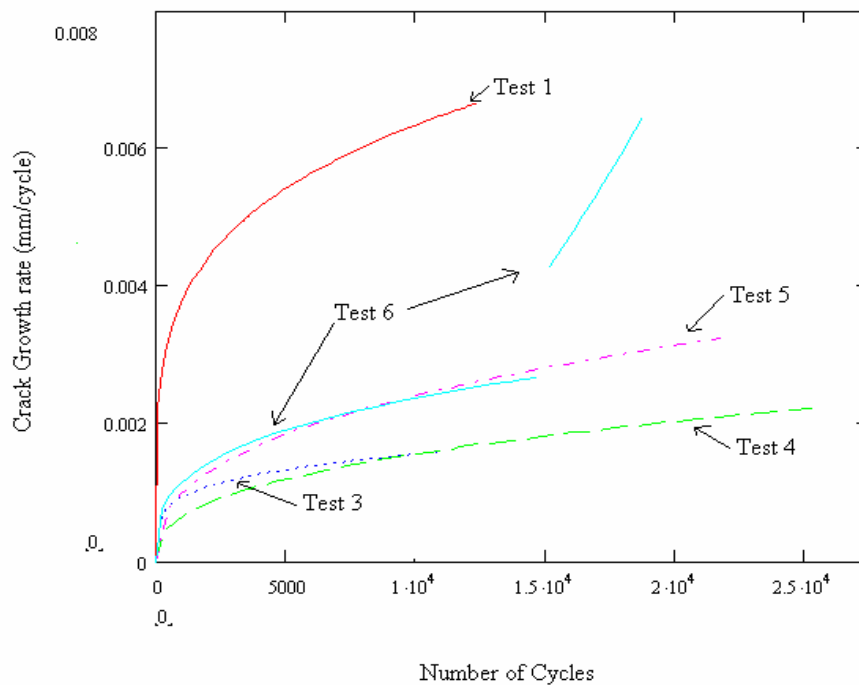


Figure 26. Crack Growth Rate vs. Number of Cycles

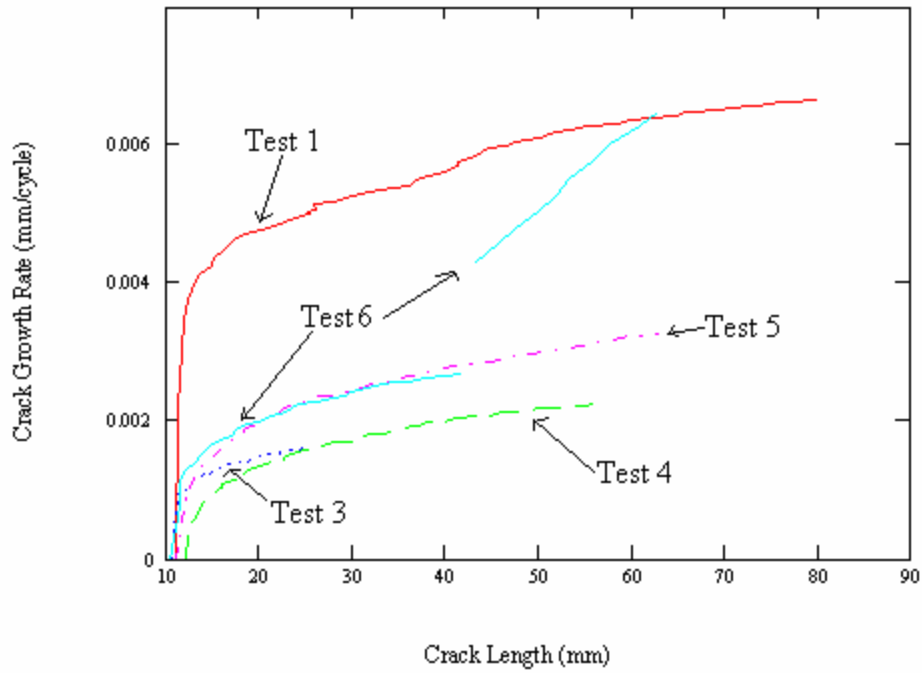


Figure 27. Crack Growth Rate vs. Crack Length.

4.2.2 Overloading and Retardation Effects

Here the overload situation is discussed, and resulting retardation effects on the crack growth, and how it applies to each of the tests. An overload during a cyclical test is where there is a cycle, or very small number of cycles that go significantly over the standard cyclical loading. After the application of an overload in a cyclical test, crack growth will be slowed. Figure 28 illustrates this retardation effect of overloads on crack propagation. [10]

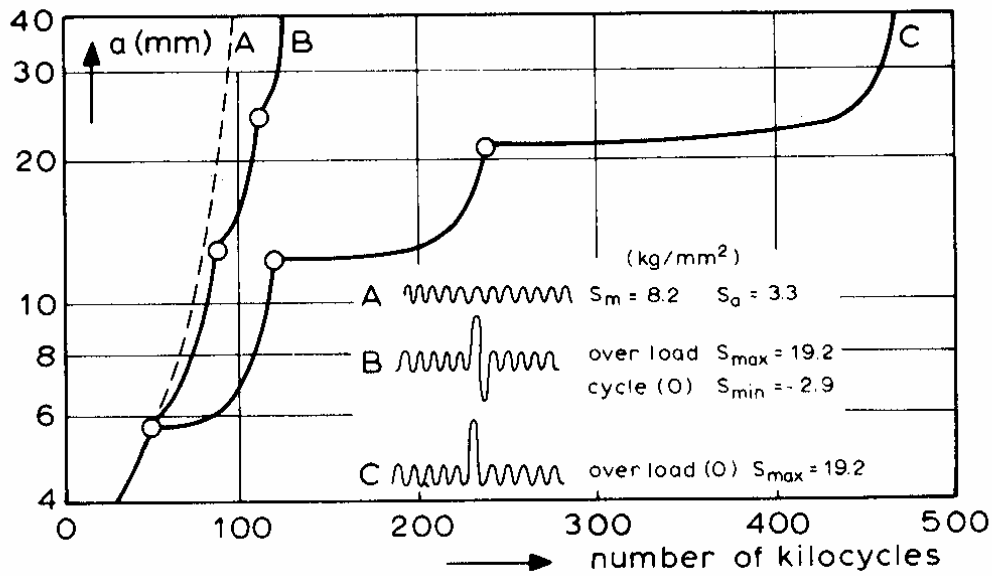


Figure 28. Retardation as a Result of Overloads (2024-T3 Al-alloy) [10]

The overload has introduced a large plastic zone in the material causing a permanent deformation region around the crack tip as shown in Figure 29. After unloading the sample, the deformed region still must fit in the surrounding elastic material. While the elastic material resumes its original size, the material in the plastic zone does not. If the surrounding elastic zone contracts upon release of the load, the plastic zone will be too large to fit in the resulting area. The elastic material will have to make it fit by exerting compressive stresses on the plastically deformed material at the crack tip. The residual stresses can also be seen in Figure 29. [10]

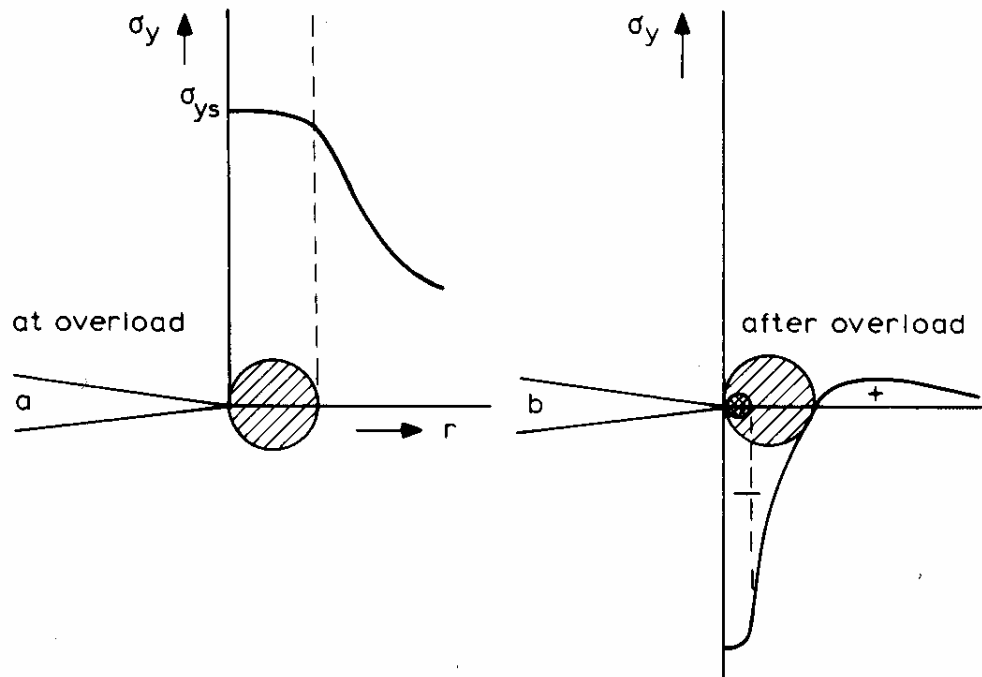


Figure 29. Residual Compressive Stresses at Crack Tip as a Result of Overload. [10]

The residual compressive stresses tend to close the crack tip over some distance. Further cycling can cause crack growth only if the residual stresses are overcome to a degree that the crack tip is opened again. As soon as the crack has grown through the area of residual stresses, the original crack propagation curve will be resumed. This explains the low growth rate after the overload. [10]

While the overload that is seen in these experiments is not extensively large, it is large enough to make a significant difference, especially when repeatedly applied. The overload occurred immediately after a crack length measurement occurred, and cycling was resumed. During tests 3 and 4, this occurred approximately every 300 cycles. These

are the two tests that are seen with the slowest crack growth. The moderate overloads at somewhat frequent intervals led to a significant retardation to the crack growth rate. Tests 5 and 6 are seen to have a slightly higher crack growth rate than those in tests 3 and 4. This is most likely due to the fact that these tests were only stopped at intervals of approximately 600 cycles. This longer testing time between overload situations allowed for the crack to grow further through the plastic zone, and begin growing somewhat quicker through the last few cycles of that segment of testing between crack length measurements. It is seen that in test 6 the crack growth begins to take off approximately 2/3 of the way through. This is where the tapered loading began, and eliminated the overload situation. The crack was then able to grow through the plastic zone and grow normally again without the retardation effects of an overload situation. Here it moves steadily to meet the crack growth rate seen in the first test.

4.2.3 Strain Measurements

How the strain values change over the life of the specimen will be examined in this section. In Figures 30 through 43 the maximum and minimum strain values versus the total crack length are examined. These appear to be the best graphs to examine how the strain changes over the life of the specimen. The crack growth rate is fairly different among the different tests, making max-min strain versus number of cycles graphs much more difficult to compare. The graphs showing the results for strain gages one and two have been split up to better show the maximum and minimum values, due to the overlapping nature of these graphs. For the exact locations of each strain gage, refer back to Figures 9 and 10.

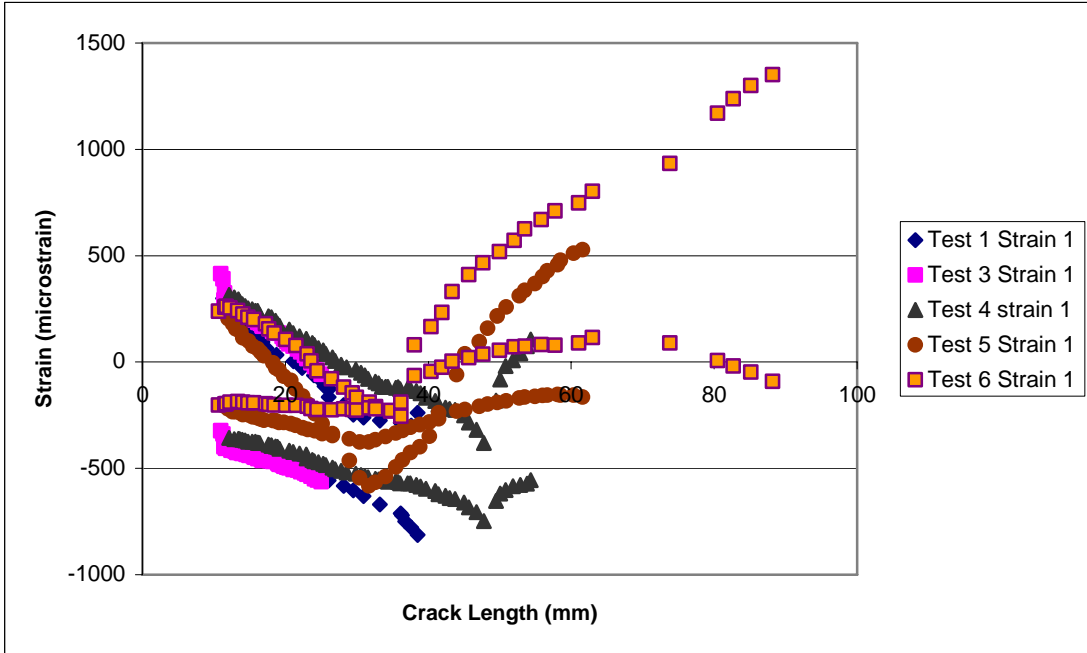


Figure 30a. Max - Min Strain Versus Crack Length (mm): Strain Gage 1

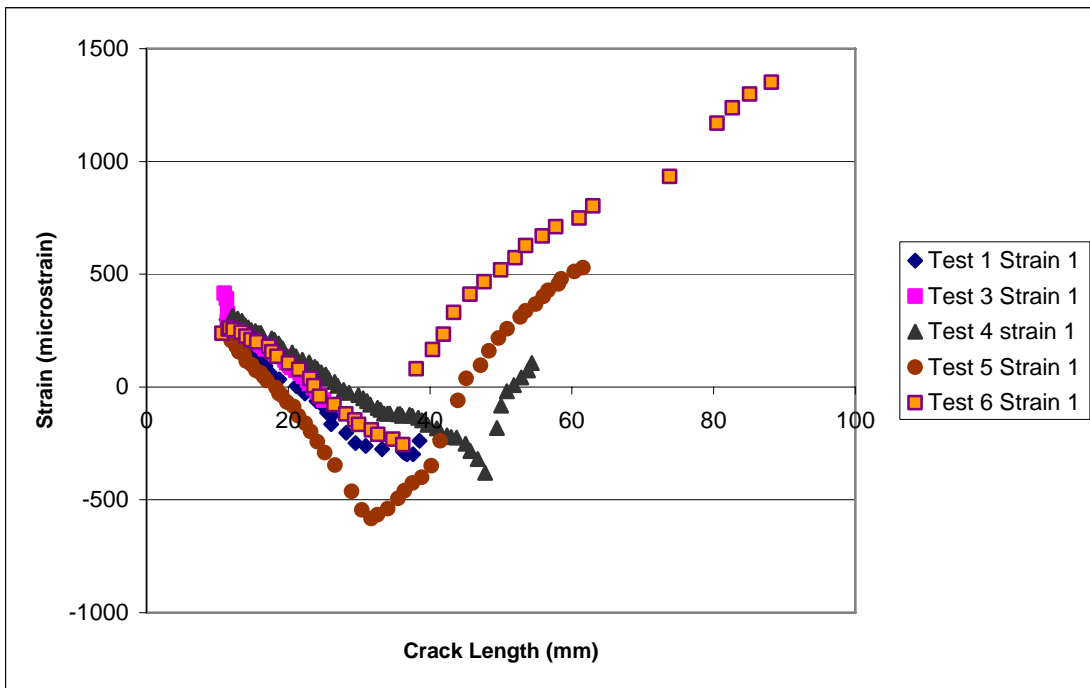


Figure 30b. Max Strain Versus Crack Length (mm): Strain Gage 1

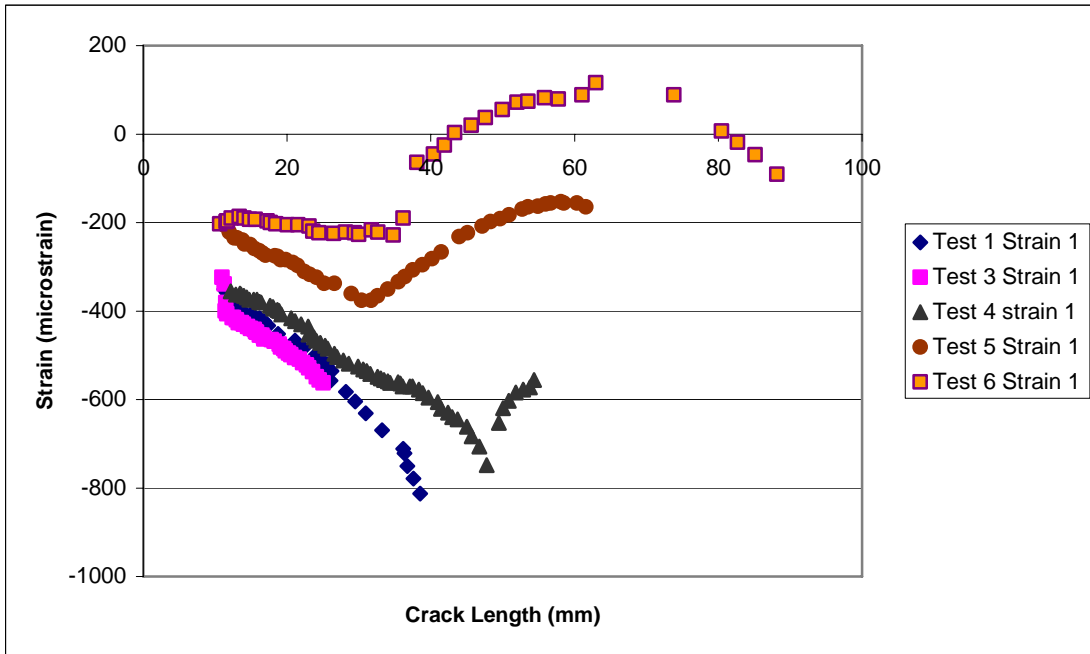


Figure 30c. Min Strain Versus Crack Length (mm):Strain Gage 1

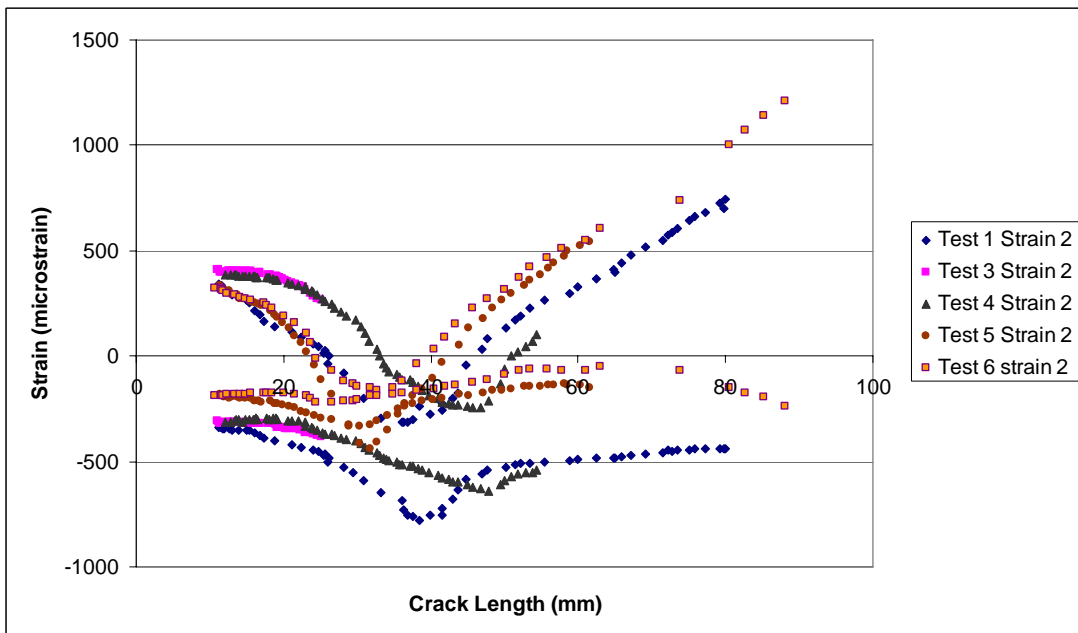


Figure 31a. Max - Min Strain Versus Crack Length (mm):Strain Gage 2

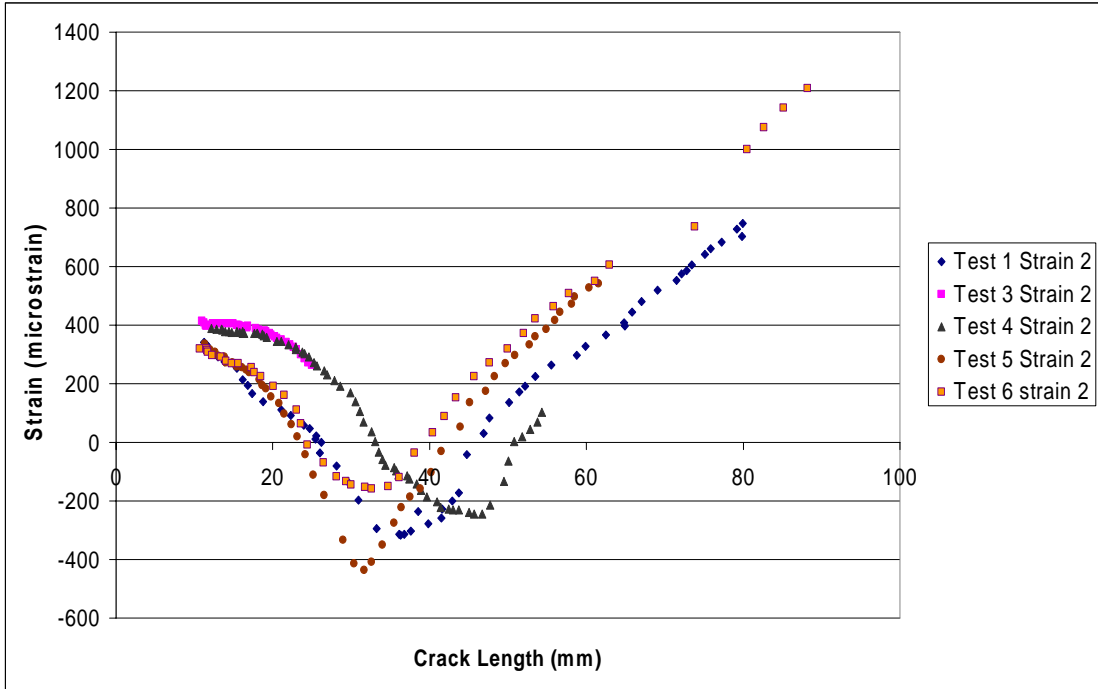


Figure 31b. Max Strain Versus Crack Length (mm):Strain Gage 2

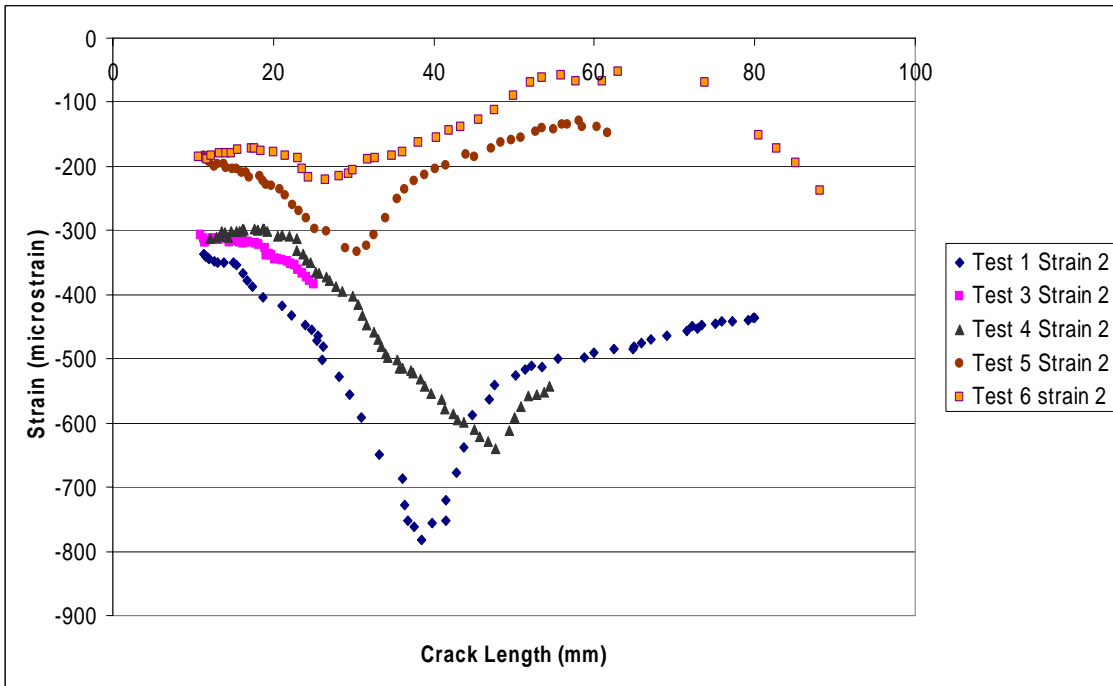


Figure 31c. Min Strain Versus Crack Length (mm):Strain Gage 2

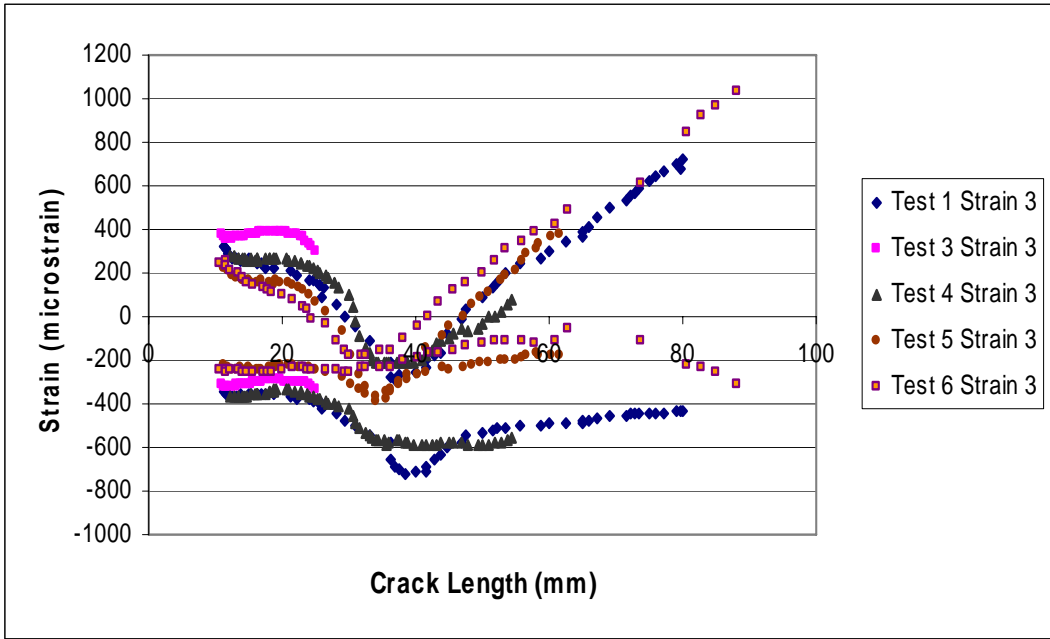


Figure 32. Max - Min Strain Versus Crack Length (mm):Strain Gage 3

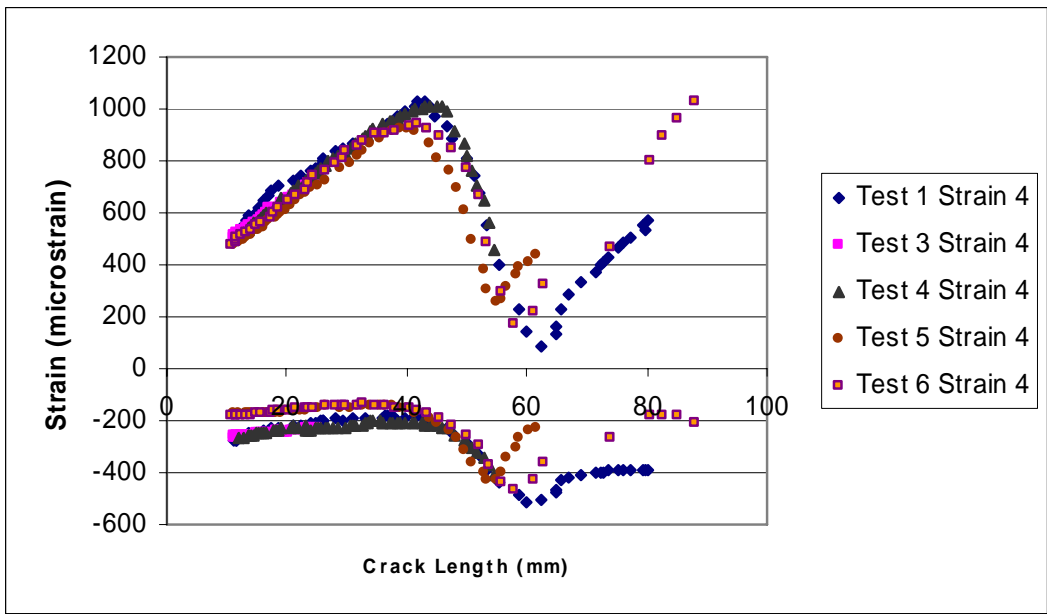


Figure 33. Max - Min Strain Versus Crack Length (mm):Strain Gage 4

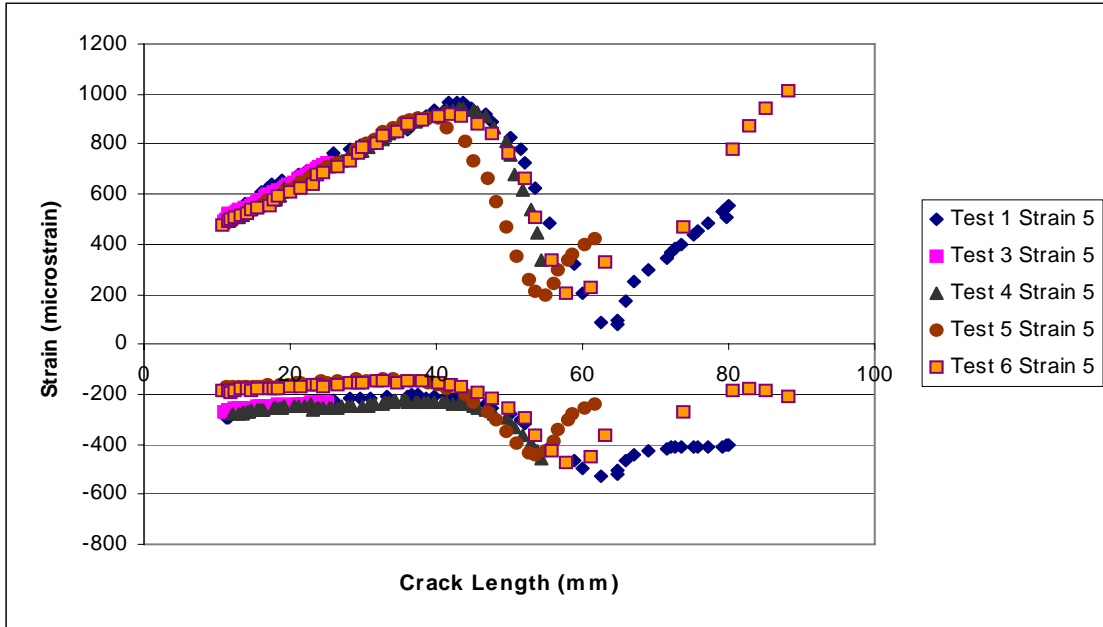


Figure 34. Max - Min Strain Versus Crack Length (mm):Strain Gage 5

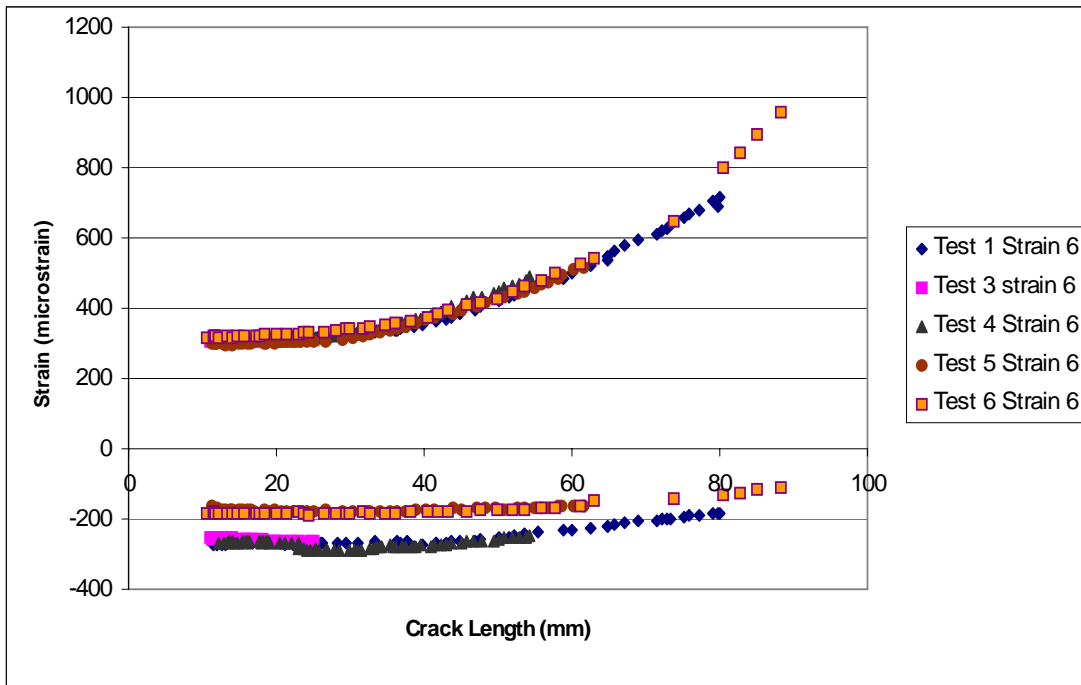


Figure 35. Max - Min Strain Versus Crack Length (mm):Strain Gage 6

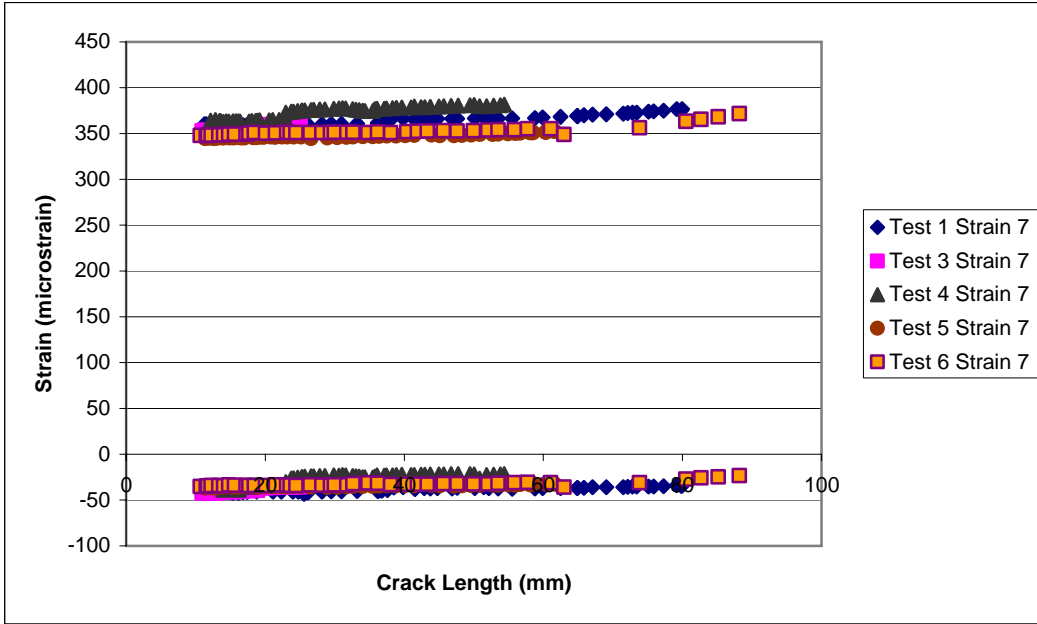


Figure 36. Max - Min Strain Versus Crack Length (mm):Strain Gage 7

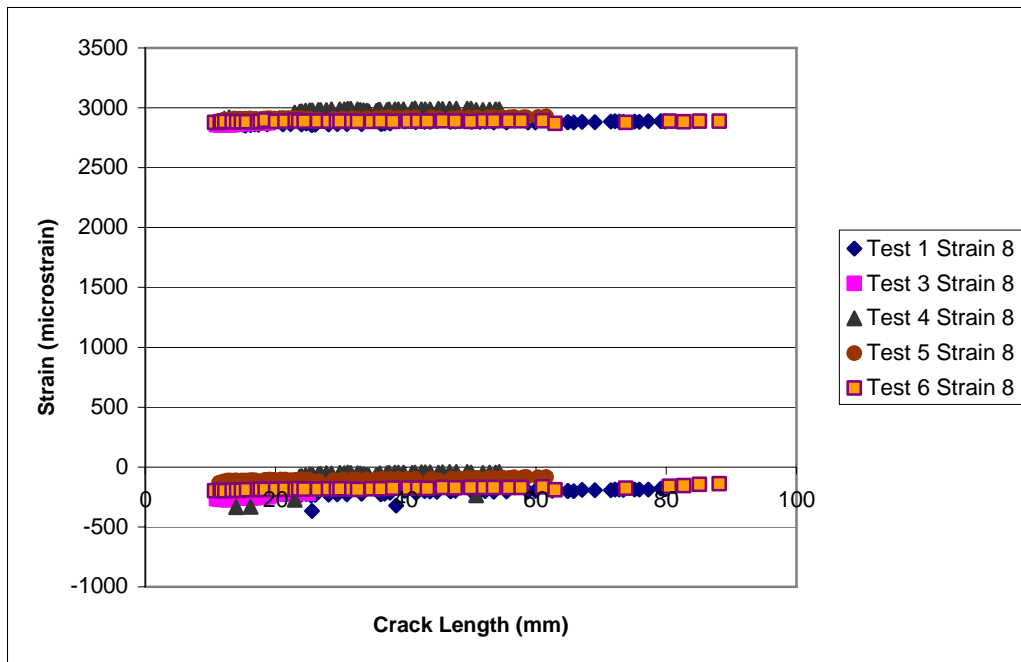


Figure 37. Max - Min Strain Versus Crack Length (mm):Strain Gage 8

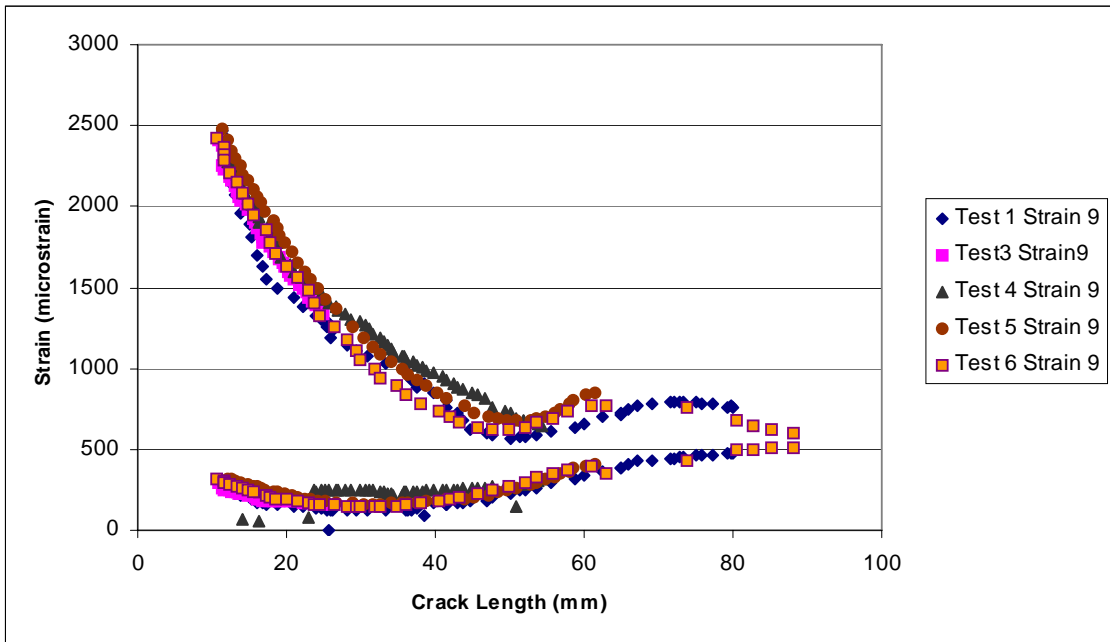


Figure 38. Max - Min Strain Versus Crack Length (mm): Strain Gage 9

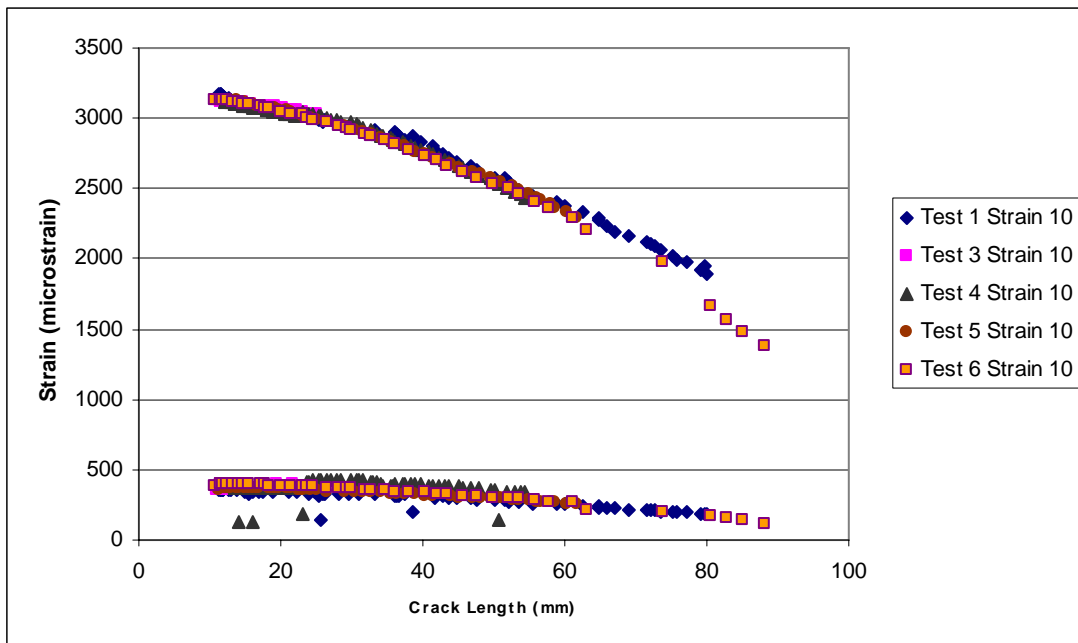


Figure 39. Max - Min Strain Versus Crack Length (mm): Strain Gage 10

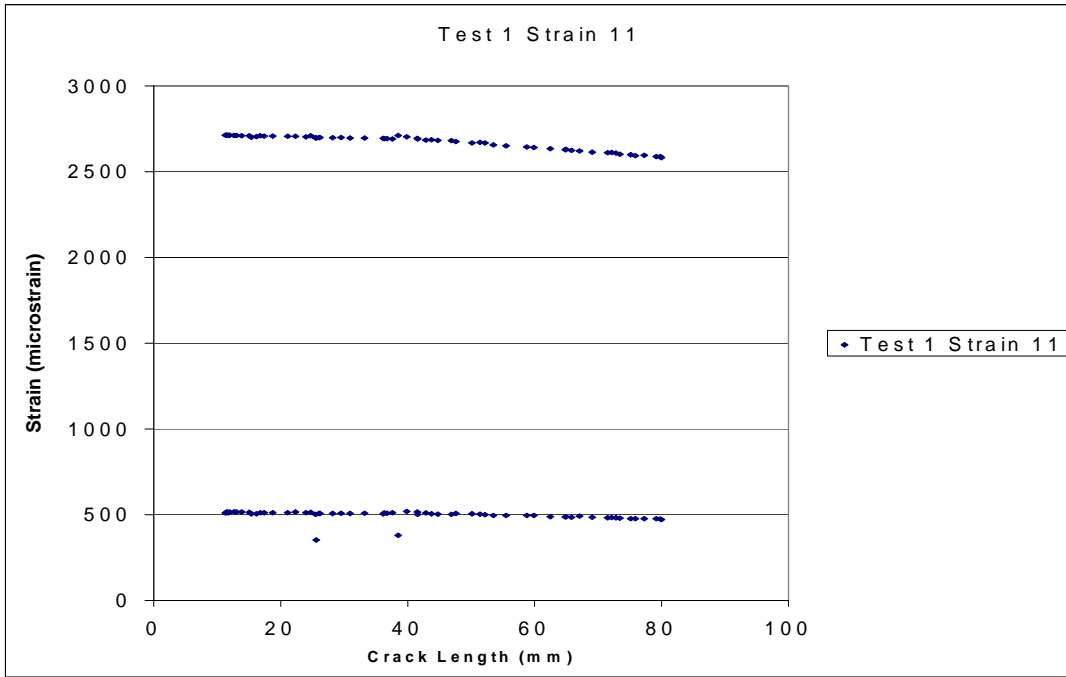


Figure 40. Max - Min Strain Versus Crack Length (mm):Strain Gage 11

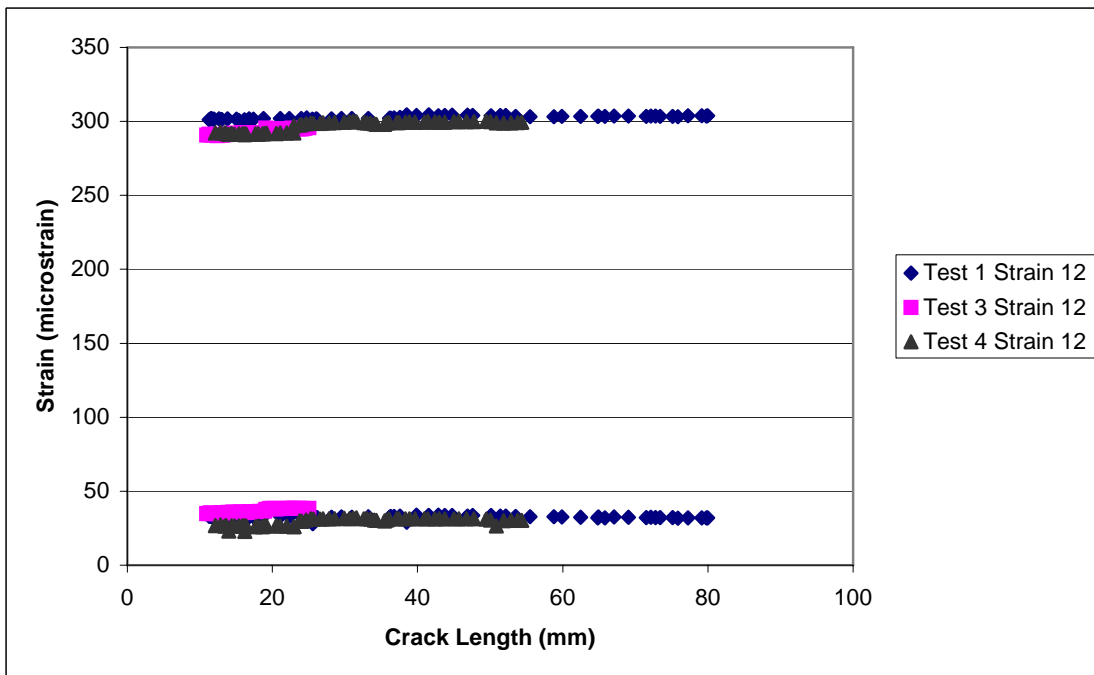


Figure 41. Max - Min Strain Versus Crack Length (mm):Strain Gage 12

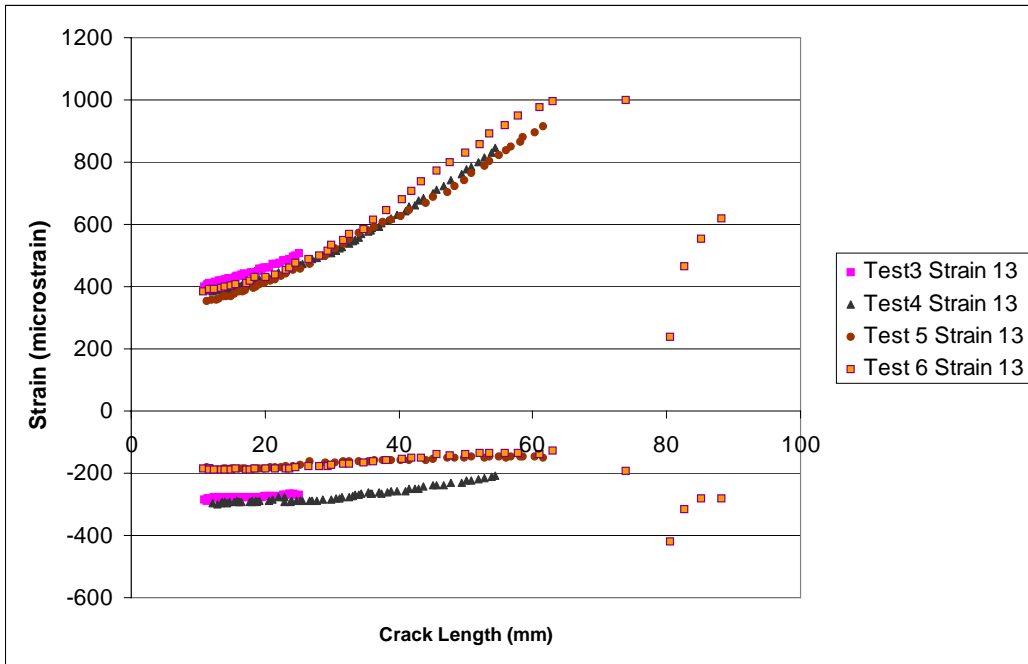


Figure 42. Max - Min Strain Versus Crack Length (mm): Strain Gage 13

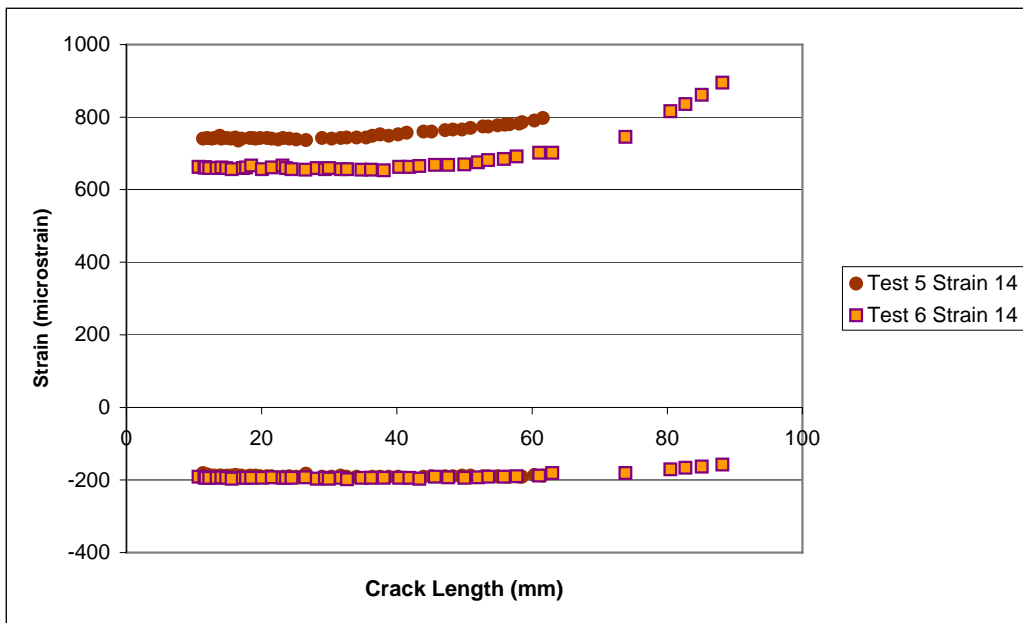


Figure 43. Max - Min Strain Versus Crack Length (mm): Strain Gage 14

Throughout all of the tests it can be seen that the strain versus crack length graphs match up very closely. The biggest differences seen in these graphs are in strains 1 through 3, the three strain gages that are right next to the crack. While these first three graphs don't match up as well as the other graphs, their features are still very similar. It can be seen that they have the same features in where the strain values decrease, and increase back up again. This region has the most irregular behavior with the crack constantly opening and closing very close to the gages, and a debond area constantly growing through these strain gages at the same time.

In looking at strains 4 and 5, the strain gages that are centered at a 12.7 mm away from the crack on the patched side, it is seen that the data curves match up extremely well. This is despite the fact that it was previously seen how the cracks have grown at different rates. Strain values are virtually identical for a given crack length despite how many cycles it took to get to that crack length. In comparing the strain graphs of strains 4 versus 9, where strain 9 is the corresponding strain on the unpatched side of the specimen, while it is seen that the graphs look fairly different, the peaks and valleys lie very close to each other comparatively.

Strain 13 at the next furthest distance away from the crack at 25.4 mm distance is the last strain gage to record the peak and valley features that are seen among strains 1-5 and 9. And in this graph it only starts falling off after the total crack length reaches 76.2 mm, which is also the width of the patch. These sudden dips in the strain values seem to match up to where the debond area behind the patch reaches that strain gage. In the strain gages 2.54 mm away from the crack, the strain values bottom out at about 33.02 mm to

43.18 mm. For the strain gages centered at 12.7 mm away from the crack it is seen that the strain values bottom out about 58.42 mm to 63.5 mm. And with strain gage 13 the strain dips down at about 78.74mm.

In strains 6 and its reverse on the back side of the panel, strain 10, the peaks and valleys in the strain values aren't seen, but a similar rise in strain 6 at 50.8 mm away from the crack is seen as was seen in strain 13 at 25.4 mm away from the crack. In the conditions of strains 6, and correspondingly strain 10, the strains similarly rose, strain 6, or fell, strain 10, they just didn't have the debond reach the area underneath those gages. In all of the strain gages on the patch, most notably the ones somewhat away from the crack, not as much with strains 1 through 3, it is seen that the strain values rise to a strain value of 1000 microstrain, and then they drop off as the debond area hits them. The results are slightly different on strains 1 through 3 in that those strain values don't have that initial rise.

While the strains on the patch didn't rise much above 1000 microstrain, it is seen that the strains off of the patch on the aluminum surface rise to as high as 4000 microstrain. However these higher strain values are those furthest away from the crack, with little change throughout the test, strains 7, 8, 11, and 12. With strains 9 and 10, on the aluminum surface, but on the back side of the patch the strains start out at somewhat high values of maximums of 2500 to 3100 microstrain, but quickly drop off.

When looking at these curves of strain versus crack length, and how well they line up on top of each other, it is seen that being able to measure the strain value on the patch can give a good measurement of how large the crack size is underneath. However it is

also seen that certain strain locations will be better than others in this regard. Strain values very close to the crack can be somewhat erratic and unreliable, while strain values just a little distance away will give very accurate results, with quick rises and quick falls. Strain would however need to be monitored somewhat closely, if using strains in locations similar to strains 4 and 5 that rise and fall. In measuring the strain it should be noted whether the strain value is associated with the first portion or the second portion of the curve. This is where comparing strain values to strains 6 or 13 would give a good number as to where on the crack growth curve the data would fall.

Strains 4 and 5 give the quickest initial rises with very accurate data through about 4.064 mm where they start to fall off fairly steeply. At that point strain 13 is rising fairly quickly and will also be a good measurement of what the crack length is.

However, in real world applications getting the strain values needed in order to determine the crack length underneath the patch would be much harder to do. The greatest change in values were at the highest stress loads of up to 194 MPa. It may not be advised, and may be difficult, to subject the aircraft or patched system to these higher loads where the biggest difference and most accurate strain results are seen. The minimum values at 7.35 MPa are much more constant. Significant changes are only seen at the 7.35 MPa range in stresses 1 through 3 up to 50.8 mm, however the strain values are erratic. Strains 4 and 5 are very constant through 40.64 mm, at the minimum stress values, but then have a noticeable dip and rise in the ranges of 143.18mm to 63.5 mm. It would likely be easier and more practical to subject the aircraft or other patched system to these sorts of loads in order to determine strain, however it still would not be simple.

If loads of 7.35 MPa could be applied and monitored at the strain values at this 12.7 mm location, the dip occurring around 4.32 mm could be seen and it would know that the patch is approaching the end of it's life.

Figure 44 to 57 show the change in strain values over the length of the tests. These numbers are the maximum strain minus the minimum strain as plotted out in Figures 31-43. In looking at the change in strain values for strain gages 9 through 11 on the back of the panel, we see that it is continually decreasing as the crack gets larger, where the lowest change in strain values are closest to the crack. In this instance the loading is required to go around the crack more and more as the crack gets larger. The stresses are now decreasing in the aluminum nearest the crack, as it increasingly flows around the crack tips in the aluminum further away from the center line that the strain gages are on, in addition to more and more of the center loading flowing through the patch.

It is seen in the change in strains on the patched side, that it is increasingly growing as more loading is flowing through the patch. On strain gages 1 through 5 and 13, areas where the change in strain decreases is seen for a time before it begins to rise again. This appears to be where the debond is growing over the strain gage. This will be shown more definitively when the shape of the debond is looked at in a later section. With no debonds below the strain gage, the gage produces a strain value based on the stresses through the combined aluminum/composite material. When the debond appears below the strain gage, the strain values are no longer based on the combined aluminum/composite, but only on the composite patch, as they are now separated. With

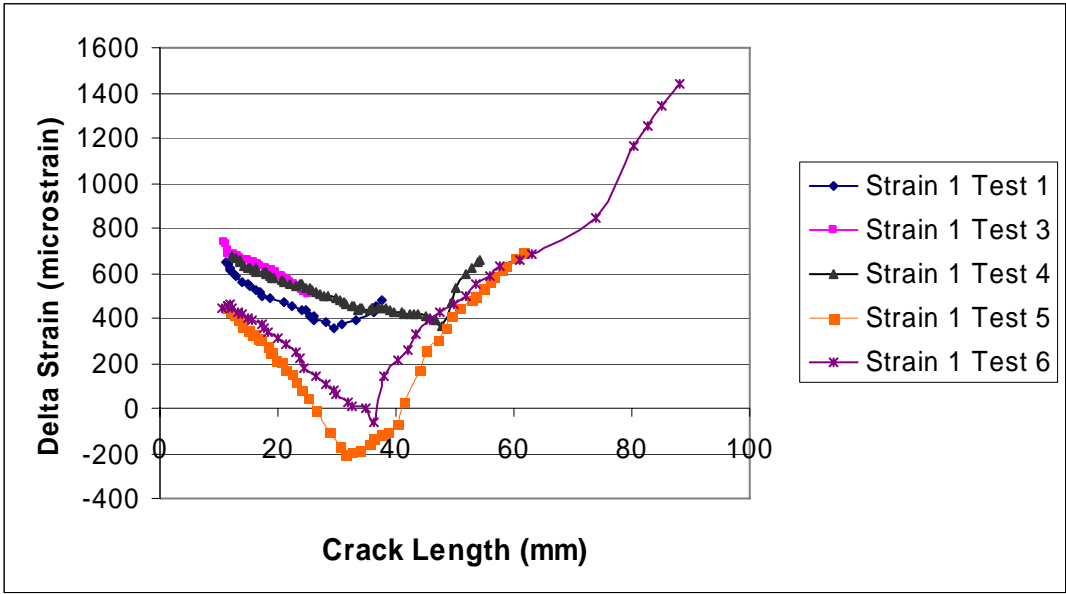


Figure 44. Change in Strain Versus Crack Length (mm):Strain Gage 1

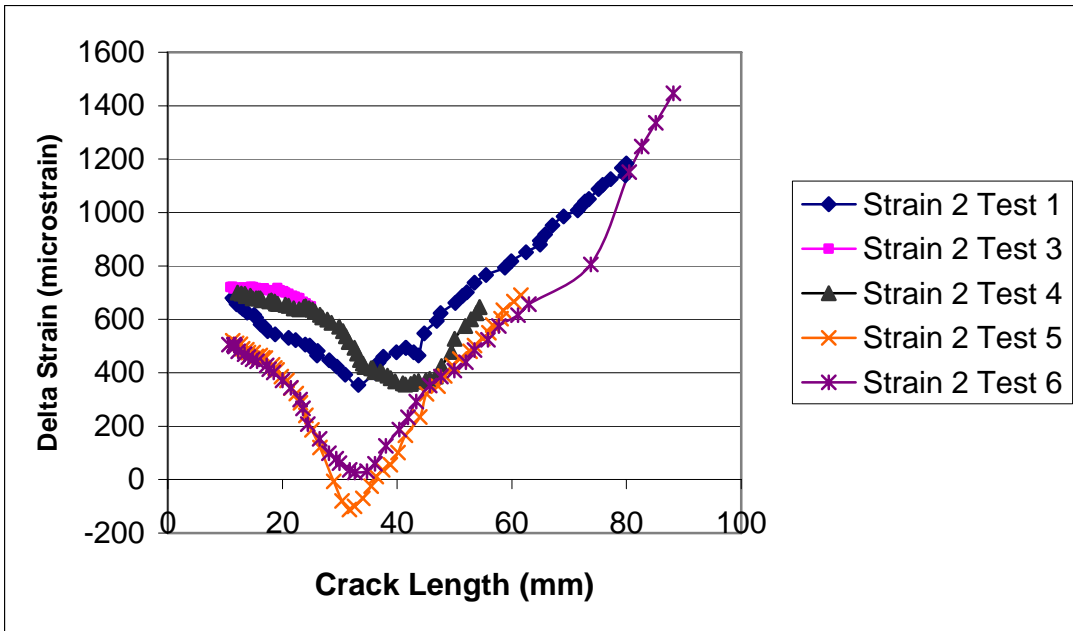


Figure 45. Change in Strain Versus Crack Length (mm):Strain Gage 2

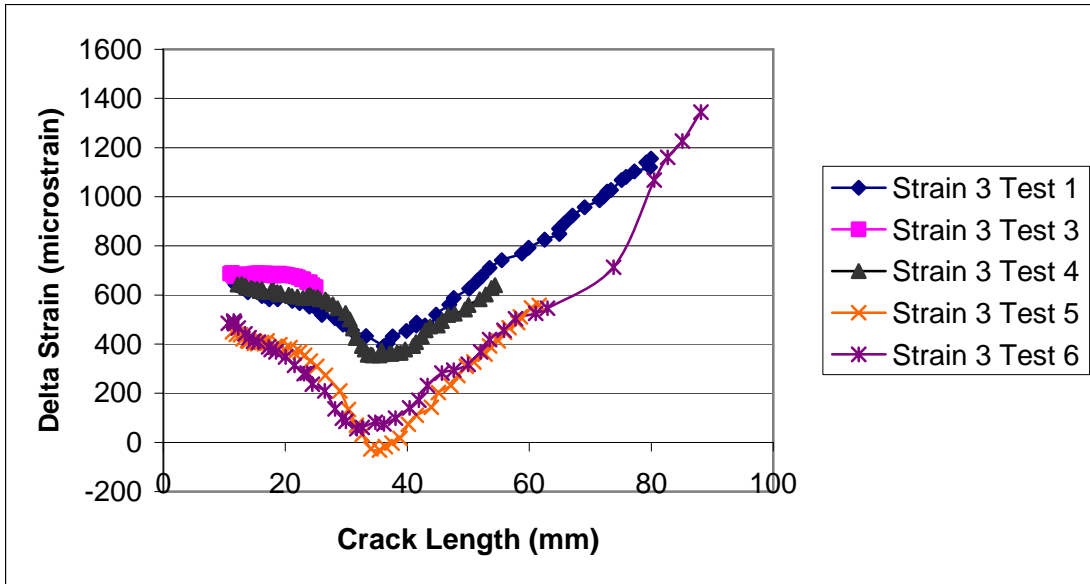


Figure 46. Change in Strain Versus Crack Length (mm): Strain Gage 3

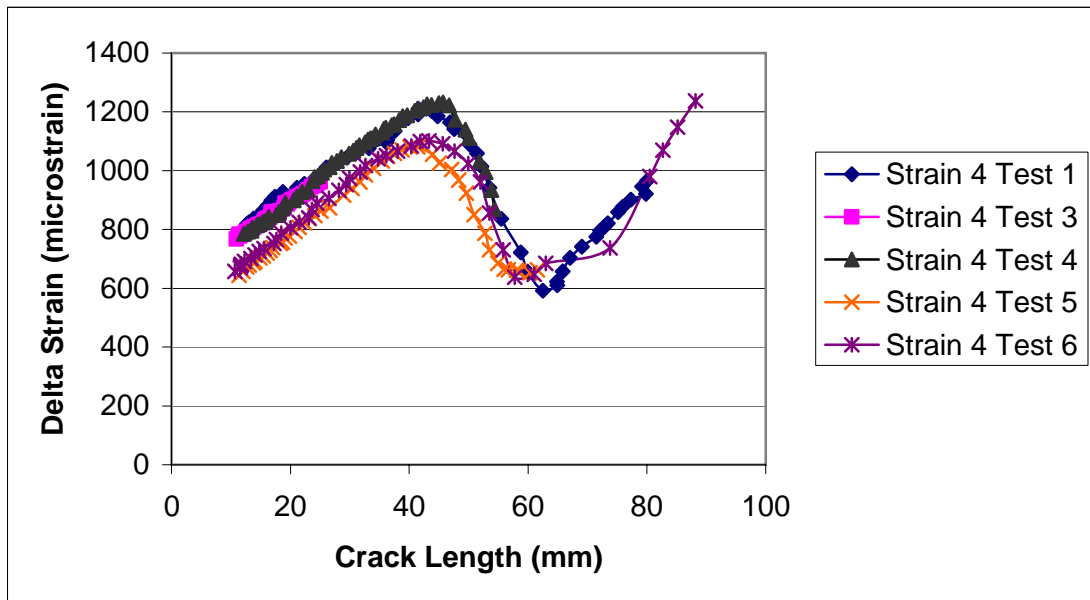


Figure 47. Change in Strain Versus Crack Length (mm): Strain Gage 4

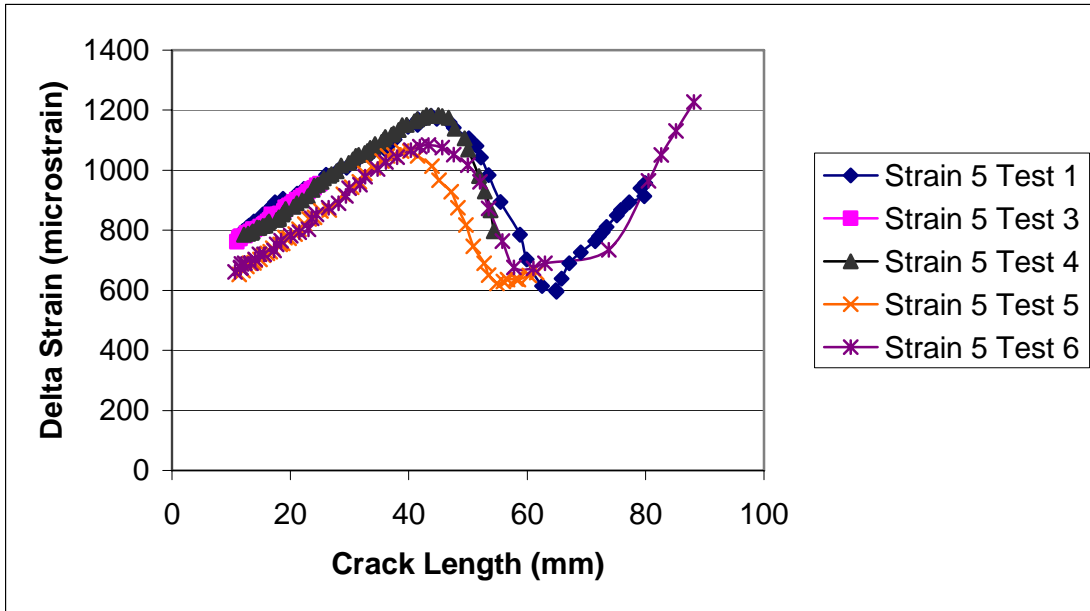


Figure 48. Change in Strain Versus Crack Length (mm):Strain Gage 5

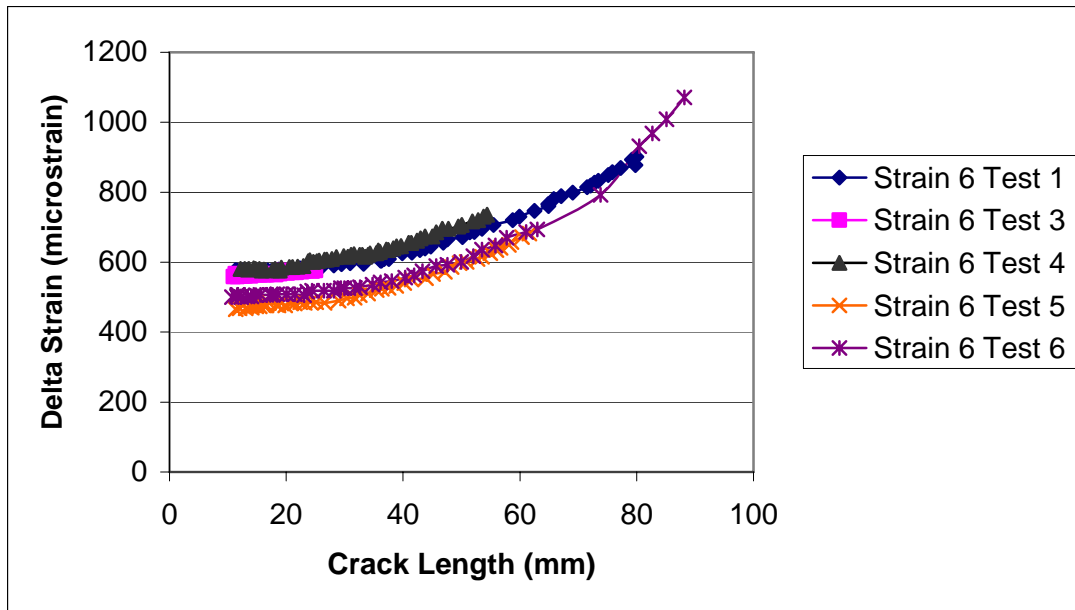


Figure 49. Change in Strain Versus Crack Length (mm):Strain Gage 6

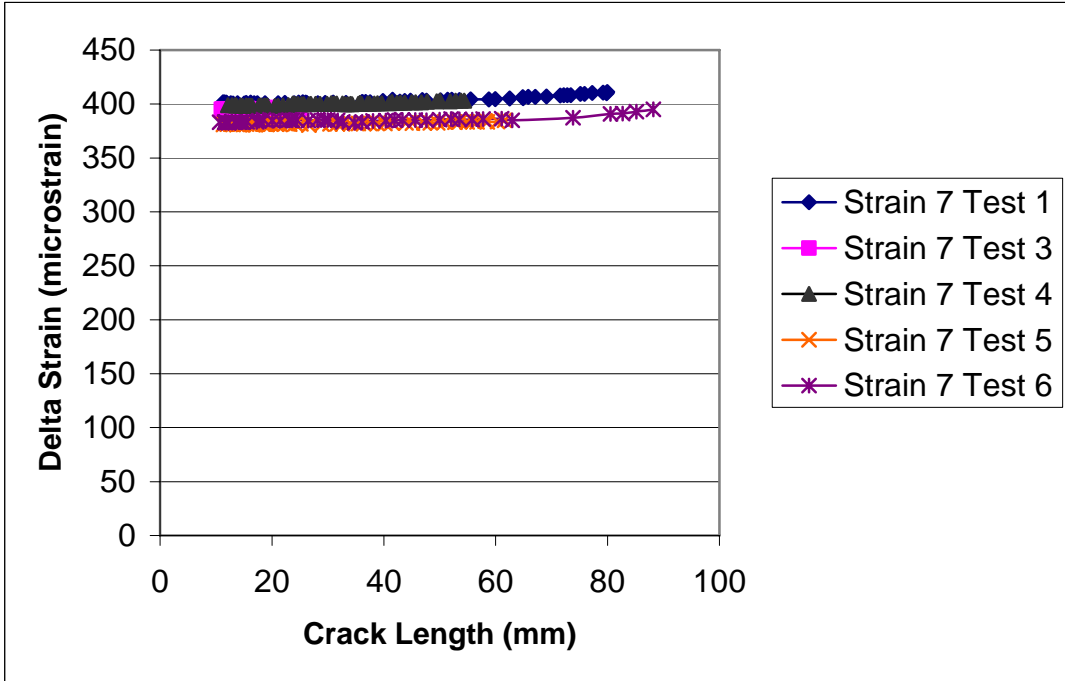


Figure 50. Change in Strain Versus Crack Length (mm):Strain Gage 7

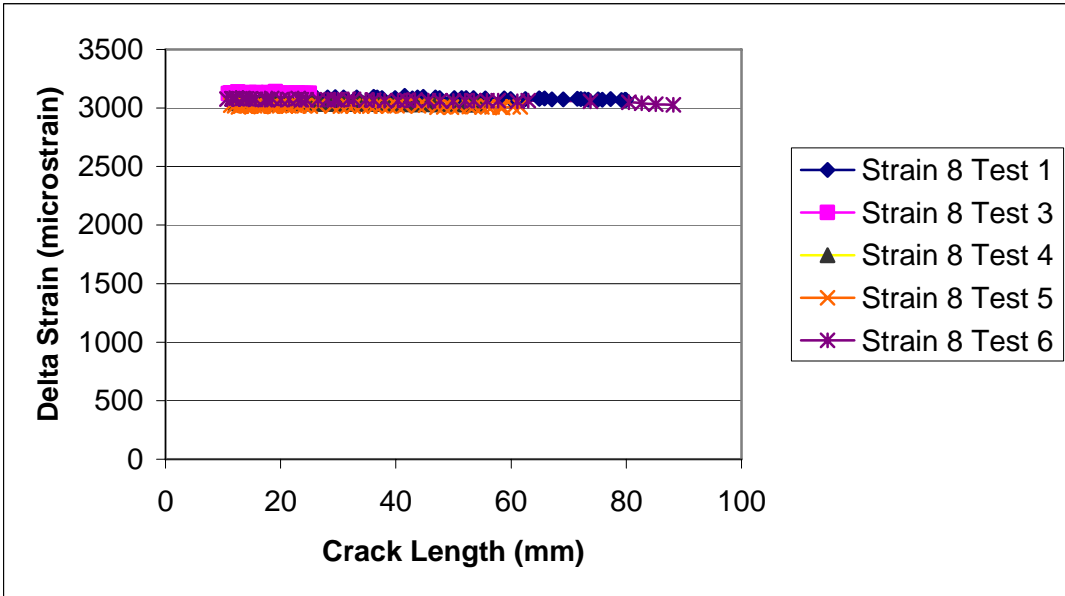


Figure 51. Change in Strain Versus Crack Length (mm):Strain Gage 8

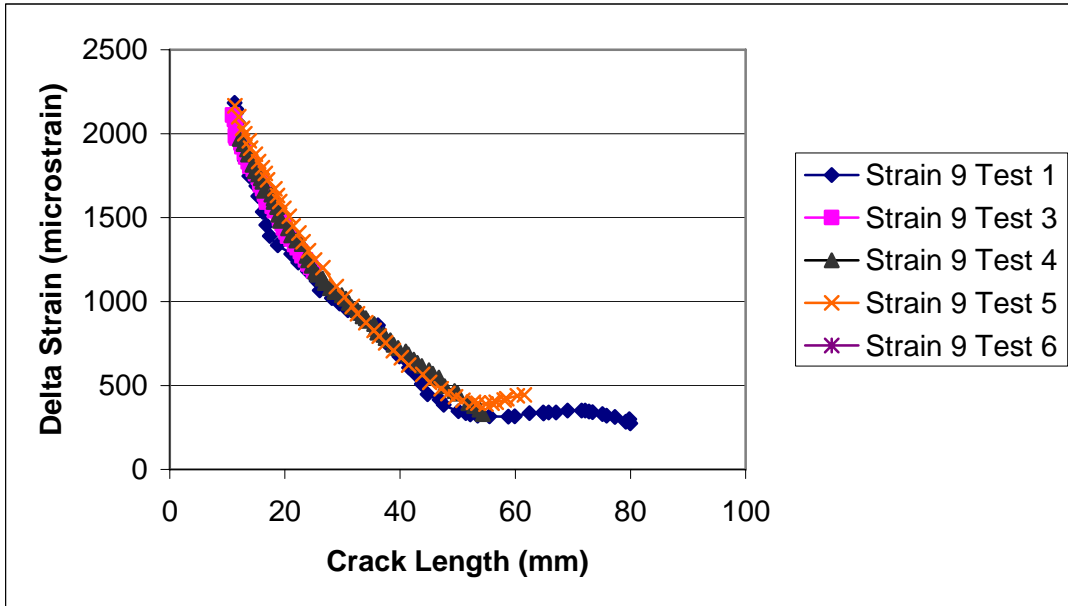


Figure 52. Change in Strain Versus Crack Length (mm):Strain Gage 9

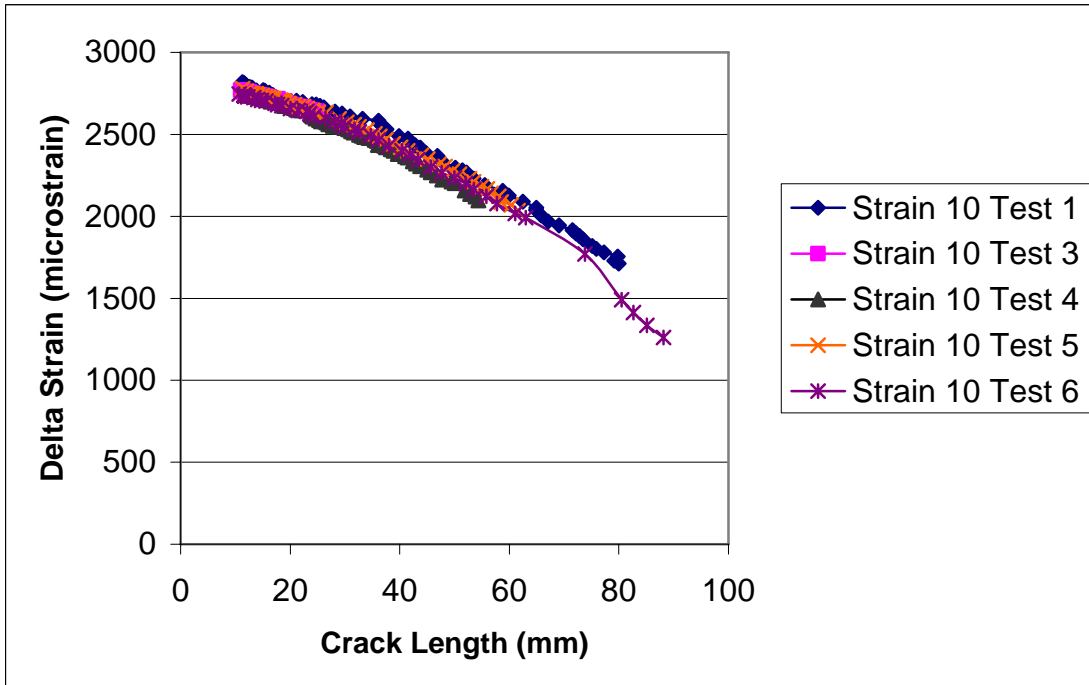


Figure 53. Change in Strain Versus Crack Length (mm):Strain Gage 10

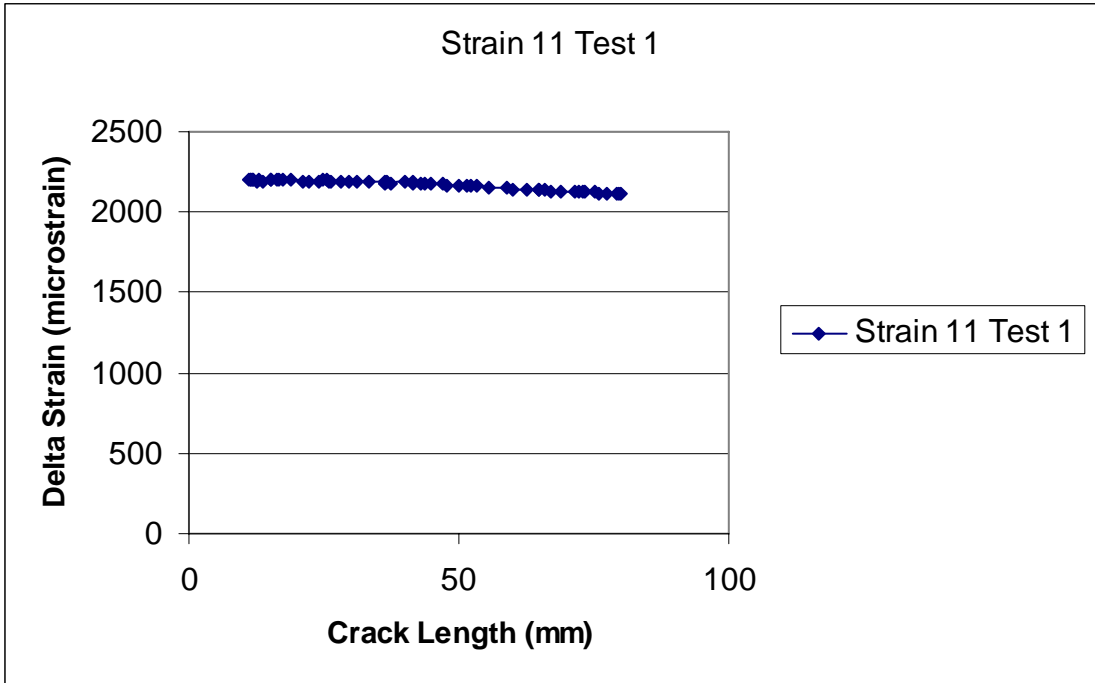


Figure 54. Change in Strain Versus Crack Length (mm):Strain Gage 11

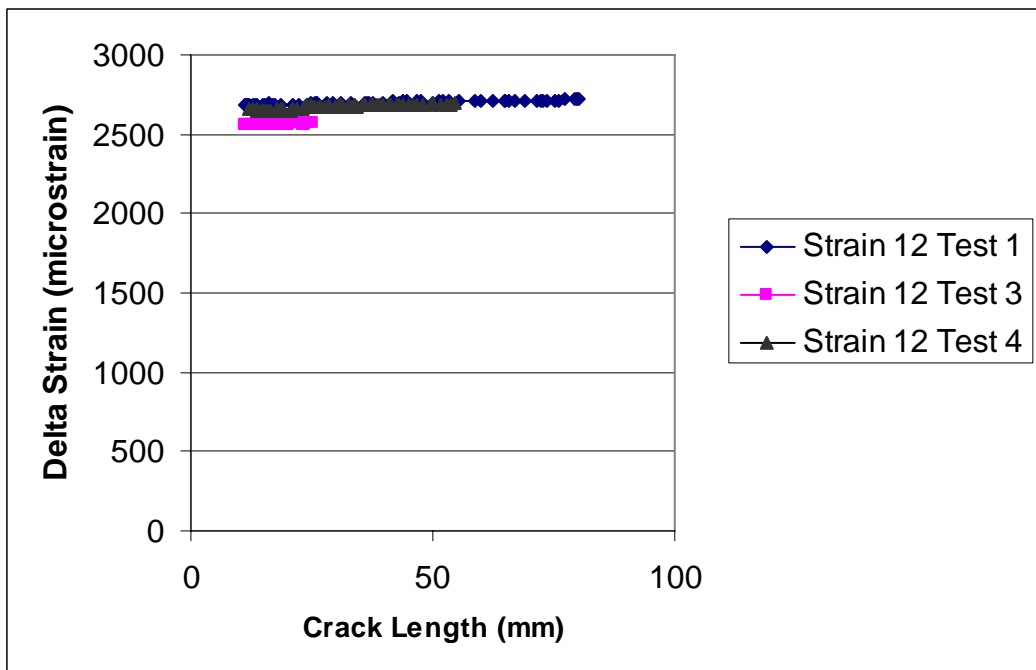


Figure 55. Change in Strain Versus Crack Length (mm):Strain Gage 12

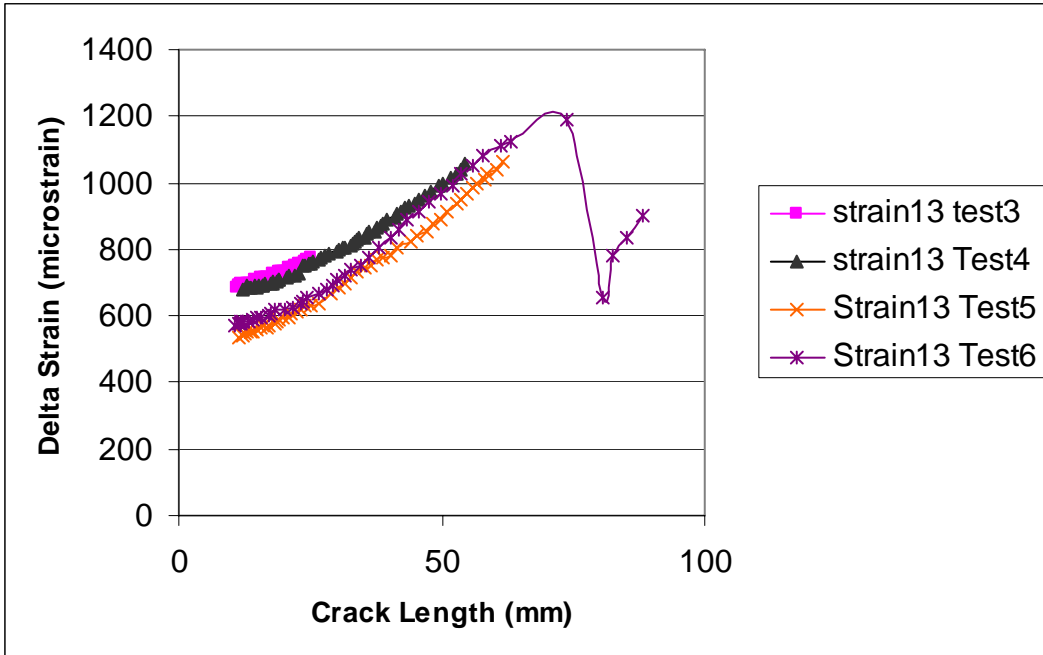


Figure 56. Change in Strain Versus Crack Length (mm):Strain Gage 13

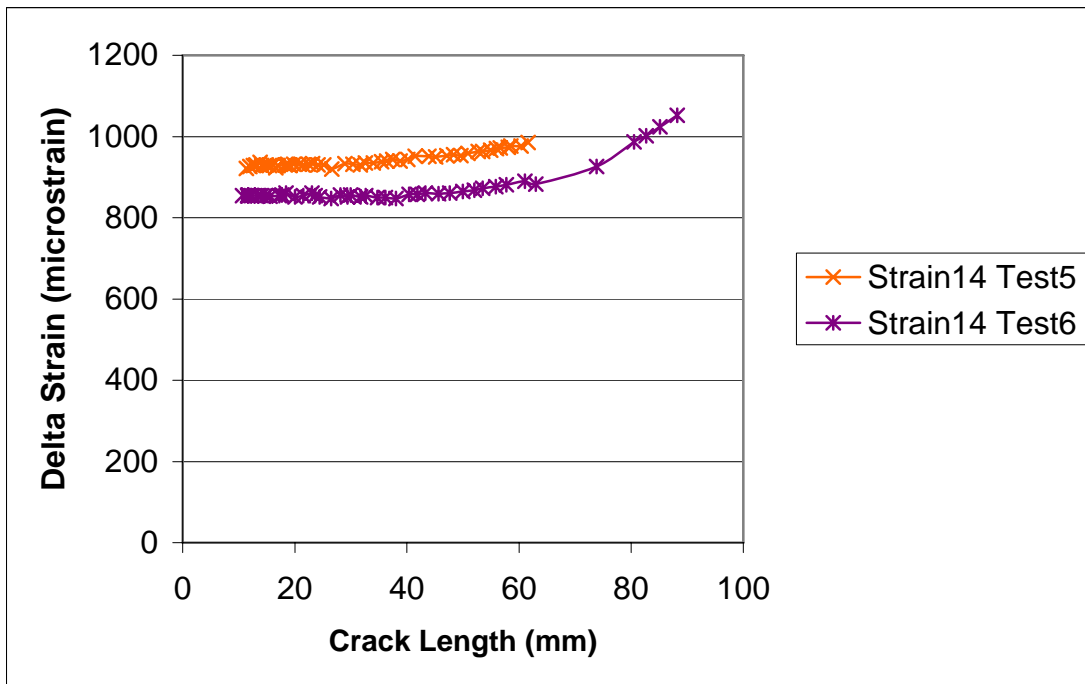


Figure 57. Change in Strain Versus Crack Length (mm):Strain Gage 14

the composite patch having the higher modulus of elasticity, the strains are lowered now that they are based on the patches modulus of elasticity and not a combined modulus of elasticity. However when the debond fully grows over the strain gage, the strains continue to rise again, as the stresses are continually flowing more through the patch, and less through the aluminum, as the crack length grows.

4.3 Tensile loading and fracture

This section will cover the tensile loading of these experiments and where its fracture points are based on the current crack length. Table 13 compares the crack length to the stress at which the specimen broke.

Table 13. Fracture Strength with Associated Crack Length

Test No.	Crack Length (mm)	Strength
1	76.2	N/A
2	11.43	603 MPa
3	25.4	603 MPa
4	55.88	559 MPa
5	63.5	475 MPa
6	91.44	195 MPa

In test one, the crack was grown to the width of the patch and then the test was halted. The specimens in tests two and three broke very near the ultimate strength of the material, however they did not break in the gage section, but broke at the grips. This is not totally unexpected. The gage section is 127 mm wide. The grip section is 152.4 mm

wide with three 12.7 mm holes straight across, giving it an effective width of 114.3 mm with stress concentrations at the bolt holes. In test number four where the crack grew to 55.88 mm before it was subjected to tensile loading broke at 559 MPa in the gage section with the patch making a clean break right along the crack. This test got into the yield zone of the aluminum before it fractured. Test number five grew the crack just slightly longer, at 63.5 mm total width, however it did not have the clean break that occurred in test number four where both the specimen and patch broke along the crack line. In test five the majority of the patch did not break, but had a catastrophic debonding. The patch broke into three separate long strips that were expelled from the specimen at fracture, not breaking along the crack line. Only a very thin amount of the patch was left fully attached to the specimen and broke in half along the crack line. In test 6 the specimen was not put under any tensile load but was fatigued until it broke, with the maximum fatigue loading being set to 194 MPa. This specimen had a clean debond, where the patch was still fairly strongly attached to the top half of the specimen when it broke, but was cleanly stripped away from the bottom half of the specimen.

4.4 Debonds

4.4.1 Photographic and Acoustic Imaging

Some of the debonds that occurred beneath the patch as the crack grew and the specimens broke will now be examined. They will be looked at in successive order of crack length at fractures. The first specimens to be looked at are the specimens from test two and test three (see Figures 58 and 59). Test two was a pure tensile test with no crack growth. In this image no debonding around the initial hole is seen. However some

lighter areas did show up, which may be possible air bubbles under the patch due to an imperfect bonding. These possible bubbles can be seen in most all of the scanned images.

For the test two scan, the crack was grown from 11.43 mm to 25.4 mm before it was put under tensile loading. In this image no definitive debonding is seen. There appears to be a possible oval shaped disbond around the crack with a little lighter coloring in that area, however those who did the scans do not believe this to be a debond.

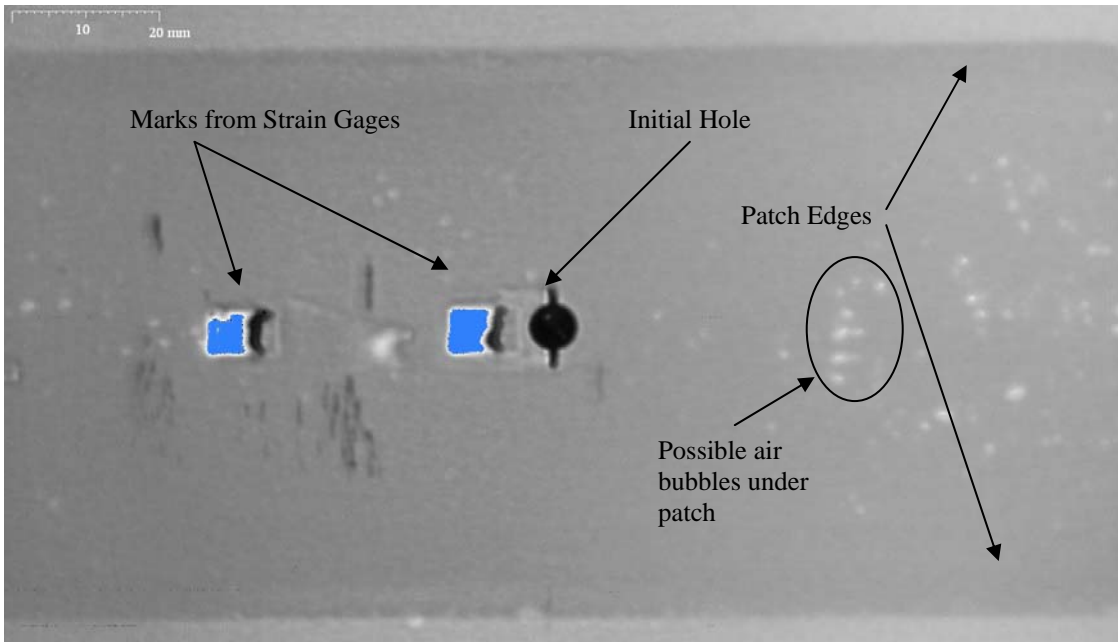


Figure 58. Test 2 Acoustic Microscopy Image.

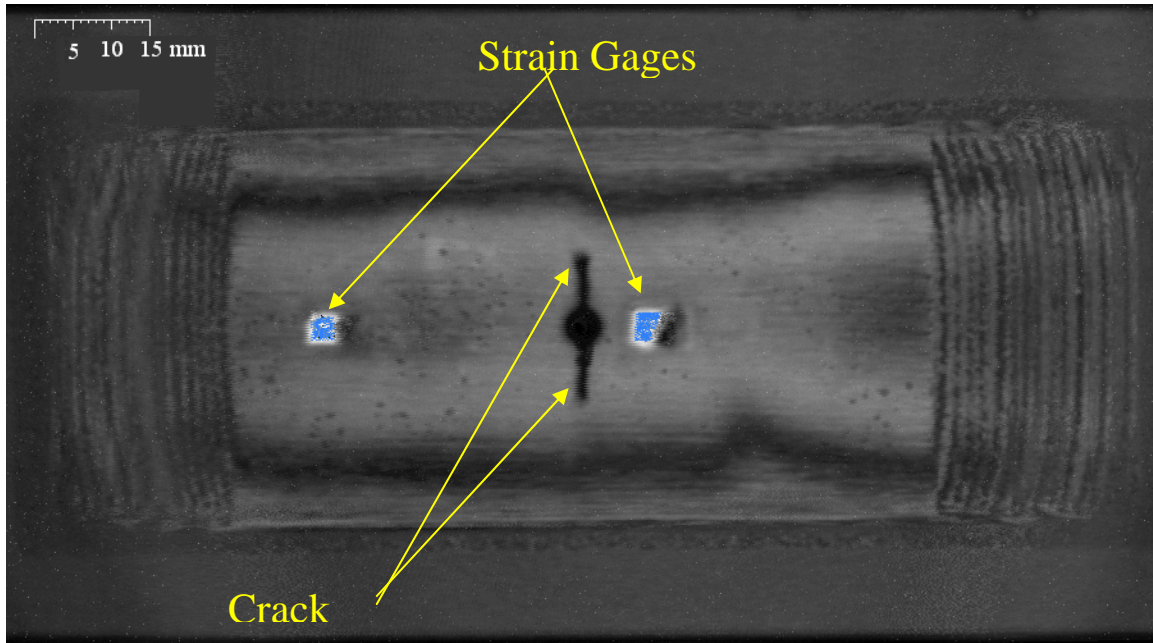


Figure 59. Test 3 Acoustic Microscopy Image.

The rest of the samples show significant debonding. Test four and test five had their cracks grow to 55.88 mm and 63.5 mm respectively before they were put under tensile loading to failure (See Figures 60 through 63). Specimen four broke the patch in two, right down the crack line. In Figure 60 it is seen that the large disbond area going all the way to the edge of the patch at the full three inches. The height of the circular debonds are measured to be 57.15 mm on the left, and 43.18 mm on the right. It is not completely clear why this debond grew in the unsymetric manner that it did.

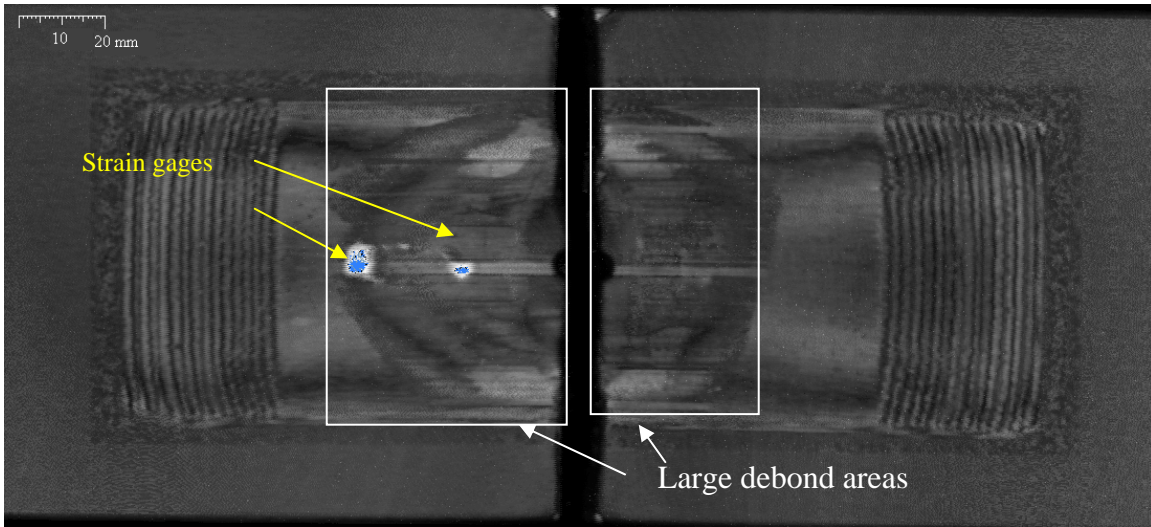


Figure 60. Acoustic Microscopy Image of Test 4 Specimen.

In test five, as seen in Figures 61 through 63 there was no patch left on the specimen to scan for debonds. However, the shape of the debond on the aluminum specimen and on the back of the patch can be seen fairly clearly. It is seen that in this test, most clearly in Figure 63 that this debond is unsymmetric in a different way, in that the debond is greater to the left side of the patch in this figure. This is almost certainly due to the fact that in this test the crack grew faster on that side than it did on the other. At a total crack length of 63.5 mm there was a difference in crack growth of 3.81 mm on the one side compared to the other. The unsymmetric crack growth would lead to the unsymmetric debond area.

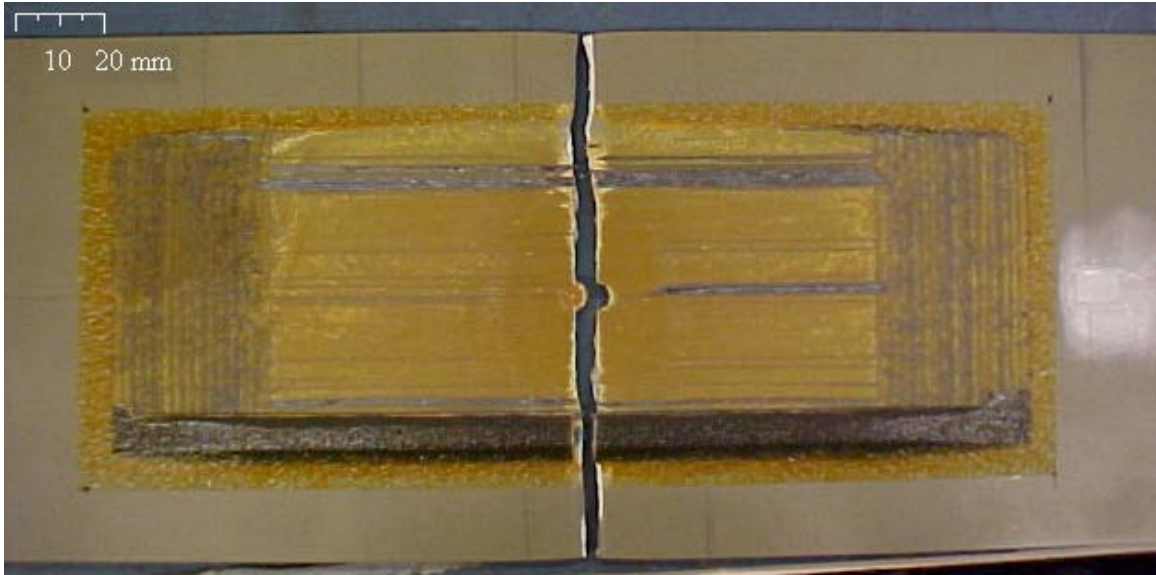


Figure 61. Photographic Image of Test 5 Specimen.



Figure 62. Close Up Photo of Test 5 Specimen



Figure 63. Photo of the Back Side of the Patch of Test 5 Specimen

Tests one and six grew the crack without any tensile loading. Test one grew the crack to the edge of the patch at 76.2 mm, whereas in test six the crack was grown until failure at 91.44 mm. These debonds are seen in Figures 64 to 66. In the scanning acoustic microscopy image of test one it is seen that while the crack grew to the full length of the patch, the debond oval stopped a little short. This specimen has the most symmetric of the debond areas. This could very well be due to the fact that this was also the only specimen to not be tested to failure. The irregular shapes of some of the other debonds could be partially from the failure loads that they were subjected to. This debond area appears to be a near perfect oval 76.2 mm in length and 43.18 mm total width.

Specimen six grew the crack to failure, and when the specimen failed the patch was smoothly stripped off of the bottom half of the specimen, leaving it attached to only the top half of the specimen. In its scanning acoustic microscopy image, a clearly defined oval debond can not be seen. When the specimen failed, it was enough to fully strip away the bonding from the lower half of the specimen. Some additional debonding certainly occurred in the top half at failure, leaving it nearly all debonded in the top half also. In Figure 66 the shape of how the debond grew before failure is seen. Here in this image the oval debond shape can be seen. A curve has been drawn to better identify this debond. Here the debond is seen to go to the edge of the 76.2 mm patch, and grew 33.02 mm from the center line.

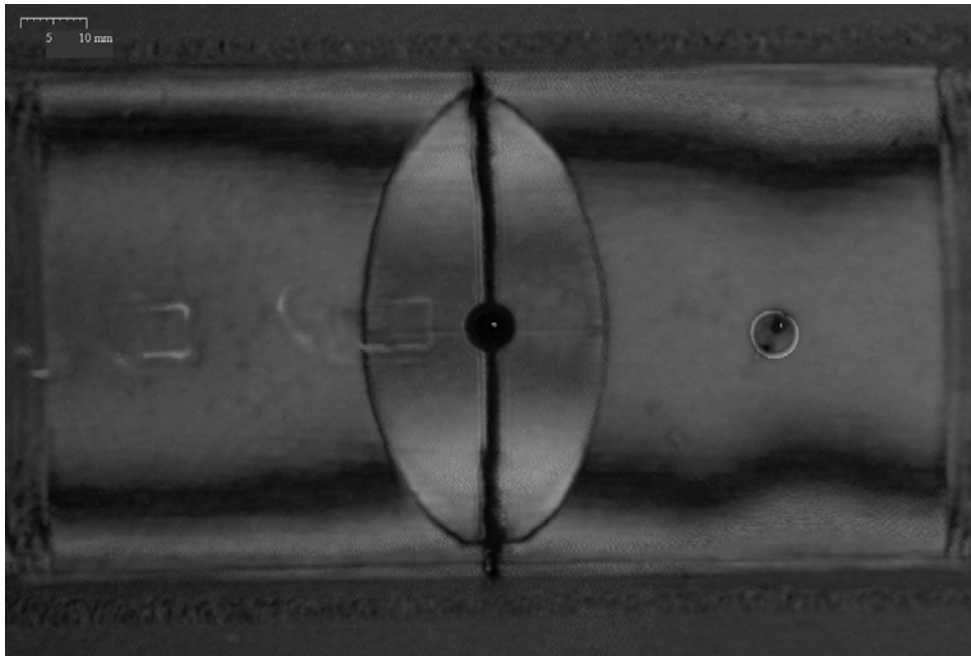


Figure 64. Acoustic Microscopy Image of Specimen from Test 1

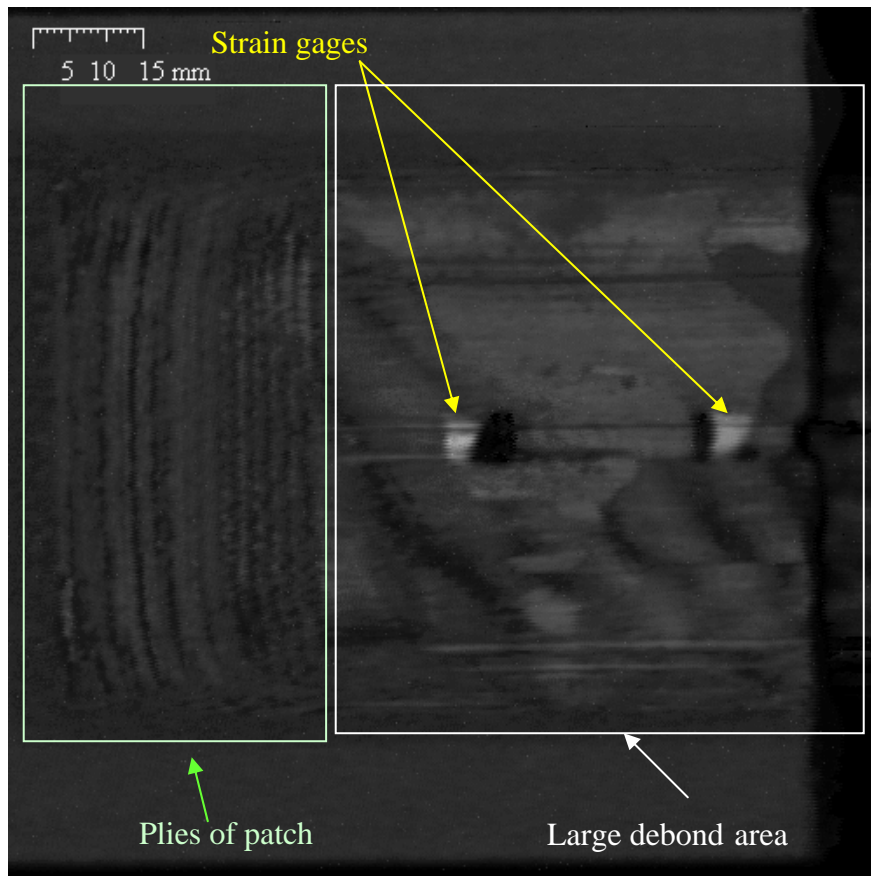


Figure 65. Acoustic Microscopy Image of Specimen from Test 6

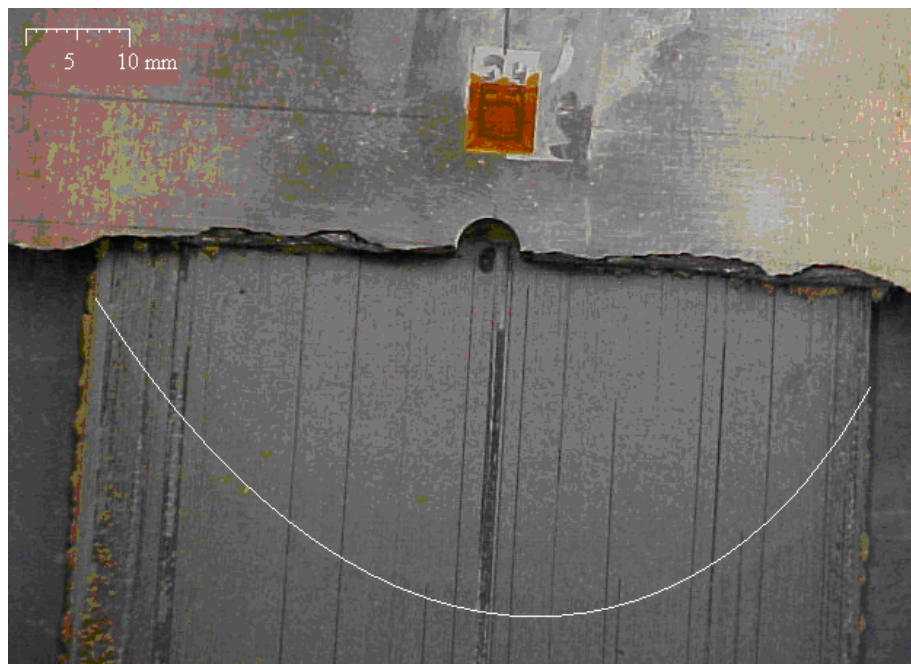


Figure 66. Photo Image of Specimen 6 Patch Debond Area.

4.4.2 IR Imaging

During each test, various Thermal IR pictures were taken. The test would be paused to try to get an IR picture of the debond area underneath the patch. The samples were then rapidly heated up using the heat gun. Due to the different rates of heating of the trapped air in the debond area, the debond should heat up at a different rate than the rest of the sample. In some tests the IR pictures were able to detect the debonds better than others. The thermal IR camera was unreliable in these tests to effectively detect debonds. In the early tests, debonds were unable to be detected. In test 6 only the initial machined hole was able to be detected even though there most certainly was a large debond at this measurement of 63 mm. (Figure 67) One thing that led to additional difficulties were the numerous strain gages that were applied to the system. The gages, wires, and tape that were all on the specimen, hinder the view of potential debonds, in that they have an all together different IR signature themselves. The best IR pictures occurred when the finished specimen was removed from the machine. In test four an IR image was taken of one of the broken halves of the specimen. (Figure 68) In this IR picture there was the advantage of the specimen no longer being gripped in the machine, which provided initial strains in the specimen even with no load, as seen previously in Table 9 In test 5 some noticeable debonds were seen in the final IR picture taken at a crack length of 63 mm. (Figure 69) While the debonds can be seen, it is difficult to get an accurate determination of the true debond size.

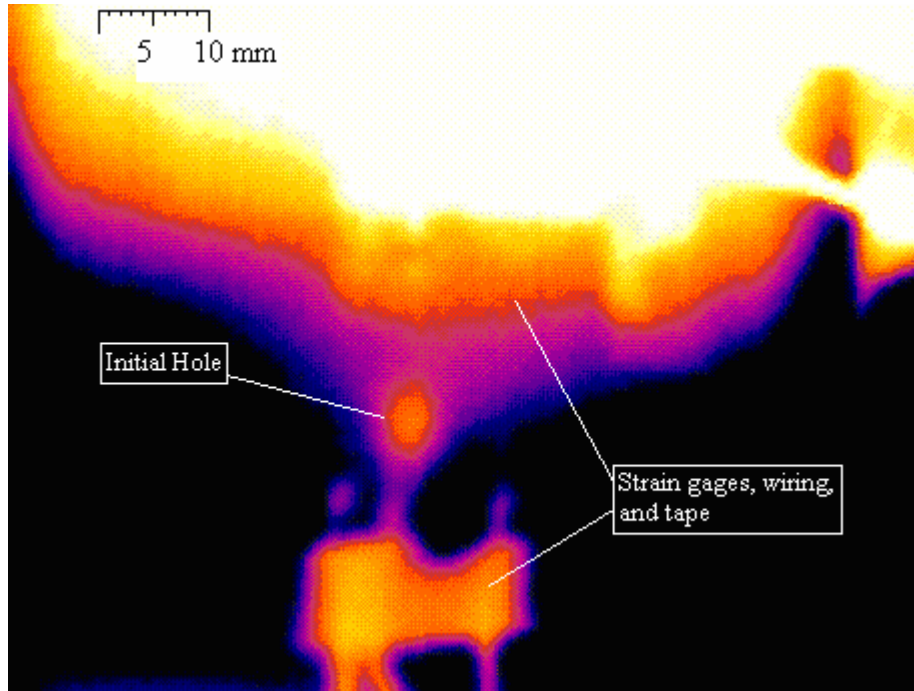


Figure 67. Thermal IR Scan of Test 6 Sample at 63 mm Crack Length

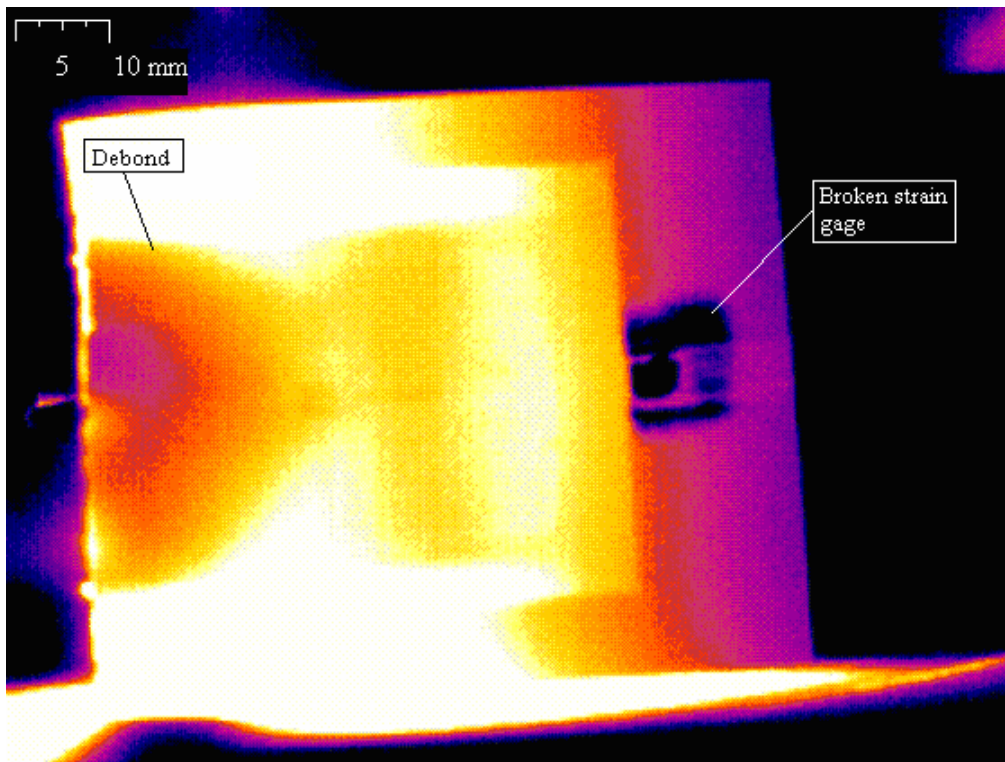


Figure 68. Thermal IR Scan of Test 4 Sample After Failure.

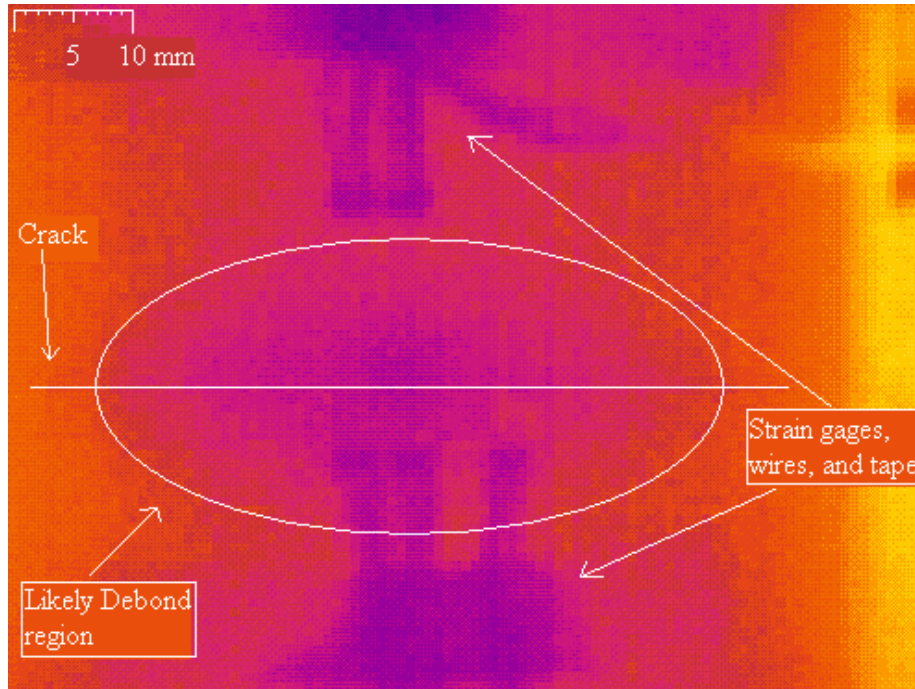


Figure 69. Thermal IR Scan of Test 5 Sample at 63 mm Crack Length

4.5 Data Comparisons

Here some of the previous data will be put together. There are several images of the debonds behind the patch that can be compared to the strain versus crack length curves (Figures 30 through 43). It was seen in Figure 64 that the debond width, at a length of 76.2 mm, was 43.18 mm. When looking at the strain gages that were centered at 2.54 mm and 12.7 mm away from the crack, the valleys in the strain readings occurring at successively larger crack lengths are seen.

With specimen 6 a similar debond shape is seen. This specimen also had a strain gage at the 25.4 mm point, and it is seen that towards the very end of the test, that strain gage showed a sudden drop in the strain readings at the point that the debond would have grown underneath its gage.

With these tests it has been seen that this Boron/Epoxy patch is very good at holding the load of the cracked specimen. With crack lengths of 11.43 mm and 25.4 mm, the patch held the entire load. Even at a crack length of 55.88 mm, the patch held the load past the yield strength of the aluminum, working nearly as well as if no patch was there. It wasn't until the crack grew to 63.5 mm that the specimen broke at stresses less than the yield strength. Even when the crack was grown by fatiguing to failure, it took a crack length of 91.44 mm before it broke with the 76.2 mm wide patch. Here it will be interesting to look at what loads an uncracked specimen would fracture, given the same crack length (see Table 14)

Table 14. Crack Length Comparison:
Real Loads to Theoretical Loads with No Patch

Crack Length	Fracture	w/o patch
11.43 mm	603 MPa	382 MPa
25.4 mm	603 MPa	251 MPa
55.88 mm	559 MPa	152 MPa
63.5 mm	474 MPa	137 MPa
76.2 mm	N/A	114 MPa

At the initial crack length, a specimen without a patch can theoretically only hold 382 MPa. This number is nearly identical to those seen in previous dummy tests on unpatched specimens. Without the patch, the specimen would break under fatigue loading by the time it reached a crack length of 50.8 mm. With the patch the crack was able to grow up to 91.44 mm before the specimen finally broke.

In looking at the shape of the debond in the acoustic scans, and the IR images, it is seen that the shape of the debond is an oval shape that is approximately two to two and

a half times as long as it is wide. In addition it is seen in Figure 64 that the length of the crack leads the debond somewhat. In this figure, the total crack length is about eight millimeters longer than the debond. It is expected that the tips of the crack would lead the debond as the tips of the crack are still very narrow, in addition to starting with an initial crack length of about 11.4 mm. If this information is extrapolated out an interesting relationship is seen with the shape of the debond versus the strain readings. For the shape of the debond as related to the crack length the following relationship will be used:

$$W_D = (2a - 10)/2.5 \quad (12)$$

where W_D is the width of the debond, and $2a$ is the total crack length.

This relationship appears to roughly hold true for the life of the specimen. With this relationship we will look again at the strain values on gages 1-5 and 13. Strain gages one through three, while centered at 2.54 mm away from the crack, were placed right on the crack line which would be why the strain values are seen decreasing right away in Figures 44-46. On strain gage four the strain values are seen to drop off around 40 mm, and on gage five around 45 mm. When a crack length of 40 mm is put into equation 12 an approximate debond width is seen to be 12 mm. Strain gages four and five were centered 12.7 mm away from the crack line. As strain gage five is slightly off center, the debond reaches it slightly later than strain gage four, which explains why the drop off in strain values occurs slightly later at strain gage five. In Figure 56 for the strain values for strain gage 13, a drop off in strain values is seen to occur at around 75 mm. Using a

crack length of 75 mm in equation 12, an approximate debond width of 26 mm is found. This corresponds to strain gage 13 being centered at 25.4 mm away from the crack.

Here it has been shown that the irregularities in the strain values are directly related to debond growth over that region. However while the debond will cause a temporary decrease in the strain, the strain values will increase later on as the debond has completely passed over the region of the strain gage.

V. Summary, Conclusions, and Recommendations

The purpose of this study was to investigate mechanical properties of the cracked aluminum specimen with the bonded composite patch. This study closely examined the strain data on and near the composite patch. The data was then analyzed to determine the mechanical properties and behavior of the patch and its effects on the crack growth rates. The fatigue tests showed the growth of the crack throughout the life of the specimen. The tensile tests showed the different strengths of the specimen at different crack lengths.

During these tests, some results were as expected, however many were not as originally expected. In this study varying overload situations caused different crack growth rates among the specimens. While this was not initially desired, it helped to examine how the strain changed over the crack length with varying crack growth rates. Here it was seen that the strain values were directly proportional to the crack length, with no noticeable dependence on the crack growth rate. For strains a little ways away from the crack, the crack length could be determined fairly closely by the strain value alone. While the overload situation caused a retardation in the crack growth rate, it was seen in test six that when this overload situation is removed, the crack growth rate will begin to rise again to approach and then in time match the crack growth rate of the specimen that had little or no retardation.

While an overload situation was not to be the intended investigation of this study, we were able to see its retardation effects on the crack growth. Often times a repaired structure will not receive a perfect cyclical loading over its life. An aircraft will

frequently run into turbulence in its operation which will produce a similar overload situation, with the resulting retardation effects on the rate of crack growth.

While we knew that the repair would strengthen the specimen significantly, these tests gave us data as to exactly how well the patch held. It was seen that through a crack length of approximately 56 mm the patch held the specimen together at stresses beyond the yield strength of the aluminum. Only after this point does the strength of the patched specimen fall below that of an unpatched one. The patch does still hold strong beyond this point, and was seen to work well up to crack lengths of the patch itself.

In this study debonding behind the repair was also examined. It was seen how the debond grew behind the patch, and the effects that it had on the strain on the portions of the patch above the debond area. It was seen how the strain on the patch grew steadily until the debond approached. When the debond grew through the patch the strain decreased in that area, then after the debond fully grew over the region the strain began to continually grow again. It was also seen that the shape of the debond was consistent among the tests prior to fracture. Using this information, strain gages along the center line will tell us the width of the debond. Since the proportional shape of the debond remains fairly consistent, knowing the width of the debond will also give the length of the debond, and the debond size. Using strain gages to monitor the debond size will tell us the crack length, and give a good warning as to when the specimen will break. The debonds were best seen growing over the strain gages 12.7 mm and 25.4 mm away from the crack. The 12.7 mm distance strain gages first saw the debond at a crack length of about 40 mm, with a patch width of 76.2 mm. The strain gage at 25.4 mm away from the crack didn't see the debond, until a crack length of 75 mm, nearly the length of the patch.

If only one strain gage were to be used to detect the debond, and predict failure, a strain gage centered at 20 mm away from the crack would work very well. It would see the debond approach as the crack length was approximately 60 mm in length. This is also just beyond the point where the strength of the specimen falls below that of the uncracked aluminum. From the tests performed this correlates to about 85% of the specimen life.

This study examined the retardation effects of overloads on composite patched aluminum specimens, however unintentional. Very little has been done in research in examining retardation effects on a composite patched specimen. Additional research in this could be done with controlled overloads at specified intervals, as opposed to the unintentional overloads that were seen in this study.

In gathering mechanical data on the patch additional research could be done. If additional strain gages were placed in the area of the debond growth, the effects of the debond on strain values could be more closely examined. Strain gages were primarily put down the center of the specimen. It may be useful to get additional strain readings along the crack further away from the center line to see what the strain values are on the patch at the crack tips when the crack is much longer. In any future tests it is recommended to have strain gages more focused within this debond region to better see how the strain values change in the patch as the debond grows beneath it. This would give a better picture of the shape of the debond as it grew and give better predictions of the life of the specimen based on the strain readings alone.

Bibliography

1. Manes, Bryan. "US Air Force Aging Aircraft Challenges" Electronic Document. USAF Aging Aircraft Program Office, 3 March 2005.
2. USAF Aging Aircraft Program Office, "TAI & Avg Age a/o 30 Sep 04" Electronic Document, 30 September 2004.
3. USAF Aging Aircraft Program Office, "DSL Chart Updated" Electronic Document, 2002
4. Bureau of Accident Investigation. "Aircraft Accident Report: Aloha Airlines, Flight 243, Boeing 737-200, N73711, Near Maui, Hawaii, April 28, 1988" Report No. NTSB/AAR-89/03. Washington: National Transportation and Safety Office, 14 June 1989.
5. Avraam, Jason B. *Fatigue Response of Thin Stiffened Aluminum Cracked Panels Repaired with Bonded composite*. MS thesis, AFIT/GMS/ENY/01M-01. School of Engineering and Management, Air Force Institute of Technology (AU), Wright-Patterson AFB OH, March 2001 (ADA390430)
6. Baker, A.A. "Introduction and Overview" in *Advances in the bonded Composite Repair of Metallic Aircraft Structure Volume 1*, Kidlington, Oxford, UK: Elsevier Science Ltd, 2002.
7. Kelly L.J. "Introductory Chapter" in *Bonded Repair of Aircraft Structures*. Dordrecht, The Netherlands: Martinus Nijhoff Publishers.
8. Air Force Joint Technology Applications Office. *Composite Patches for Metallic Structures*. No. TT-89034. Wright-Patterson AFB OH, 29 August 1989 (AD-B143611).
9. Boeing. "Structural Health Monitoring for Bonded Repairs, Plan for Supplemental Coupon Testing"(Revision A) 16 April 2004
10. Broek, David *Elementary Fracture Mechanics*(fourth revised edition), Dordrecht, The Netherlands: Kluwer Academic Publisher, 2002
11. Conley, David S. *Fatigue Response of repaired thick aluminum panels with bondline flaws*. MS thesis, AFIT/GAE/ENY/99M-03. School of Engineering and Management, Air Force Institute of Technology (AU), Wright-Patterson AFB OH, March 1999 (ADA361591)
12. Fredell, R. S. *Damage Tolerant Repair Techniques for Pressurized Aircraft Fuselages*. PhD dissertation. Delft University of technology, Delft, The Netherlands, June 1994 (WL-TR-93-3134)

13. Schubbe, Joel J. *Thickness Effects on a Cracked Aluminum Plate with Composite Patch Repair*. Air Force Institute of Technology (AU), Wright-Patterson AFB OH, June 1997
14. Herakovich, Carl T. *Mechanics of Fibrous composites*, New York: John Wiley & Sons Inc, 1998
15. Reinhart T.J. “Surface treatments for bonded repairs of metallic components” in *Bonded Repair of Aircraft Structures*, Dordrecht, The Netherlands: Martinus Nijhoff Publishers.
16. Sutherland, Bill J. “Boron Doubler Reinforcement Modification F-111 Wing Pivot Fittings.” Status Report. Sacramento Air Logistics Center. 01 January 1993
17. Hart-Smith L.J. “Design and analysis of bonded repairs for metal aircraft structures” in *Bonded Repair of Aircraft Structures*, Dordrecht, The Netherlands: Martinus Nijhoff Publishers.
18. Baker, Alan and others. *Advances in the bonded Composite Repair of Metallic Aircraft Structure Volume 2*. Kidlington, Oxford, UK: Elsevier Science Ltd, 2002.
19. Walker K.F. and Rose L.R.F. “Case History: F-111 Lower Wing Skin Repair substantiation” in *Advances in the bonded Composite Repair of Metallic Aircraft Structure Volume 2*, Kidlington, Oxford, UK: Elsevier Science Ltd, 2002.
20. Guijt C. and Mazza J. “Case History: F:16 Fuel Vent-hole Reparis” in *Advances in the bonded Composite Repair of Metallic Aircraft Structure Volume 2*. Kidlington, Oxford, UK: Elsevier Science Ltd, 2002.
21. Fredell R. and Guijt C. “Glare Patching Efficiency Studies” in *Advances in the Bonded Composite Repair of Metallic Aircraft Structure volume 1*. Kidlington, Oxford, UK: Elsevier Science Ltd, 2002.
22. Denney, Jason J. *Fatigue Response of Cracked Aluminum Panel With Partially Bonded Composite Patch*. MS thesis, AFIT/GAE/ENY/95D-7. School of Engineering and Management, Air Force Institute of Technology (AU), Wright-Patterson AFB OH, December 1995.
23. MatWeb “Aluminum 7075-T6; 7075-T651,” *Online Material Data Sheet*, (May 6, 2005) <http://www.matweb.com/search/SpecificMaterial.asp?bassnum=MA7075T6>,
24. MatWeb “Specialty Materials 5521 Boron Epoxy Prepreg Tape”, *Online Material Data Sheet*, (May 6, 2005) <http://www.matweb.com/search/SpecificMaterial.asp?bassnum=PSPEC00>,

25. Welter, John T. "Scanning Acoustic Microscopy Description" Electronic Document. Air Force Research Laboratory Materials and Manufacturing Directorate (AFRL/ML) February 16, 2005.

26. Saada, Adel S. *Elasticity Theory and Applications*, Malabar: Krieger Publishing company, 1993

Vita

Captain Michael A. Hansen was born in Normandy Park, Washington. He graduated from Evergreen Lutheran High School, Des Moines, Washington, in 1996. He then entered the University of Washington and graduated with a Bachelor of Science in Aeronautical and Astronautical Engineering in June of 2000. On August 23, 2000 he entered the United States Air Force Officer Training School and was commissioned a 2nd Lieutenant on November 17, 2000. Captain Hansen's first assignment was to the National Air and Space Intelligence Center, Wright-Patterson AFB, OH. Captain Hansen entered the Air Force Institute of Technology in August 2003.

REPORT DOCUMENTATION PAGE

*Form Approved
OMB No. 074-0188*

The public reporting burden for this collection of information is estimated to average 1 hour per response, including the time for reviewing instructions, searching existing data sources, gathering and maintaining the data needed, and completing and reviewing the collection of information. Send comments regarding this burden estimate or any other aspect of the collection of information, including suggestions for reducing this burden to Department of Defense, Washington Headquarters Services, Directorate for Information Operations and Reports (0704-0188), 1215 Jefferson Davis Highway, Suite 1204, Arlington, VA 22202-4302. Respondents should be aware that notwithstanding any other provision of law, no person shall be subject to a penalty for failing to comply with a collection of information if it does not display a currently valid OMB control number.

PLEASE DO NOT RETURN YOUR FORM TO THE ABOVE ADDRESS.

1. REPORT DATE (DD-MM-YYYY) 13-06-2005		2. REPORT TYPE Master's Thesis		3. DATES COVERED (From – To) Aug 2003 – Jun 2005	
4. TITLE AND SUBTITLE Mechanical Behavior of Cracked Panels Repaired with Bonded Composite Patch				5a. CONTRACT NUMBER	
				5b. GRANT NUMBER	
				5c. PROGRAM ELEMENT NUMBER	
6. AUTHOR(S) Hansen, Michael, A., Captain, USAF				5d. PROJECT NUMBER JON#04-192	
				5e. TASK NUMBER	
				5f. WORK UNIT NUMBER	
7. PERFORMING ORGANIZATION NAMES(S) AND ADDRESS(S) Air Force Institute of Technology Graduate School of Engineering and Management (AFIT/EN) 2950 Hobson Way WPAFB OH 45433-7765				8. PERFORMING ORGANIZATION REPORT NUMBER AFIT/GA/ENY/05-J01	
9. SPONSORING/MONITORING AGENCY NAME(S) AND ADDRESS(ES) AFRL/VASA Mr. Mark Derriso Bldg 65, WPAFB Mark.Derriso@wpafb.af.mil				10. SPONSOR/MONITOR'S ACRONYM(S)	
				11. SPONSOR/MONITOR'S REPORT NUMBER(S)	
12. DISTRIBUTION/AVAILABILITY STATEMENT APPROVED FOR PUBLIC RELEASE; DISTRIBUTION UNLIMITED.					
13. SUPPLEMENTARY NOTES					
14. ABSTRACT This research focuses on investigating the mechanical behavior of cracked aluminum panels repaired with bonded boron/epoxy composite patches. The effects of crack initiation and growth on the residual strength of the repaired panels are characterized. This research establishes a correlation between damage modes, residual strength and evolution of strain within as well as outside the patch. Monotonic tensile tests on specimens with a perfectly bonded patch were used to determine the base line strength. Likewise, fatigue tests on specimens with a perfectly bonded patch served to establish baseline fatigue life. In addition, several specimens with a perfectly bonded patch were subjected to different fractions of the expected fatigue life, introducing damage, which were quantified by NDE techniques. These specimens were then subjected to a monotonic tensile test to failure in order to characterize the residual strength and the evolution of strain within and outside the patch, and the correlation between the disbonds and strain measurements at various locations on the specimen. This research looks to help in extending the service life of military and commercial aging aircraft, by using bonded composite patches on developing cracks in the structure. Bonded composite patches may be able to replace the crack patching technique of using bolted joints, which have the disadvantage of requiring holes to be machined in the metallic structure, which decreases its load-carrying capacity, creating stress concentrations and sites for crack initiation. In this study it was learned how the strain values increase as the crack grows. And despite differing crack growth rates, the strain values followed the growth of the crack closely throughout all the tests. The effects of overload situations were seen, and how this produces a retardation effect in the rate of growth of the crack.					
15. SUBJECT TERMS Bonded Composite Repair, Fatigue, Tensile, Crack Growth, Stress, Strain, Strength, Overload, Retardation, Crack Patching, Fracture, Debond, Scanning Acoustic Microscopy, Adhesive, Aging Aircraft,					
16. SECURITY CLASSIFICATION OF:		17. LIMITATION OF ABSTRACT UU	18. NUMBER OF PAGES 113	19a. NAME OF RESPONSIBLE PERSON Your Advisor-name	
REPORT U	ABSTRACT U			c. THIS PAGE U	19b. TELEPHONE NUMBER (Include area code) (937) 255-3636, ext 4587; e-mail: Shankar.mall@afit.edu